

Reducing the cover-to-diameter ratio for shallow tunnels in soft soils

Vu Minh, Ngan

DOI

[10.4233/uuid:e35c4735-1f6f-4e4c-b7b8-130f68a7dd02](https://doi.org/10.4233/uuid:e35c4735-1f6f-4e4c-b7b8-130f68a7dd02)

Publication date

2016

Document Version

Final published version

Citation (APA)

Vu Minh, N. (2016). *Reducing the cover-to-diameter ratio for shallow tunnels in soft soils*. [Dissertation (TU Delft), Delft University of Technology]. <https://doi.org/10.4233/uuid:e35c4735-1f6f-4e4c-b7b8-130f68a7dd02>

Important note

To cite this publication, please use the final published version (if applicable).
Please check the document version above.

Copyright

Other than for strictly personal use, it is not permitted to download, forward or distribute the text or part of it, without the consent of the author(s) and/or copyright holder(s), unless the work is under an open content license such as Creative Commons.

Takedown policy

Please contact us and provide details if you believe this document breaches copyrights.
We will remove access to the work immediately and investigate your claim.

Reducing the cover-to-diameter ratio for shallow tunnels in soft soils

Reducing the cover-to-diameter ratio for shallow tunnels in soft soils

Proefschrift

ter verkrijging van de graad van doctor
aan de Technische Universiteit Delft,
op gezag van de Rector Magnificus prof. ir. K.C.A.M. Luyben,
voorzitter van het College voor Promoties,
in het openbaar te verdedigen op
maandag 12 september 2016 om 12:30 uur

door

Minh Ngan VU

Civiel ingenieur
Nationale Universiteit van Civiele Techniek, Hanoi, Vietnam,
geboren te Hanoi, Vietnam.

Dit proefschrift is goedgekeurd door de

promotor: prof. ir. J.W. Bosch

copromotor: dr. ir. W. Broere

Samenstelling promotiecommissie:

Rector Magnificus,

Prof. ir. J.W. Bosch,

Dr. ir. W. Broere,

voorzitter

Technische Universiteit Delft

Technische Universiteit Delft

Onafhankelijke leden:

Prof. ir. A.F. van Tol,

Prof. dr. T.H. Vo,

Prof. dr. -Ing. M. Thewes,

Prof. dr. ir. A. Bezuijen,

Prof. dr. ir. J.G. Rots,

Technische Universiteit Delft

Hanoi University of Mining and Geology

Ruhr-Universität Bochum

Universiteit Gent

Technische Universiteit Delft, reservelid

Overige leden:

Dr. ir. K.J. Bakker,

Technische Universiteit Delft



Keywords: tunnelling, stability, tunnel lining, ground movement, volume loss

Printed by: Ipskamp Printing, Enschede

Copyright © 2016 by M.N. VU

ISBN 978-94-028-0028-9

An electronic version of this dissertation is available at

<http://repository.tudelft.nl/>.

All rights reserved. No part of the material protected by this copyright notice may be reproduced or utilized in any form or by any means, electronic or mechanical, including photocopying, recording or by any information storage and retrieval system, without written consent from the author.

To Mai Lan, Minh Hang and Chinh Duong

ABSTRACT

Despite the fact that shallow tunnels have the benefits of low short-term construction costs and long-term operational costs primarily due to the shallow depth of the station boxes, the limited understanding of shallow tunnelling in soft soils is an obstacle to the development of shallow tunnels in urban areas. This study carries out a theoretical investigation of the effects of reducing the cover-to-diameter ratio C/D for shallow tunnels in soft soils.

In stability analysis, the uplift, face stability and blow-out mechanisms are investigated. This study investigates interactions between the TBM and surrounding soil in tunnelling process, the stability of the TBM is not taken into account. The relationship between the C/D ratio and the required thickness-to-diameter ratio d/D as well as the required support pressures will be derived in various soils. Ranges of support pressures are also estimated for the TBM.

Structural analysis is carried out for the variation of deformations and internal forces of the tunnel lining when reducing the C/D ratio. Since the conventional design models are not suitable in the case of shallow tunnels a new structural analysis model, which includes the difference between loads at the top and at the bottom of the tunnel, is proposed. Optimal C/D ratios with various d/D ratios for shallow tunnels in soft soils are also derived.

With respect to ground movement analysis, this research investigates the areas affected by shallow tunnelling with a preliminary assessment of the risk of building damage by investigating surface and subsurface soil displacements. These areas are determined for different tunnel diameters in various soil types and are then compared to recent studies. The total volume loss is estimated at the tunnelling face, along the TBM, at the tail and includes long-term consolidation settlements. By combining empirical models from the literature and the proposed new models, the volume loss components are estimated both for short-term construction and for the long-term consolidation effects. This shows that a no volume loss is feasible in shallow tunnelling with careful control of the support pressure.

The boundaries of the influence zones in shallow tunnelling are identified and discussed on the basis of various case studies. The effects of the soil parameters on the influence areas are also investigated.

From these calculations, the limits and optimal C/D ratios for shallow tunnelling are deduced and recommendations and solutions for improving the shallow tunnelling process are proposed in this dissertation.

ACKNOWLEDGEMENTS

I consider it an honour to work with Prof. Ir Johan W.Bosch and Dr. Ir Wout Broere in this research. Johan, your speech at the first meeting about PhD studies has been lived in my mind “You are here not only for your PhD study, the more important achievement is the improvement of yourself”. It has changed my attitude of the PhD study. I have a special thank for Wout, who has worked patiently with me-a recruit in tunnelling-not only for discussing and assessing to my sudden and strange ideas, but also with special guidance and even English correction. Without your help, I think it would be impossible to write this acknowledgement. Johan and Wout, your guidance and suggestions in research process are really wonderful and I would like to express my profound gratitude and appreciation to you.

The research in this dissertation was supported by the Ministry of Education and Training of Vietnam (Project 322), Hanoi University of Mining and Geology, Geo-Engineering Section and Valorisation Centre in Delft University of Technology. I am very grateful for their support and for the opportunity to carry out this research.

For the period of my PhD study, I am grateful for the time spent with roommates and colleagues in the GeoEngineering Section. Patrick Arnold, thanks for your kind help not only on many things in a PhD study such as Latex and Matlab, but also many life problems. Nor Hazwani Md. Zain, Rafael Rodriguez Ochoa, Rui Rui and Hongfen Zhao who made me feel comfortable. I will remember the time with colleagues in GeoEngineering during BBQ, drinking events and especially, football matches between the United Nation team from Geo-Engineering section and Vietnamese team in TU Delft.

For the Vietnamese community in Delft and in the Netherlands, I cannot find words to express my gratitude to you. I cannot image how I could live in Delft without you. Thanks for the help from Chi and Phuong when I first came here. VDFC is a wonderful football club, I have had many amazing moments in some tournaments.

This work would never been completed and perhaps begun without the support from my family. I would like to thank my papa, mama and my younger sister, Dieu for your support. My wife, Mai Lan, thank you so much for your love, support, encouragement and patience. For my daughter, Minh Hang, it is really happy to see you growing up every morning. Thanks to my son, Chinh Duong who breathes new life into my research.

CONTENTS

Abstract	vii
Acknowledgements	ix
1 Introduction	1
1.1 Aims of this research	3
1.2 Outline of this dissertation	4
2 Stability analysis of shallow tunnels	7
2.1 Introduction	8
2.2 Uplift	9
2.3 Failure body models	11
2.3.1 Literature review concerning stability of tunnel face	11
2.3.2 Wedge stability model	15
2.4 Blow-out	21
2.5 Combination analysis	33
2.6 Conclusion	37
3 Structural analysis of shallow tunnels	41
3.1 Introduction	42
3.2 Structural lining design	44
3.2.1 Influence of load and overburden on lining models	44
3.2.2 Influence of ground-lining interaction	46
3.2.3 A case study of Second Heinenoord Tunnel	48
3.3 Impacts of overburden on tunnel lining	52
3.4 Conclusion	58
4 Ground movements and effects on buildings	71
4.1 Introduction	72
4.2 Ground movement definitions and risk assessment	72
4.2.1 Ground movement definitions	72
4.2.2 Risk of building damage assessment	78
4.3 Effects of the C/D ratio on surface settlement	80
4.4 Effects of the C/D ratio on subsurface settlement	85
4.5 Conclusion	89
5 Volume loss in shallow tunnelling	91
5.1 Introduction	92
5.2 Volume loss at the tunnelling face	93
5.3 Volume loss along the shield	97

5.4	Volume loss behind the shield	100
5.4.1	Volume loss at the tail	103
5.4.2	Volume loss due to consolidation	106
5.5	Total volume loss and case studies	110
5.5.1	Total volume loss.	110
5.5.2	Case studies	115
5.6	Conclusion	119
6	Impact factors of influence zones	121
6.1	Introduction	122
6.2	On the variation of influence zones with different categories of damage risk assessment	122
6.3	Effects of soil parameters on influence zones	129
6.4	Conclusion	132
7	Conclusions and Recommendations	135
7.1	Conclusions.	136
7.2	Recommendations for future research	139
	Bibliography	141
A	Blow-out model	151
A.1	Uniform support pressure	151
A.2	Linear support pressure with gradient δ_p	153
B	Ground movement	155
	List of Symbols	157
	Summary	161
	Samenvatting	163
	Curriculum Vitae	165

1

INTRODUCTION

You are here not only for your PhD study, the more important achievement is the improvement of yourself.

Johan W.Bosch

Although tunnels are often designed well below foundation level in urban areas, shallow tunnels have many benefits with regards to the short-term construction costs and the long-term operational expenses. There are, however, limits to shallow tunnelling in urban areas with soft soil conditions, which should be investigated and solved. This chapter provides an overview of the general background to shallow tunnelling, the aims of this research and the outline of this dissertation.

The demand for infrastructure in urban areas is increasing due to economic developments and the growth of urban populations. Even though the construction costs are higher, underground infrastructure is a sustainable and safe construction choice for cities. Tunnels have become an important part of public underground infrastructure all over the world.

Tunnel boring machines (TBM) are widely used in the construction of underground infrastructure in urban areas due to the fact that disturbance at surface level can be reduced significantly during the construction and their ability to limit settlements and damage to existing buildings. In an environment with soft overburden, particularly in soft Holocene layers, buildings are generally built on pile foundations. The tunnel is often designed well below the pile tip level. There are two reasons for doing this: to reduce interaction between the tunnelling process and the piles, and to avoid having to drive through old abandoned piles that are still present below the streets. This results in relatively deep track tunnels and also in deep station boxes.

When the tunnels are located at more shallow levels, above the pile tip level, this largely eliminates the impact on the pile bearing capacity due to the ground movement at the tip of the piles. This then reduces the required depth of the station boxes and therefore also the construction costs. Other benefits are the low operational cost in the long-term and the shorter travelling time from the surface to the platforms. Tunnelling in such conditions is only possible if there are no or hardly any obstacles in the subsurface of the streets. A shallow tunnel, with a low cover-to-diameter ratio C/D may introduce unforeseen or new limits, for example related to the face stability, the lining structure or ground movements and the subsequent impact on nearby structures. Also, the stability of the TBM and the tunnelling process may become an issue. For this reason, the focus of this study is on the impact of shallow tunnelling in soft soils.

Firstly, the properties of the soil around the tunnel have important effects on the tunnelling face stability. With a shallow cover, if the support pressures at the tunnelling face are too small, the tunnelling face will collapse and the soil will move towards the TBM. When the support pressures are too large, this leads to problems of uplift, blow-out or fracturing. Furthermore, the relatively large difference between the support pressures at the top and the bottom of the tunnel and the relatively small bandwidth between the maximum and minimum support pressures, compared to moderate and deep tunnels, should be taken into account.

Secondly, reducing the C/D value leads to a change in the overburden load on the tunnel lining. A common method used in structural tunnel design has been proposed by [Duddeck and Erdmann \(1985\)](#). Both his continuum model and the model without a reduction in ground pressures at the crown are valid for moderate and deep tunnels with a depth $C \geq 2D$. In shallow tunnels with a C/D ratio of less than 1, the overburden pressure on the crown and the invert is significantly different and the loads, which are used in Duddeck's models, will not be realistic.

Thirdly, underground construction in urban areas often leads to negative effects on existing structures on the surface and on subsurface structures. In fact, considerable damage to existing buildings due to tunnelling has been seen in many cities. To avoid or limit such damage, the extent of the area that is influenced by tunnelling should be investigated. Tunnelling usually leads to surface and subsurface settlement caused by ground

movement. Shallow tunnelling is expected to both increase the impact and magnitude of ground movement to limit the area affected. The combined set of these contrasting effects should be investigated to estimate the effect of tunnelling on existing structures. Fourthly, the prediction of surface settlement and ground movement induced by tunnelling is based on volume loss, which is the difference between the realized tunnel volume and the designed tunnel volume. Although some methods for estimating volume loss during design have been proposed, most are based on experience gained from previous projects, with a limited understanding of tunnelling processes. In order to optimize the shallow tunnelling process, the relation between volume loss and machine parameters and tunnelling management needs to be studied.

Besides investigating stability problems and the influence of shallow tunnelling on existing nearby buildings, protective methods also are effective approaches when seeking to minimize the negative effects of tunnelling projects in urban areas. These methods might be applied to improve the tunnelling process, to reinforce surrounding soil and/or to strengthen existing nearby buildings. These protective methods are often determined and decided on the basis of the required technical parameters estimated from the impact analysis of shallow tunnelling.

1.1. AIMS OF THIS RESEARCH

On the basis of the above analysis, the effects and possibilities of shallow tunnelling in soft soil will be investigated in this dissertation. This identifies the areas that require improvement methods for safe shallow tunnelling.

The first aim is to solve the stability problems of shallow tunnelling relating to uplift, blow out and tunnelling face stability. The limits to the C/D ratio when tunnelling in soft Holocene layers are investigated by looking into several aspects of shallow tunnelling.

The second target is to solve the structural design problem for shallow tunnels. Since there are insufficient analysis models for tunnelling with shallow covers, this study proposes a new structural model for shallow tunnels, which will include significant differences between loads at the top and bottom of the tunnel. From this structural analysis, optimal C/D ratios can then be derived for various soil parameters and tunnels.

Thirdly, an investigation into the effects of shallow tunnelling on surface buildings with shallow foundations, deep foundations and pile systems will be carried out. The extent of influence areas due to tunnelling can be determined with allowable design values for the preliminary risk assessment.

The next part studies volume loss, which is derived from tunnel boring machine parameters and construction management. The relationship between volume loss and the process around the tunnelling machines will be investigated. An optimal way of conducting construction management and establishing possible developments for new tunnelling machines may be proposed.

The fifth part will provide the discussion on the combination of all the above aspects of shallow tunnelling. The impact of soil parameters on zones affected by shallow tunnelling will be investigated.

In this study, the driveability of the TBM in soft soils, which was studied in [Broere et al. \(2007\)](#) and [Festa \(2015\)](#), is not included because it is a very different field of expertise and recent projects show that the driveability issues can be dealt with.

1.2. OUTLINE OF THIS DISSERTATION

Chapter 2 deals with stability issues in tunnelling. Uplift, wedge stability and blow-out will be investigated. New models for blow-out are presented. The range of the support pressures depending on C/D ratios and limits is shown.

Chapter 3 investigates the effects of overburden on the tunnel structure. A new model for the structural analysis of shallow tunnels is introduced to calculate the impact of the C/D ratio on internal forces and deformations of the lining. Optimal C/D ratios for tunnels in various soil are derived.

The next chapter deals with ground movements and the effects on existing nearby buildings. These include the relative influence distances from existing buildings to the tunnel axis and the influence zone on subsurface structures.

Volume loss at the tunnelling face, along the shield, as well as at and behind the tail are detailed in Chapter 5.

Chapter 6 investigates the combined results and impact factors on the extent of the influence zones induced by shallow tunnelling.

The final chapter draws conclusions and provides recommendations for optimizing shallow tunnelling in soft soil.

An overview of this dissertation and the journal papers it is based on are given in Figure 1.1.

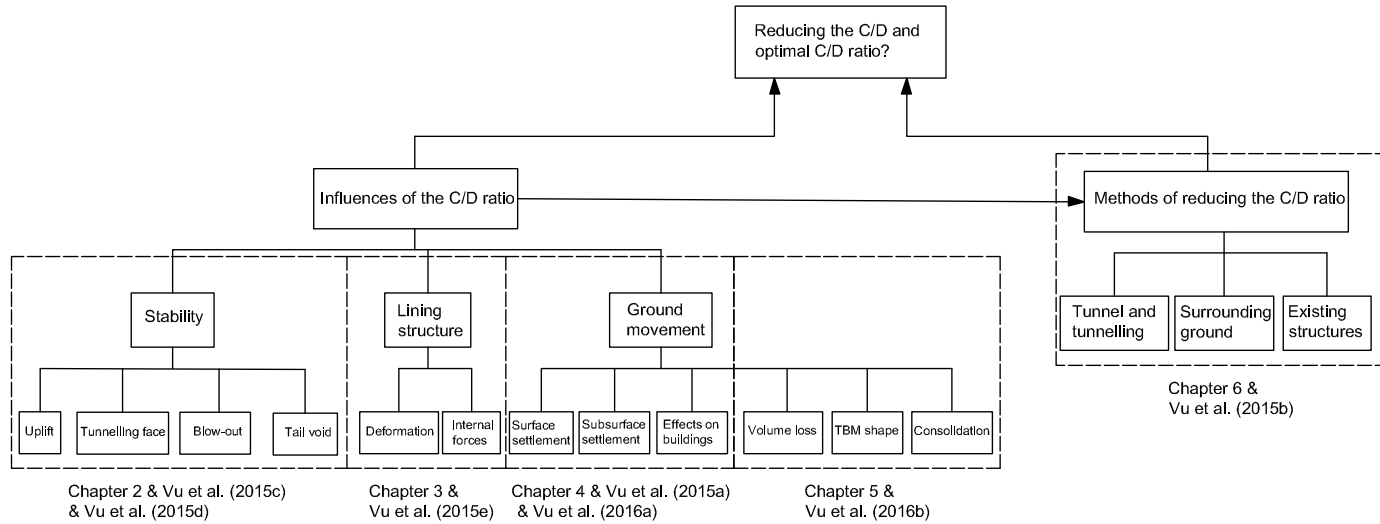


Figure 1.1: Research structure

2

STABILITY ANALYSIS OF SHALLOW TUNNELS

Keeping the tunnel safe and operational during use

Peck, Ralph B

Reducing the cover of shallow (metro) tunnels can lower construction costs by lowering cost of the station boxes, increase safety and lower operational costs in the long-term. For bored tunnels there are normally minimal depth requirements stemming from design and construction. The aim of this chapter is to investigate the effects of the cover-to-diameter ratio C/D on the stability of tunnelling process. Several models to analyze the tunnel stability were investigated and were applied for a case study in a typical Dutch soil profile with soft Holocene soil layers. The range of the support pressures in TBM machines, especially in EPB, when tunnelling in soft soil is derived for varied C/D ratios in different soil conditions. On the basis of the analysis results, some design optimizations are proposed for shallow tunnels in soft soil.

This chapter is based on papers that have been published in ITA WTC 2015 Congress and 41st General Assembly [Vu et al. \(2015d\)](#) and Tunnelling and Underground Space Technology [Vu et al. \(2015c\)](#).

2.1. INTRODUCTION

One of the most important requirements of tunnelling in cities is to maintain existing buildings and infrastructure systems. In the case of tunnelling carried out in urban areas and especially the historical areas, there may be a risk of damage to buildings, for instance due to the collapse of the tunnel face and the subsequent surface settlement. Therefore, it is necessary to control the support pressures at the tunnelling face, around the TBM and at the tail to prevent unexpected displacements in the surrounding ground and surface settlements.

In tunnelling, the support pressures should not only be high enough in order to avoid the ground moving into the excavation chamber but also low enough to prevent fracturing and blow-out. Although recent models in stability analysis for tunnelling can supply the maximum and minimum support pressures, when tunnelling with a shallow cover and taking into account a minimum of allowable fluctuation of the support pressures in practice, there will be a limit C/D ratio for tunnelling in soft soils.

Although that tunnel construction with a shallow cover is technically feasible is shown for example by the constructions of the Oi Area Tunnel, Japan (Miki et al., 2009), the Zimmerberg Base Tunnel, Switzerland (Matter and Portner, 2004), or microtunnelling and pipejacking in soft ground, see Stein (2005), it is not clear to what extent this is true in soft soils below the water table, as found in many delta areas. Therefore, it is necessary to prevent the uplift and take into account the pore pressure in calculating the support pressures.

Numerous authors have looked into the stability of the tunnel in soft soils such as Broms and Bennermark (1967); Atkinson and Potts (1977); Davis et al. (1980); Kimura and Mair (1981); Leca and Dormieux (1990); Anagnostou and Kovári (1994); Jancsecz and Steiner (1994); Chambon and Corté (1994); Broere (2001); Bezuijen and van Seters (2005) and Mollon et al. (2009a). However, they have not explicitly investigated the stability of very shallow tunnelling. This chapter looks into several aspects of shallow overburden tunnelling and seeks the limits to C/D ratios when tunnelling in soft Holocene layers. Various geotechnical influences on the tunnel will be studied and the effects of a low C/D ratio will be modelled. In this study, it is assumed that infiltration influences are minimal, as these are not taken into account. This analysis is carried out with a number of ideal soil profiles which are derived from Amsterdam North-South metro line project (Gemeente-Amsterdam, 2009), consisting of a single soil type with most important properties as defined in Table 2.1, where γ is volumetric weight, φ is the friction angle, K is the initial coefficient of lateral earth pressure, c is cohesion, C_s is compression constant, C_{swel} is swelling constant, ν is Poisson's ratio and E_s is the stiffness modulus of the ground.

In this chapter, section 2.2 will investigate the failure of uplift and propose requirements of cover depth as well as the thickness of the tunnel lining. Section 2.3 will study recent failure models and investigate the wedge models to estimate the relationship between minimum required support pressures and C/D ratios. In section 2.4, the instability of tunnels due to blow-out will be studied and models to calculate the maximum required support pressures are proposed. Section 2.5 is the combination of all aspects on tunnel stability analysis in order to estimate the relation between required support pressures and C/D ratios. Conclusions of geotechnical analysis for tunnelling stability are pre-

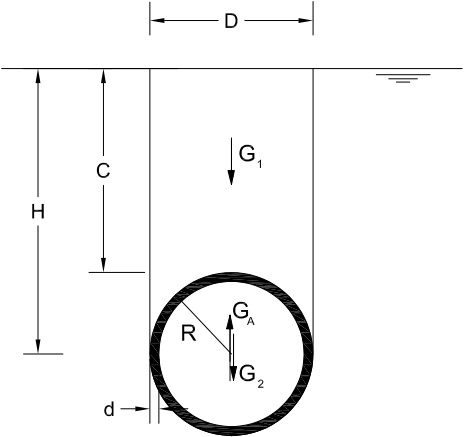


Figure 2.1: Uplift calculation

sented in Section 2.6.

2.2. UPLIFT

In tunnelling design, failure by uplift should be assessed as a permanent stability assessment. Uplift of bored tunnels is indicated in several studies such as Bakker (2000); NEN-EN 1997-1 (1997). In offshore industry, there are models of uplift stability for oil and gas pipeline are proposed by Trautmann et al. (1985); Ng and Springman (1994); White et al. (2001) which present various sliding blocks and inclined failure surfaces. In this study, the model with vertical slip surfaces (Figure 2.1) which has a diameter D soil volume above the circle tunnel is proposed for analysis. Assuming that the ground water level is at the surface, the tunnel is loaded by the following vertical forces: the weight of the tunnel G_2 , the weight of overlaying soil layers G_1 and the uplift force G_A . The uplift force G_A on the tunnel can be estimated according to the Archimedes's prin-

Table 2.1: Soil parameters used in design of Amsterdam North-South metro line project (Bosch and Broere, 2009; Gemeente-Amsterdam, 2009)

Soil type	$\gamma(kN/m^3)$	$\varphi(^{\circ})$	$K(-)$	$c(kN/m^2)$	$C_s(-)$	$C_{swel}(-)$	$v(-)$	$E_s(kN/m^2)$
Sand	20	35	0.5	-	-	-	0.2	20000
Clayey sand	17.9	35	0.4	2	-	-	0.2	12000
Clay	16.5	33	0.5	7	100	1000	0.15	10000
Organic clay	15.5	20	0.65	5	80	800	0.15	5000
Peat	10.5	20	0.65	5	25	250	0.15	2000

ciple as:

$$G_A = \gamma_w \frac{\pi}{4} D^2 \quad (2.1)$$

where γ_w is the volumetric weight of water and D is the diameter of the tunnel. The weight of the tunnel lining G_2 follows from:

$$G_2 \approx \pi \gamma_T D d \quad (2.2)$$

where d is the thickness of the tunnel lining and γ_T is the weight unit of the tunnel lining (concrete).

The weight of the soil layers above the tunnel G_1 is given by:

$$G_1 \geq DH\gamma' - \frac{\pi}{8} D^2 \gamma' \quad (2.3)$$

where γ' is the effective volumetric weight of soil.

In the construction phase, it is assumed that friction between the tunnel lining and surrounding ground is not included in the vertical equilibrium (lower boundaries). If the uplift force G_A is smaller than the total of tunnel weight and the upper soil layers weight, there will be no uplift of the tunnel (although safety factors have not been included here):

$$G_A \leq G_1 + G_2 \quad (2.4)$$

or

$$\frac{\pi}{4} \gamma_w D^2 \leq \pi \gamma_T D d + DH\gamma' - \frac{\pi}{8} D^2 \gamma' \quad (2.5)$$

Such that, the required depth of the tunnel can be calculated from:

$$H \geq \frac{\pi \gamma_w D + \frac{\pi}{2} \gamma' D - 4\pi \gamma_T d}{4\gamma'} \quad (2.6)$$

From Figure 2.1, the depth of tunnel overburden is:

$$C = H - \frac{D}{2} \quad (2.7)$$

From Equation 2.6, the minimum required ratio of C/D can be calculated as:

$$\left(\frac{C}{D}\right)_{min} = \frac{\pi \gamma_w}{4\gamma'} - \frac{\pi d \gamma_T}{D\gamma'} - \frac{1}{2} + \frac{\pi}{8} \quad (2.8)$$

Assuming the unit weight of tunnel lining $\gamma_T = 24 \text{ kN/m}^3$, the relation between the minimum required ratio of C/D and the unit weight of soil for the various thickness-to-diameter ratios of the tunnel segment d/D is shown in Figure 2.2. For example, for a reference tunnel in clayey sand ($\gamma = 17.9 \text{ kN/m}^3$) with $d/D = 1/20$, the minimum C/D ratio of 0.41 is found. For the case of $d/D = 1/10$, the cover $C = 0$ and therefore the ratio $C/D_{min} = 0$ when $\gamma' = 2.92 \text{ kN/m}^3$. This means that there is no risk of uplift when the cross section of the tunnel is designed with $d/D = 1/10$ or including ballast weight to a similar effect and the soil has a unit weight γ' more than 3 kN/m^3 .

Based on Equation 2.8, Figure 2.3 indicates the required ratio d/D and the minimum required ratio C/D in various soil types. In these conditions, the minimum ratios d/D avoiding the uplift are identified as in Table 2.2 in the case of a tunnel with $C/D = 0$. This shows that given enough ballast weight, the risk of uplift can be countered even in very soft soil conditions.

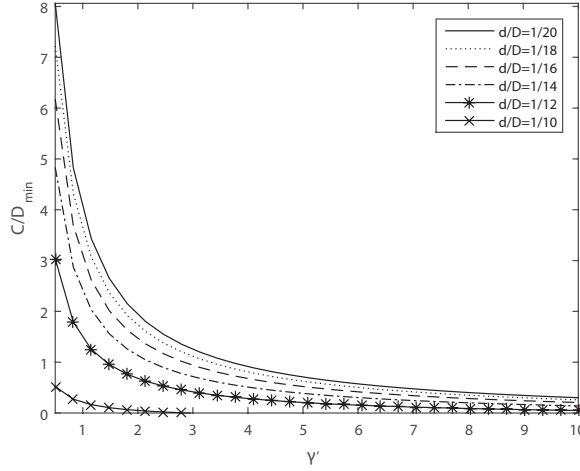


Figure 2.2: Relation between unit weight of soil and the minimum required ratio C/D

Table 2.2: Minimum required d/D

Soil type	$\gamma(kN/m^3)$	d/D
Sand	20	0.090
Clayey sand	17.9	0.093
Clay	16.5	0.095
Organic clay	15.5	0.096
Peat	10.5	0.103

2.3. FAILURE BODY MODELS

2.3.1. LITERATURE REVIEW CONCERNING STABILITY OF TUNNEL FACE

In order to evaluate the failure which is related to the stability of the tunnelling face, [Broms and Bennermark \(1967\)](#) proposed the first model which describes the vertical opening stability in an undrained cohesive (Tresca) material as can be seen in [Figure 2.4](#). Their study was carried out by theoretical analysis and experiment observations. The stability of the tunnelling face is assessed by the stability ratio N , as follows:

$$N = \frac{q_s - s}{c_u} + \frac{\gamma}{c_u} \left(C + \frac{D}{2} \right) \quad (2.9)$$

where q_s is the surface load, C is the overburden, D is the tunnel diameter, c_u is the undrained shear strength of the ground and s is the support pressure. From the laboratory test data and observations of tunnels and pipes constructed in soft clay, the opening face is stable when N is less than 6.

From [Equation 2.9](#), the minimum support pressure s_{min} for the tunnelling face can be given by:

$$s_{min} = \gamma \left(C + \frac{D}{2} \right) + q_s - N c_u \quad (2.10)$$

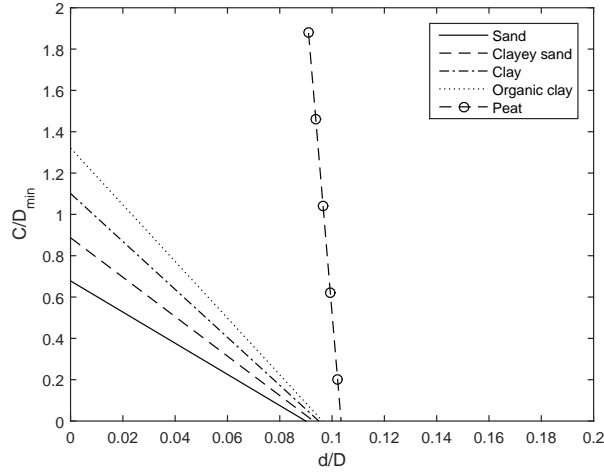


Figure 2.3: Relation between ratio of d/D and the minimum required ratio C/D

2

Davis et al. (1980) investigated the stability of two dimensional idealization of a partial unlined tunnel heading in Tresca material as can be seen in the Figure 2.5 where P is the distance between the face and the provided support point. Three different mechanisms of a shallow tunnel are derived for collapse under undrained conditions. In this study, the vertical opening theory which was presented by Broms and Bennermark (1967) is used as one of three limit cases.

The influence of the C/D ratio on the stability of the tunnel in the study of Davis et al. (1980) is shown in Figure 2.6 with the different values of $\gamma D/c_u$ ratio for upper and lower boundaries. For the values of C/D ratio higher than 3, the values of lower and upper bounds do not change with the $\gamma D/c_u$ ratio. The authors also showed that a blow-out will be a problem in the case of a very shallow tunnel and the failure mechanism is usually close to the optimum upper bound mechanism.

In their analysis of the stability of the tunnelling face (when $P = 0$), Davis et al. (1980) also derived the lower boundary of the stability ratio N for two cases of cylindrical and spherical stress fields as:

$$N_{TC} = 2 + 2\ln\left(\frac{2C}{D} + 1\right) \quad (2.11)$$

$$N_{TC} = 4\ln\left(\frac{2C}{D} + 1\right) \quad (2.12)$$

These results agree with the values of the critical stability ratio N_{TC} in laboratory and centrifuge tests from the study of Kimura and Mair (1981) on tunnel heading failures in undrained conditions (Figure 2.7).

Atkinson and Potts (1977) investigated the stability for a circular tunnel in cohesionless soil by means of theoretical and experimental methods. Their study based on a upper boundary by selecting any kinematic collapse mechanism and a statically admissible

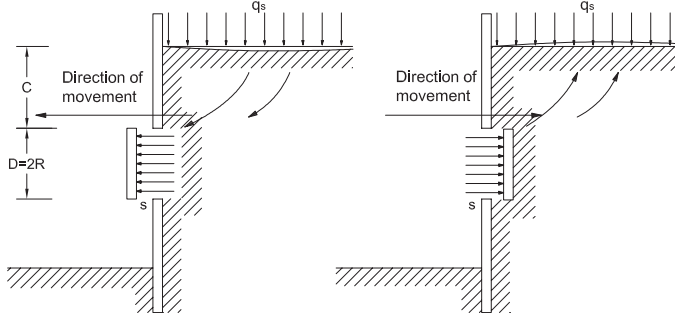


Figure 2.4: Unsupported opening in vertical hold (Broms and Bennermark, 1967)

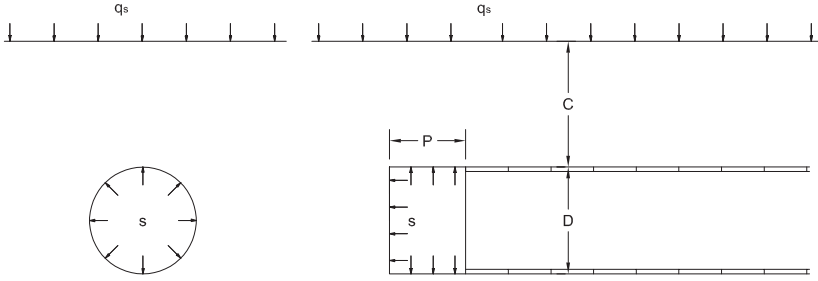


Figure 2.5: A tunnelling model in Davis et al. (1980)

lower boundary on a plane strain model is shown in Figure 2.8. The boundary of the dimensionless $s/\gamma D$ ratio is shown in Figure 2.9 in the case of $\varphi = 35^\circ$. The results of their experiments agree with the theoretical analysis. Figure 2.9 also shows that the boundaries of the support pressures are independent of the C/D ratio. The minimal support pressure is estimated by the lower boundary conditions, as follows:

$$s_{min} = \frac{\mu}{\mu^2 - 1} \gamma D \quad (2.13)$$

where:

$$\mu = \frac{1 + \sin \varphi}{1 - \sin \varphi} \quad (2.14)$$

and φ is the maximum angle of shearing resistance.

Based on the upper boundary conditions, the maximum support pressure is given by:

$$s_{max} = \frac{\gamma D}{4 \cos \varphi} \left(\frac{1}{\tan \varphi} + \varphi - \frac{\pi}{2} \right) \quad (2.15)$$

In order to investigate the stability of the tunnelling face in cohesive and frictional soils,

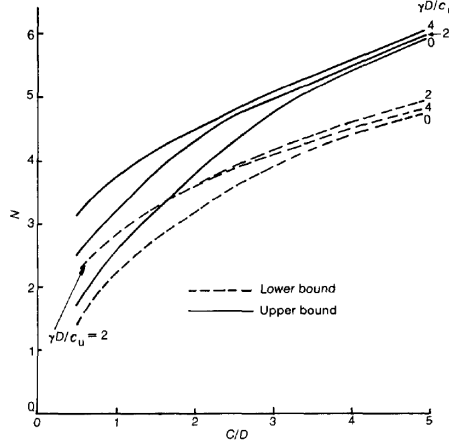


Figure 2.6: Upper and lower bound stability ratios for a plane strain unlined tunnel (Davis et al., 1980)

2

Leca and Dormieux (1990) proposed a stability criterion for the tunnelling face based on the movement of rigid conical blocks with circular cross-sections (Figure 2.10). The maximum and minimum support pressures are derived from three upper boundary solutions (Figure 2.11). Their results presented in Figure 2.9 show that the support pressures from the upper boundary conditions are independent of the C/D ratio. The support pressures are derived from these failure mechanisms as following:

$$s = N_s q_s + N_\gamma \gamma D \quad (2.16)$$

where N_s and N_γ are weighting coefficients that depend on the angle α between the axis of the cone adjacent to the tunnel and the horizontal axis. The minimum or maximum support pressures depend on the choice of the value of N_s and N_γ .

The results of this criterion were also compared to the experimental results of centrifuge tests. There is a reasonable agreement between the results of theoretical calculation and of the centrifuge tests by Chambon and Corté (1994). This comparison shows that the support pressures from the upper boundary solutions are closer to the real pressures at failure than the support pressures calculated by the lower boundary solutions. The authors also concluded that the face stability has little effect from the surcharge q_s except for very shallow tunnels and the failure zone in front of the tunnelling face has the extent smaller than a long open cut.

Mollon et al. (2009a) presented a failure mechanism to determine the critical collapse pressures of a pressurized tunnel face based on the kinematic approach of limit analysis theory. It is a three dimensional multiblock mechanism that improves from the solution of Leca and Dormieux (1990) (Figure 2.12). The support pressure is estimated as:

$$s = \gamma D N_\gamma + q_s N_s - c N_c \quad (2.17)$$

where N_γ , N_s and N_c are dimensionless coefficients depending on the size and shape of the mechanism. Their results were compared to and well agreed with the other kine-

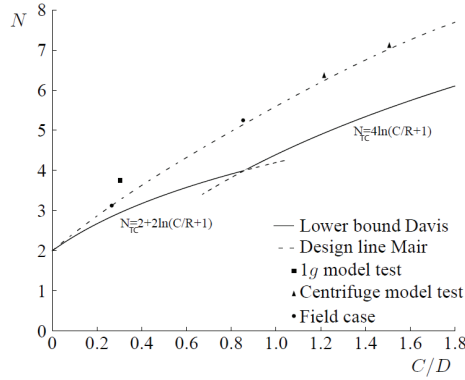


Figure 2.7: Critical stability ratio for lined tunnels (Mair and Taylor, 1999)

matic and static approaches as shown in Figure 2.13 for the load factor and the collapse pressure but there is still a considerable difference between the results of centrifuge tests and their results in the case of a purely cohesive soil.

2

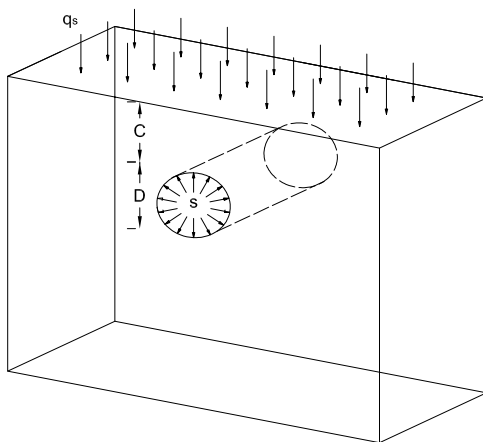
2.3.2. WEDGE STABILITY MODEL

The support pressure at the tunnelling face must be higher than or at least equal to the total of water pressure and horizontal effective soil pressure to avoid collapse. The minimum required support pressure is estimated on the basis of this equilibrium condition. Over the years, many studies have been carried out to determine the minimum required support pressure. In 1961, Horn developed the first kinematic model including a soil wedge column based upon the silo theory to assess the stability of the tunnelling face. This model consists of a wedge and overlying prismatic body (Figure 2.14).

Anagnostou and Kovári (1994) developed Horn's wedge model using the silo theory of Janssen in drained condition (Figure 2.15). In this model, the vertical surcharge pressure σ'_v acting on the wedge can be reduced by the shear stresses on the sliding surface. From the computational analysis, the effects of the shear strength parameter of the ground, the permeability and the dynamic viscosity of the suspension were taken into account in stability assessments. It was concluded that the effectiveness of slurry support depends on the infiltration distance of suspension into the ground. However, these models only deal with the case of homogeneous soil.

Jancsecz and Steiner (1994) proposed a three-dimensional model that takes into account the effects of soil arching above the tunnelling face as can be seen in Figure 2.16. The three-dimensional effect is shown in this model by the three-dimensional earth pressure coefficient K_{A3} in calculation relating to the support pressure for the stability of the tunnelling face. In this study, the minimum required support pressure can be calculated as:

$$s_{min} = \sigma'_h + p = K_{A3} \cdot \sigma'_v + p \quad (2.18)$$



2

Figure 2.8: Model test of Atkinson and Potts (1977).

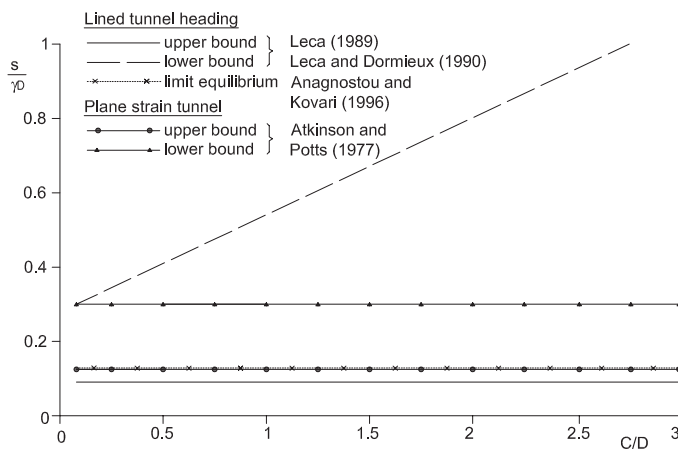


Figure 2.9: Upper and lower bounds of the support pressure for lined ($P = 0$) and unlined tunnels ($P = \infty$) (Mair and Taylor, 1999)

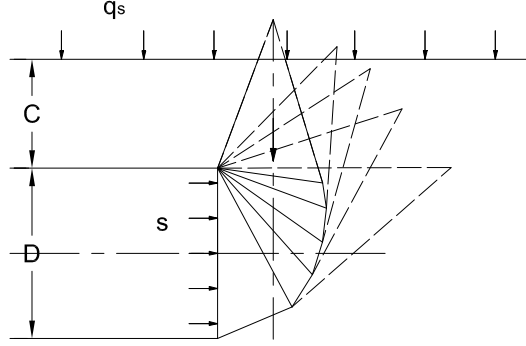


Figure 2.12: Multiblock failure mechanism by Mollon et al. (2009b)

2

In the case of surface loading $q_0 = 0 \text{ kN/m}^2$, the effective horizontal stress can be calculated as:

$$\sigma'_{h,a} = \sigma'_{v,a} K = \frac{a\gamma' - c'}{\tan\phi'} \left(1 - e^{-K \tan\phi' \frac{z}{a}} \right) \quad (2.22)$$

According to Broere (2001), three possible relaxation length a values can be estimated based on the applied wedge model:

- Without arching effect: $a = \infty$;
- With two dimensional arching effect: $a = R$;
- With three dimensional arching: $a = R \frac{1}{1 + \tan\theta}$, where θ is estimated in Jancsecz and Steiner (1994).

Three possible ways of vertical and horizontal stress distribution along the wedge body were also proposed by Broere (2001) as can be seen in Figure 2.18. The line 1 and 2 show the horizontal stress distribution in the case of without and with arching effect. The dashed line 3 presents the assumed linear distribution with the stress including arching effect at the top of the tunnel and the stress without arching effect at the bottom of the tunnel.

By comparing the results of centrifuge tests and different models with and without arching effect, Broere (2001) indicated that the model with three dimensional arching effect with coefficient of neutral horizontal effective stress K_0 is the best model to determine the minimal required support pressure in the case of a shallow tunnel. This model is applied in this study for calculating the minimum support pressure for the tunnel in varied soil parameters.

Figure 2.19 shows the relation between the effective horizontal pressures σ'_h and the C/D ratio based on Equation 2.22 for various tunnel diameters D in varied soil types. For instance, for a reference tunnel with $D = 6 \text{ m}$ in clayey sand and $C/D = 0.41$, a minimum support pressure $\sigma'_h = 3.84 (\text{kN/m}^2)$ is found. It shows that the larger the tunnel diam-

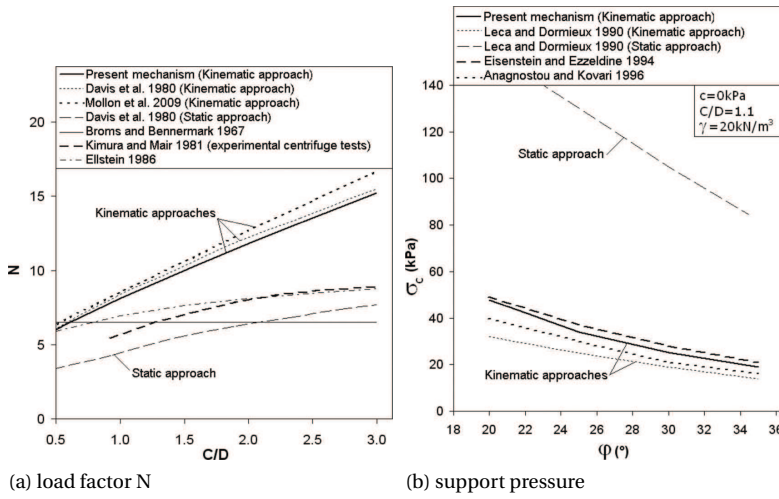


Figure 2.13: Comparison load factor N and support pressures between kinematic and static approaches (Molton et al., 2010)

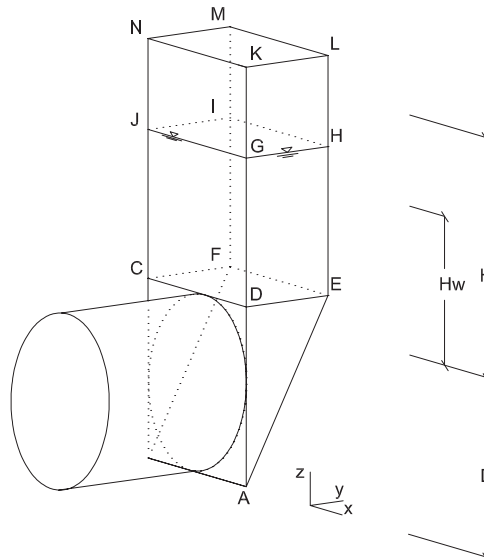


Figure 2.14: Sliding mechanism (after Horn 1961)

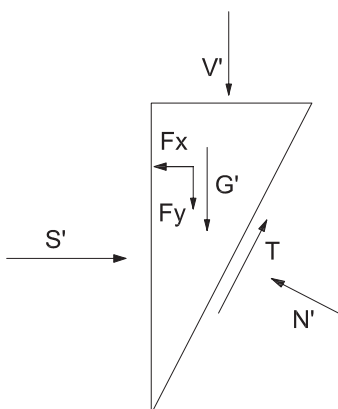


Figure 2.15: Force model according to Anagnostou and Kovári (Maidl, 2012)

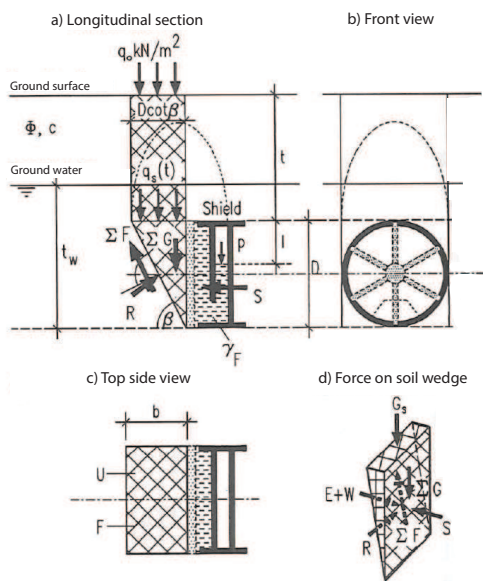


Figure 2.16: Three dimensional limit equilibrium model (Jancsecz and Steiner, 1994)

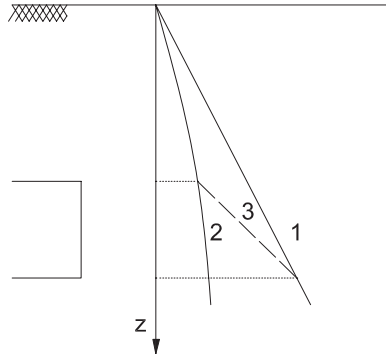


Figure 2.18: Three possible distribution of horizontal stress along the wedge sides (Broere, 2001)

2

pear between the soil column and the surrounding ground. In a more accurate blow-out model, this shear stress should be taken into account. In the equilibrium condition (Figure 2.21), the support force is at least equal to the total of the weight of the above soil column and the shear forces along two vertical sides of the two dimensional rectangular soil body. Based on this, the maximum support pressure for the tunnel face can be estimated as (excluding safety factors):

$$s_{max} = C \left(\gamma + \frac{2c + CK_y \gamma' \tan \varphi}{D} \right) \quad (2.24)$$

where K_y is the coefficient of horizontal effective stress.

In the model proposed by Balthaus (1991) (Figure 2.22), the up-lift soil body is modelled as a wedge shape, which is pushed upward when blow-out occurs. By balancing the wedge soil body weight G and the support force S , the maximum support pressure can be estimated. Safety indexes against the blow out were presented:

$$\eta = \frac{G}{S} > \eta_1 = \frac{\gamma C (B' + C \cot(45^\circ + \varphi/2))}{B' s(z_t)} > \eta_2 = \frac{\gamma C}{s(z_t)} \quad (2.25)$$

Because Balthaus's model activates a large soil body above the tunnel, the calculated result is somewhat exaggerated. Meanwhile, Broere's model (Figure 2.21) is probably too conservative. In practical tunnelling, the support pressure at the tunnelling face often changes along the vertical axis. In shallow tunnels, the difference between the required support pressures at the top and the bottom of the tunnel is large. This study proposes below new blow-out models in order to take this change into account with uniform support pressures and linear support pressures in which the effect of grouting flows is included.

In the model in Figure 2.23, the support pressure s is uniformly distributed on the perimeter of the tunnel section at the upper and lower part of the tunnel. The maximum allowable support pressure is estimated in the upper part of the tunnel in which the soil body

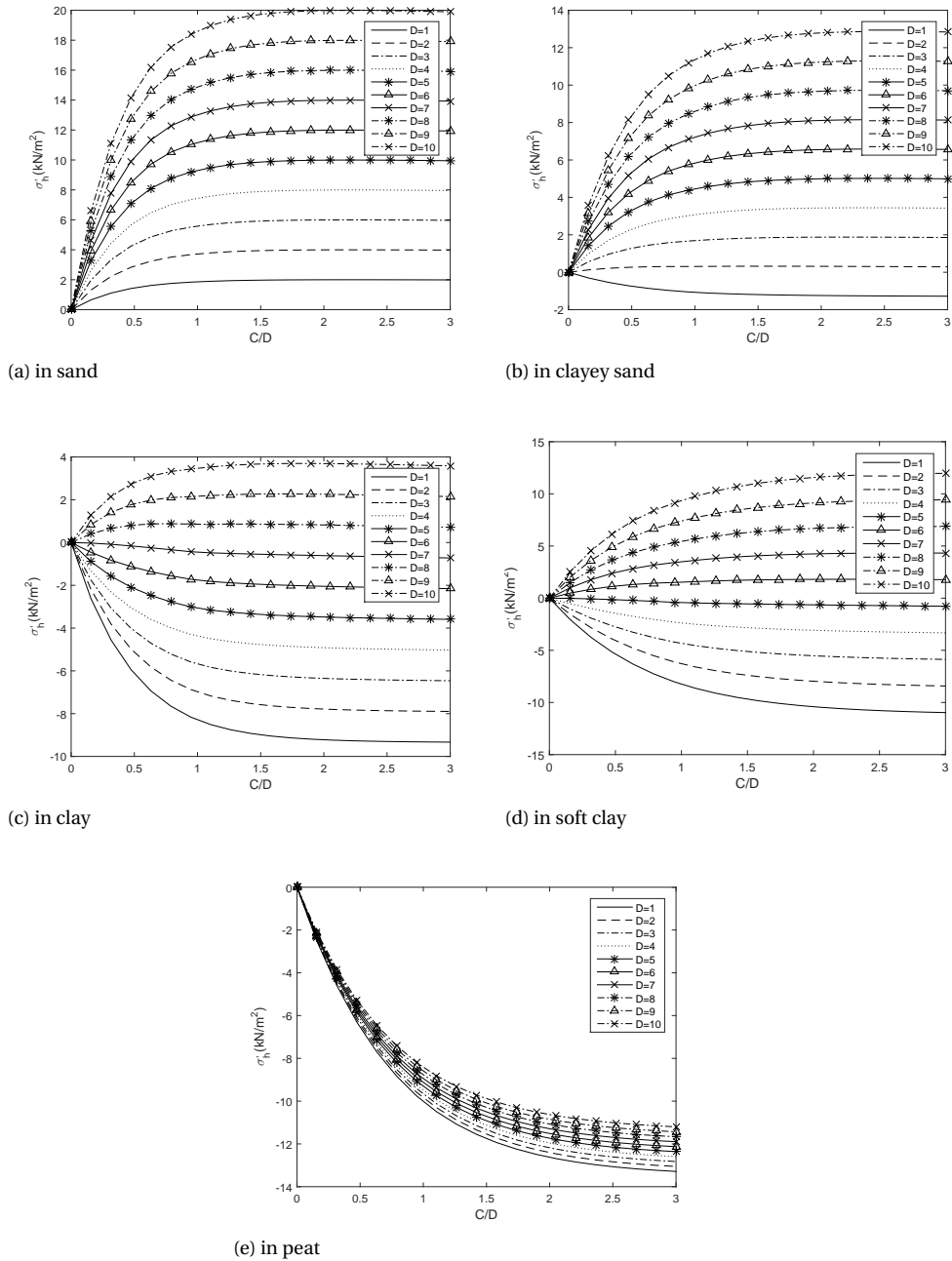
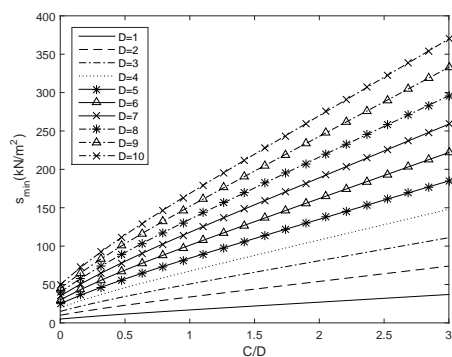
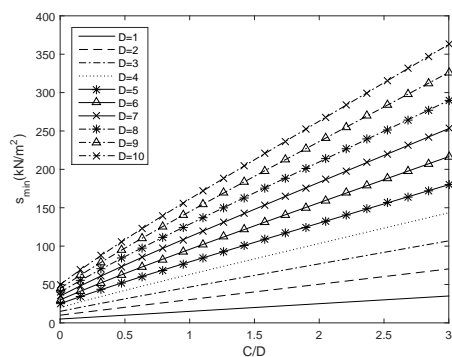


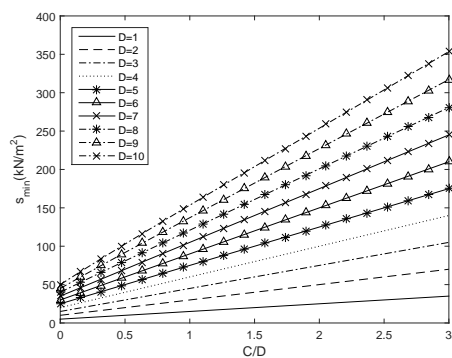
Figure 2.19: Relationship between C/D ratio and horizontal stress σ'_h with varied tunnel diameter D



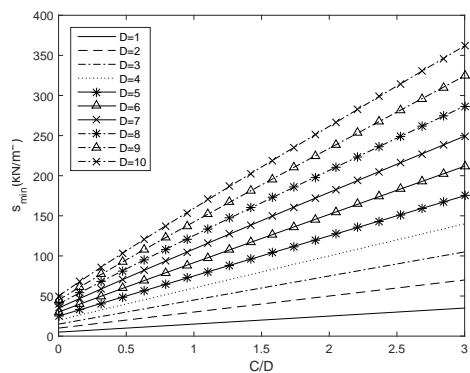
(a) in sand



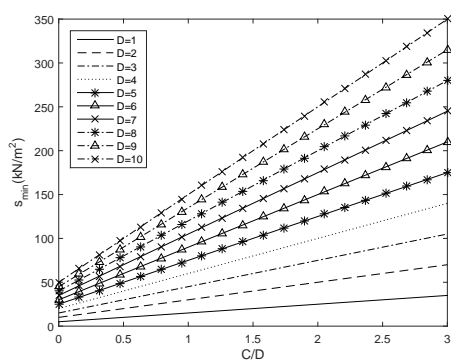
(b) in clayey sand



(c) in clay



(d) in organic clay



(e) in peat

Figure 2.20: Relationship between C/D ratio and minimum support pressures with various tunnel diameter D

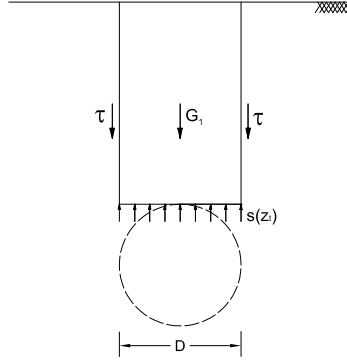


Figure 2.21: Blow-out model including friction at boundaries (Broere, 2001)

and the shear are taken into account, as follows (see Appendix A):

$$s_{t,max} = \gamma \left(H - \frac{\pi}{8} D \right) + 2 \frac{H}{D} \left(c + \frac{1}{2} H K_y \gamma' \tan \varphi \right) \quad (2.26)$$

where $H = C + \frac{D}{2}$.

It can be written as:

$$s_{t,max} = \left(\frac{C}{D} + \frac{1}{2} \right)^2 2 D K_y \gamma' \tan \varphi + \left(\frac{C}{D} + \frac{1}{2} \right) (\gamma D + 2c) - \frac{\pi}{8} \gamma D \quad (2.27)$$

For the lower part of the tunnel, the tunnel weight is taken into account. The allowable grouting pressure which is shown in Figure 2.23b, can be estimated as following equation (see Appendix A):

$$s_{b,max} = \gamma \left(H - \frac{\pi}{8} D \right) + 2 \frac{H}{D} \left(c + \frac{1}{2} H K_y \gamma' \tan \varphi \right) + \gamma_T \pi d \quad (2.28)$$

Or

$$s_{b,max} = \left(\frac{C}{D} + \frac{1}{2} \right)^2 2 D K_y \gamma' \tan \varphi + \left(\frac{C}{D} + \frac{1}{2} \right) (\gamma D + 2c) + \gamma_T \pi d - \frac{\pi}{8} \gamma D \quad (2.29)$$

Figure 2.24 presents the relationship between the maximum support pressure $s_{t,max}$ and $s_{b,max}$ at upper and lower part of the tunnel and the C/D ratio in the range of tunnel diameter D from 1 meter to 10 meters. This figure shows that the higher the ratio of C/D is, the larger the maximum support pressures are.

The in-situ data (Talmon and Bezuijen, 2005; Bezuijen and Talmon, 2005b) and experimental data (Bezuijen et al., 2006) show that the grouting pressure gradient directly behind the TBM is nearly 20 kPa/m at the start of grouting and at the end of the registration is about 7 kPa/m in monitoring. This reduction of the grouting pressure is related to the consolidation and bleeding of the grout (Bezuijen and Talmon, 2005a). The grout around

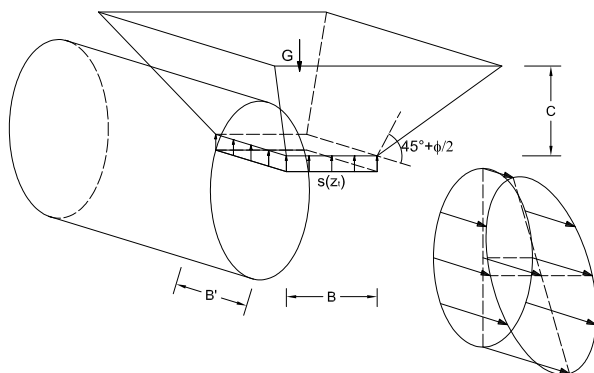


Figure 2.22: Calculation model of Balthaus for the safety against blow-out (Balthaus, 1991)

the tunnel is assumed to behave as a Bingham liquid which has a viscosity and a yield stress. This liquid has a downward movement when more grout is injected through the upper injection points of the TBM. This downward flow creates a driving force larger than the yield stress. The pressure gradient, therefore, is smaller than the gradient estimated from the density. To be more accurate with the in-situ data, the gradient of the grouting movement in the tail void should be taken into account in blow-out analysis. According to [Bezuijen and Talmon \(2008\)](#), the maximum pressure gradient δ_p is given by:

$$\delta_p = \frac{dP}{dz} = \rho_{gr} g - 2 \frac{\tau_y}{d_{gr}} \quad (2.30)$$

where ρ_{gr} is the density of the grout, g is the acceleration gravity, τ_y is the shear strength of the grout, and d_{gr} is the width of the tail void gap between the tunnel and the surrounding ground.

Figure 2.25 shows the blow-out model including a vertical pressure gradient δp . The support pressure in the upper part of the tunnel section in Figure 2.25a is given by:

$$s = s_{0,t} + \delta_p R \cos \varphi \quad (2.31)$$

where $s_{0,t}$ is the support pressure at the top of the tunnelling face.

The maximum support pressure at the top of the tunnelling face is given by (see Appendix A):

$$s_{0,t,max} = \gamma \left(H - \frac{\pi}{8} D \right) + 2 \frac{H}{D} \left(c + \frac{1}{2} HK_y \gamma' \tan \varphi \right) - \frac{\delta_p D}{4} \quad (2.32)$$

or

$$s_{0,t,max} = \left(\frac{C}{D} + \frac{1}{2}\right)^2 2DK_Y \gamma' \tan\varphi + \left(\frac{C}{D} + \frac{1}{2}\right)(\gamma D + 2c) - \frac{\pi}{8}\gamma D - \frac{\delta_p D}{4} \quad (2.33)$$

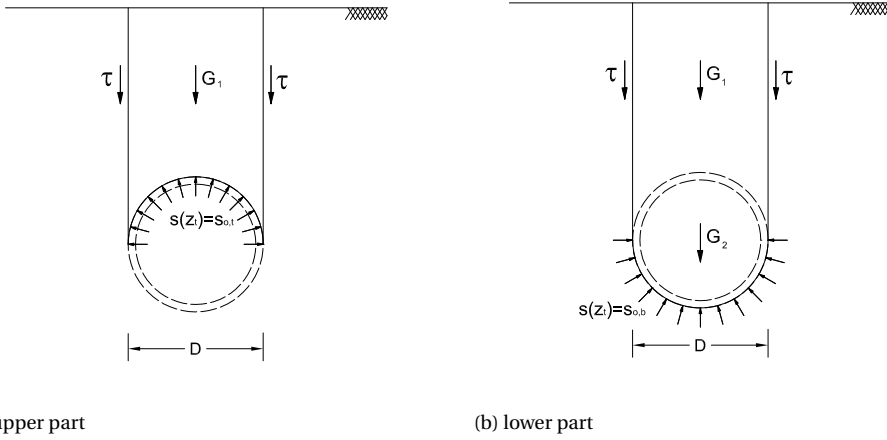


Figure 2.23: Blow-out model with uniform support pressure

In the lower part as can be seen in Figure 2.25b, the support pressure in the upper part of the tunnel section is given by:

$$s = s_{0,b} - \delta_p R \cos \varphi \quad (2.34)$$

where $s_{0,b}$ is the support pressure at the bottom of the tunnelling face.

The maximum support pressure at the bottom of the tunnelling face is given by (see Appendix A):

$$s_{0,b,max} = \gamma \left(H - \frac{\pi}{8} D \right) + 2 \frac{H}{D} \left(c + \frac{1}{2} HK_y \gamma' \tan \varphi \right) + \gamma_T \pi d + \frac{\delta_p D}{4} \quad (2.35)$$

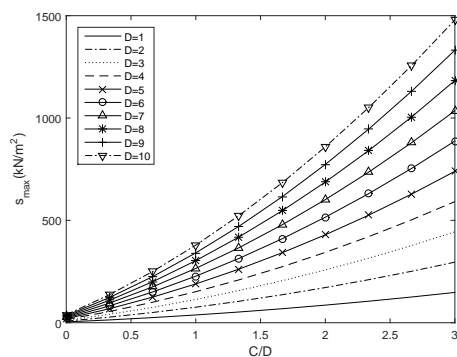
or

$$s_{0,b,max} = \left(\frac{C}{D} + \frac{1}{2} \right)^2 2DK_y \gamma' \tan \varphi + \left(\frac{C}{D} + \frac{1}{2} \right) (\gamma D + 2c) + \gamma_T \pi d - \frac{\pi}{8} \gamma D + \frac{\delta_p D}{4} \quad (2.36)$$

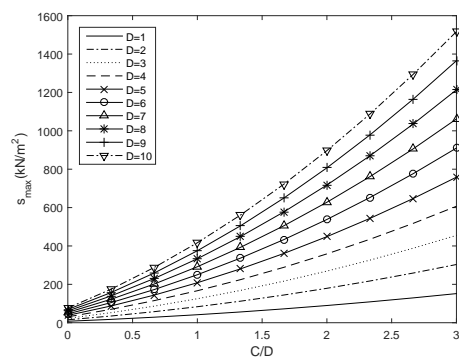
From Equation 2.33 and 2.36, the maximum support pressures can be estimated depending on the C/D ratio in the case of linearly distributed support pressures. It is assumed that the unit weight of tunnel is $\gamma_T = 24 \text{ kN/m}^3$ and the vertical gradient of the grout $a = 7 \text{ kPa/m}$. For example, for a reference tunnel with $D = 6 \text{ m}$ and $C/D = 0.41$ in clayey sand, the maximum support pressures are $s_{t,max} = 81,34 (\text{kN/m}^2)$, $s_{b,max} = 103,96 (\text{kN/m}^2)$, $s_{0,t,max} = 70,84 (\text{kN/m}^2)$ and $s_{0,b,max} = 114,46 (\text{kN/m}^2)$.

The relationship between the maximum support pressures at the upper and lower parts of the tunnel $s_{0,t,max}$ and the C/D ratio is shown in Figure 2.26 for tunnels with the diameter D from 1 meter to 10 meters in varied soil. The conclusion reached when analysing the relationship between the maximum support pressures and the C/D ratio is that the higher the ratio of C/D is, the larger the maximum support pressures are.

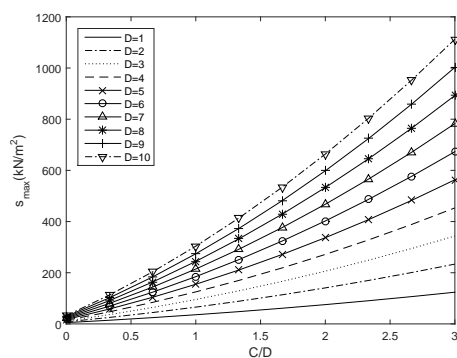
In order to evaluate the new blow-out models, the blow-out case of the Second Heinen-



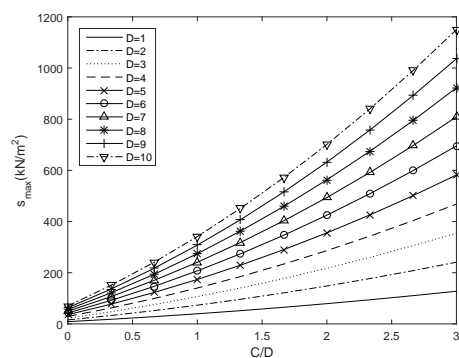
(a) in sand-upper part



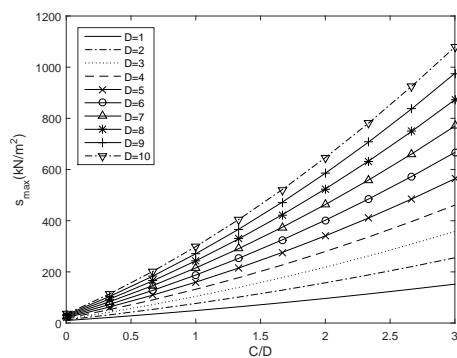
(b) in sand-lower part



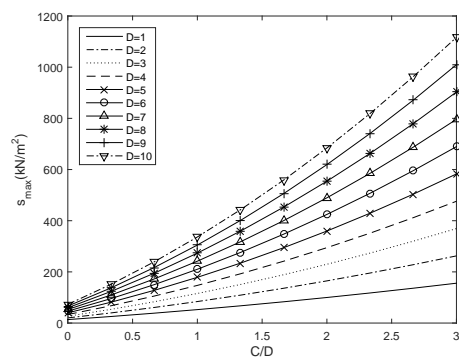
(c) in clayey sand-upper part



(d) in clayey sand-lower part

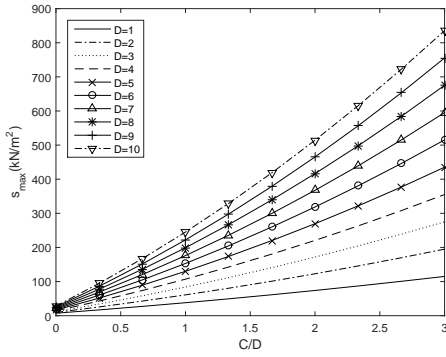


(e) in clay-upper part

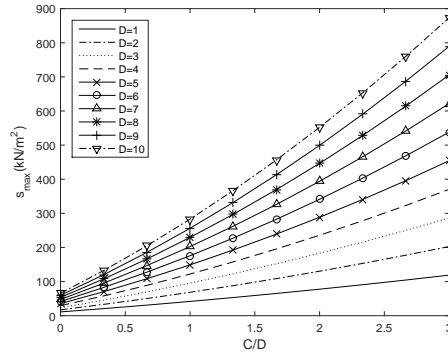


(f) in clay-lower part

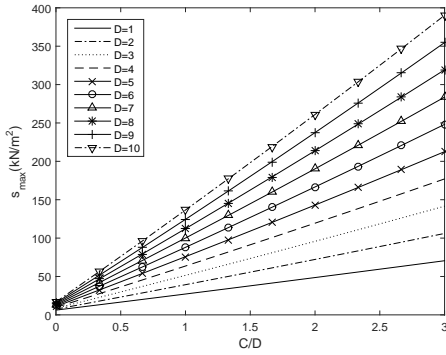
Figure 2.24: Maximum allowable support pressures at upper and lower part of the tunnel with uniform support pressures according to Equations 2.27 and 2.29 (continue in next page)



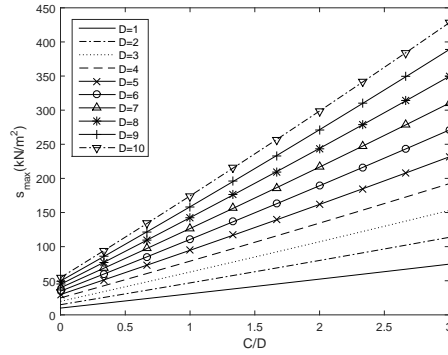
(g) in organic clay-upper part



(h) in organic clay-lower part



(i) in peat-upper part



(j) in peat-lower part

Figure 2.24: Maximum allowable support pressures at upper and lower part of the tunnel with uniform support pressures according to Equations 2.27 and 2.29

noord Tunnel in the Netherlands (Figure 2.27a) is used. A tunnel with an outer diameter of $8.3m$ was constructed below the Oude Maas river in the neighborhood of Rotterdam between 1996 and 1999. At the blow-out position, the tunnel is covered by $4m$ of Pleistocene sand with a friction angle of 36.5° . The cover depth of the tunnel is $8.6m$ in total including this sand layer and there was $11m$ of water above the soil (Bezuijen and Brassinga, 2006). Figure 2.27b shows the face pressures measured at the tunnel centre when the blow-out happened. During the blow-out, face pressure measured at the top of the tunnel was $405kPa$ and at the center of the tunnel was $450kPa$.

Figure 2.28 shows the maximum support pressures calculated with the new blow-out model, Broere's model (Figure 2.21) and Balhaus's model (Figure 2.22) for the case of the blow-out position in the Second Heinenoord Tunnel. It can be seen that the maximum support pressures at the top and the bottom of the tunnel derived from the new blow-out models are in between the maximum support pressures calculated by Balhaus's model and Broere's model. Also, the measured face pressures at the top and the center of the

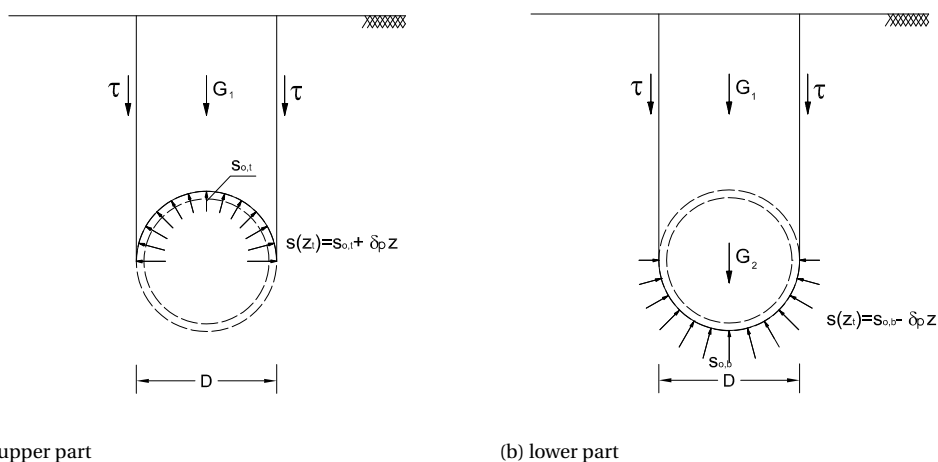


Figure 2.25: Blow-out model with vertical support pressure gradient δp

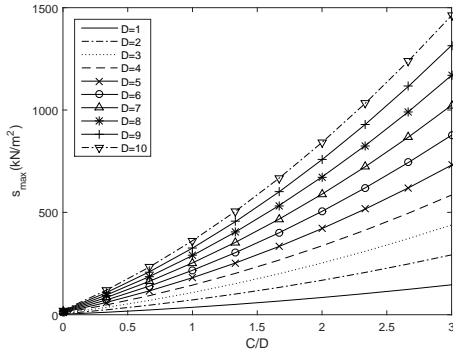
Table 2.3: Soil parameters used in centrifuge tests (Bezuïjen and Brassinga, 2006)

Soil parameters	Speswhite clay	Sand med. dens.
$\gamma_{wet} (kN/m^3)$	17	19.6
$c (kPa)$	1	8.3
Friction angle (deg.)	23	37
Dilatancy angle (deg.)	-	9
Poisson's ratio (-)	0.45	0.3
$E_{50} (MPa)$	0.53	0.4
$n (-)$	-	0.394

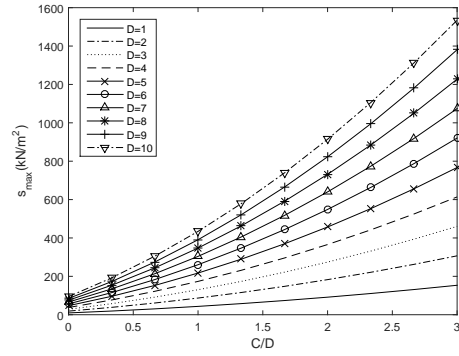
Second Heinenoord Tunnels at the blow-out position where $C/D \approx 1$ are plotted. It shows that the measured blow-out face pressures are in the range of calculated maximum support pressures with the new blow-out model for the lower and upper parts of the tunnel. The result also confirms the above statement that the maximum support pressure derived by Balhaus's model is somewhat exaggerated whereas this pressure estimate is too conservative when using Broere's model.

In order to validate with experimental data, centrifuge tests performed by GeoDelft and supervised by COB in order to investigate the grouting process (Brassinga and Bezuïjen, 2002) are used to compare to the analysis results derived from the new models, Balhaus's model and Broere's model. These centrifuge tests were carried out with a tube representing a tunnel lining which has an outer diameter of 130mm and an inner diameter of 125mm as can be seen in Figure 2.29. The 25mm tail void in this model was directly filled by a bentonite slurry. The bentonite pressure was increased until the blow-out occurred in order to measure the maximum support pressures. The soil parameters used in these centrifuge tests are shown in Table 2.3. The maximum grouting pressures measured in these centrifuge tests are shown in Figure 2.30.

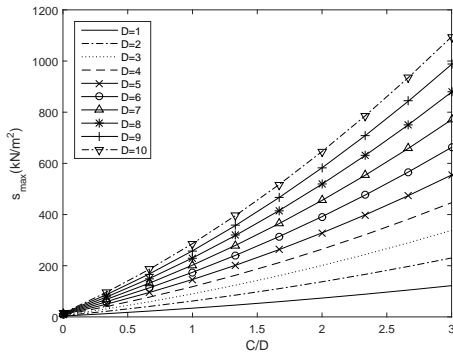
The first centrifuge experiment was carried out with a tunnel covered by sand and at



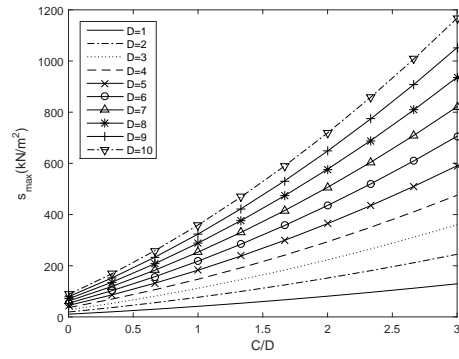
(a) in sand-upper part



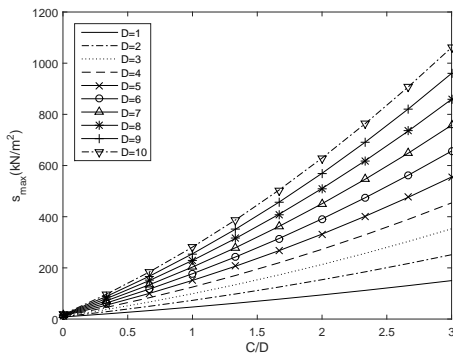
(b) in sand-lower part



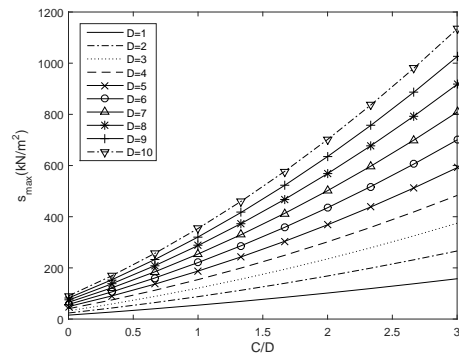
(c) in clayey sand-upper part



(d) in clayey sand-lower part

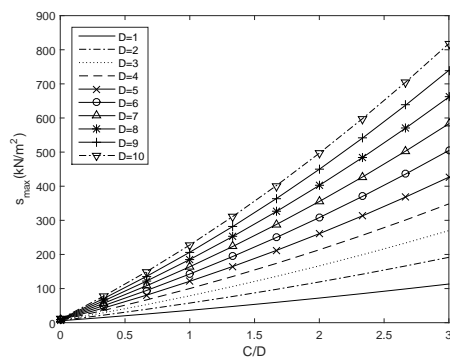


(e) in clay-upper part

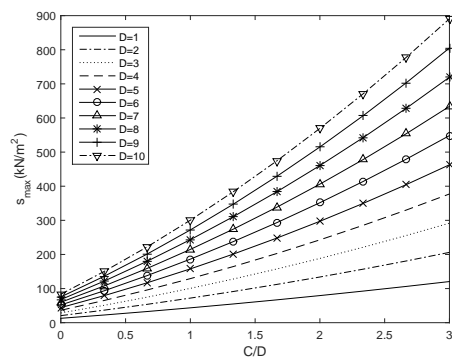


(f) in clay-lower part

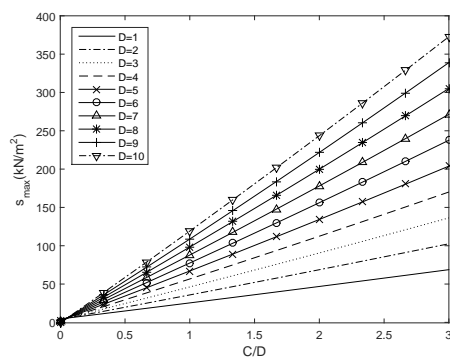
Figure 2.26: Maximum allowable support pressures at upper and lower part of the tunnel with linear support pressures according to Equations 2.33 and 2.36(continue in next page)



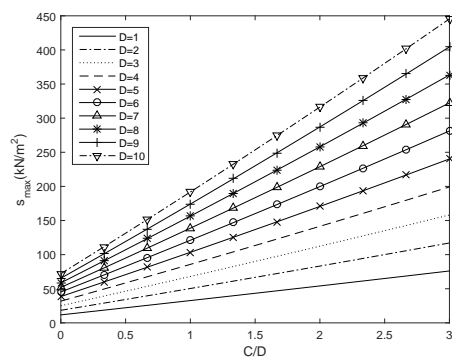
(g) in organic clay-upper part



(h) in organic clay-lower part



(i) in peat-upper part



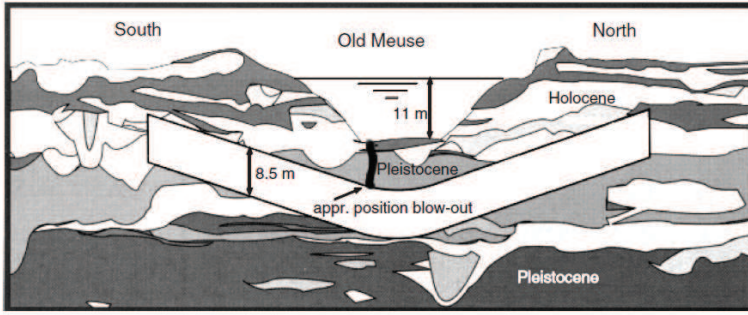
(j) in peat-lower part

Figure 2.26: Maximum allowable support pressures at upper and lower part of the tunnel with linear support pressures according to Equations 2.33 and 2.36

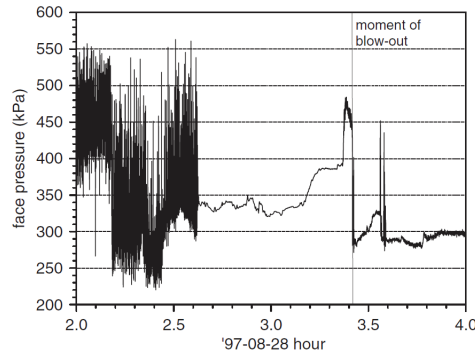
150g. This centrifuge test represented a large tunnel with a diameter of $18.75m$, the tube was covered by $0.2m$ saturated sand with the parameters as shown in Table 2.3. The maximum excess bentonite pressure was measured as $620kPa$.

The second and third tests were carried out at 40g and represented a tunnel with diameter $D = 5m$ covered by sand and clay. There was a sand layer of $77.5mm$ above the tunnel. A clay layer of $170mm$ is above this sand layer and $5mm$ sand layer is on the top. The water level is at the top of the $5mm$ sand layer. The result in the second centrifuge test shows that failure was reached at a pressure of $190kPa$. In the third centrifuge experiment with the same condition as the second test, the measured maximum excess bentonite pressure was of $215kPa$.

Figure 2.31 shows a comparison between the analytical results derived from the new models, Balhaus's model and Broere's model for these centrifuge test results. This figure also shows that the value of maximum support pressure derived by the new model is in between Balhaus's model and Broere's model with the soil conditions used in these cen-



(a) Scheme of the Second Heinenoord Tunnel and the blow-out position



(b) Face support pressure measurement at the tunnel centre during blow-out

Figure 2.27: Blow-out at the Second Heneinoord Tunnel (Bezuijen and Brassinga, 2006)

trifuge tests. It can be seen that the measured maximum support pressures in these centrifuge tests are approximately the maximum pressure calculated from the new models, while the maximum support pressure derived from Balthaus's model is larger and the results from Broere's model are smaller in comparison in these case. These results indicate that a more accurate result can be reached when applying the new model to maximum support pressure calculation.

2.5. COMBINATION ANALYSIS

In order to analyse the effects of the C/D ratio on the required support pressures, the uplift, blow-out and wedge stability models are combined with safety indexes for the cases of tunnels in sand, clayey sand, clay, organic clay and peat. The following safety indexes are used in calculating: $\eta_{blow-out} = 1.1$ for blow-out; $\eta_{uplift} = 1$ for uplift, $\eta_{porepressure} = 1$ for pore pressure, and $\eta_{\sigma'_h} = 1.5$ for effective horizontal pressures, in line with Broere (2001).

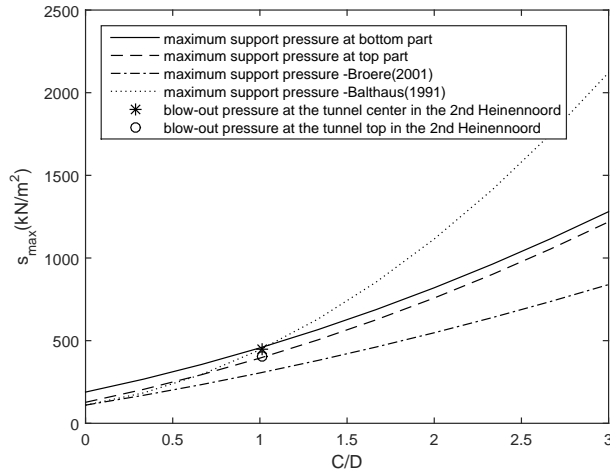
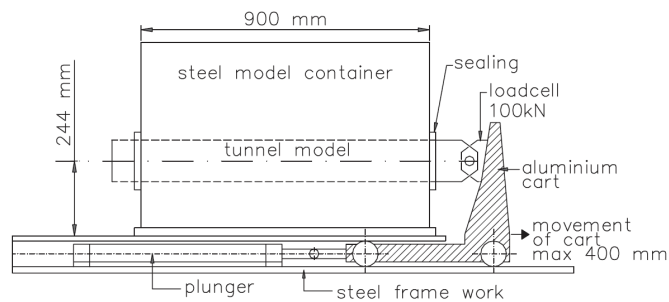
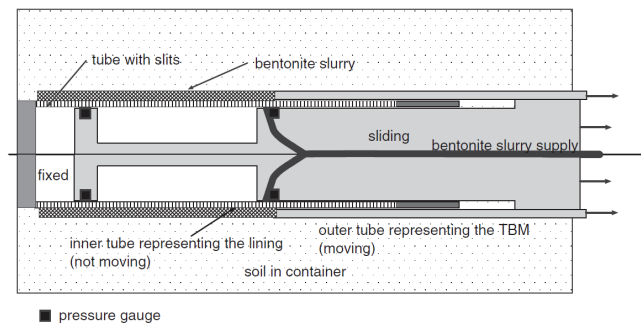


Figure 2.28: A comparison of maximum support pressures calculated from new blow-out models, Broere's model, Balhaus's model and in the Second Heinennoord Tunnel case



(a) Side view



(b) Sketch of the module made to simulate the grouting process

Figure 2.29: Sketch of centrifuge tests in Bezuijen and Brassinga (2006)

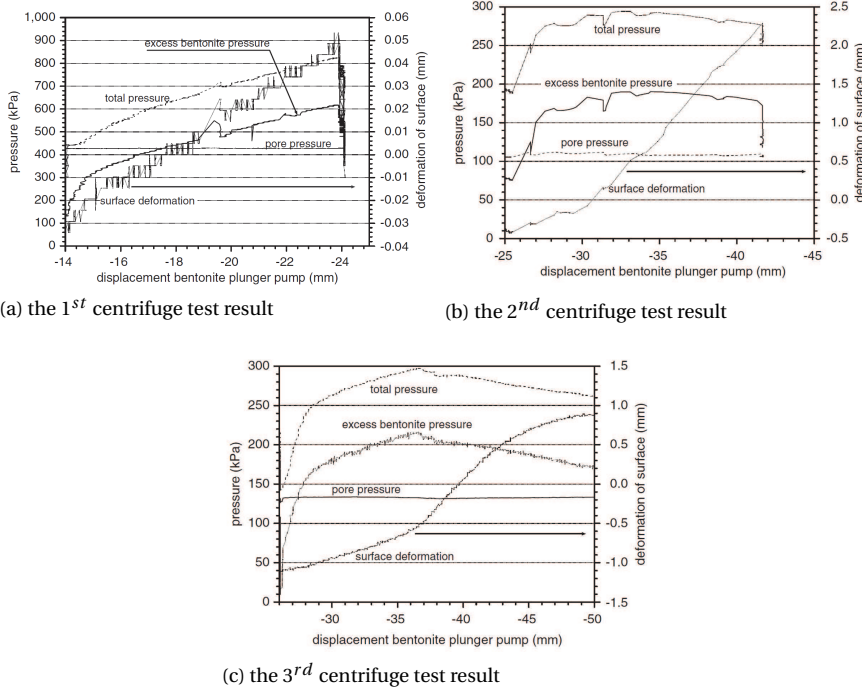


Figure 2.30: Measured pressures in centrifuge tests in [Bezuijen and Brassinga \(2006\)](#)

For uplift, safety index $\eta_{uplift} = 1$ is applied to Equation 2.8 as:

$$\left(\frac{C}{D}\right)_{min} = \frac{\frac{\pi\gamma_w}{4\gamma_g} - \frac{\pi d\gamma_T}{D\gamma_g} - \frac{1}{2} + \frac{\pi}{8}}{\eta_{uplift}} \quad (2.37)$$

For the minimum support pressure, safety index $\eta_{\sigma'_h} = 1.5$ is applied to effective horizontal pressures and $\eta_{porepressure} = 1$ is applied to pore pressure in Equation 2.18 as:

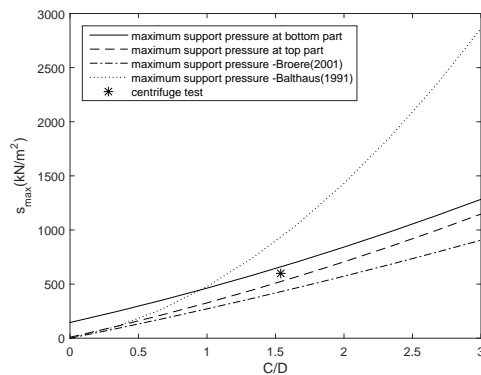
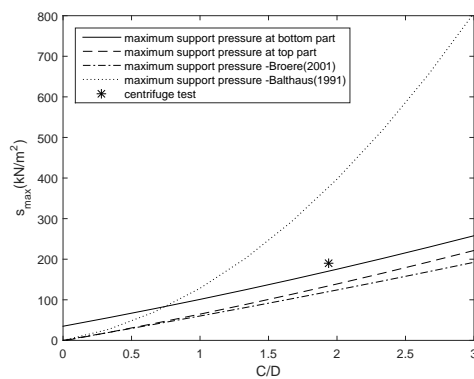
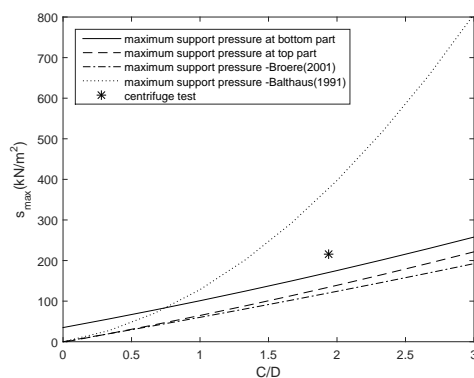
$$s_{min} = \eta_{\sigma'_h} \sigma'_h + \eta_{porepressure} p \quad (2.38)$$

For the maximum support pressure, safety index $\eta_{blow-out} = 1.1$ is applied to the values of maximum support pressures derived from blow-out condition :

$$s_{max} = \frac{s_{blow-out}}{\eta_{blow-out}} \quad (2.39)$$

where $s_{blow-out}$ is the maximum support pressure derived from Equations 2.26, 2.28, 2.32 and 2.35.

Figure 2.32 shows that tunnels in sand, clayey sand, clay or organic clay can be designed with very shallow overburden by changing the design of the tunnel segments, in particular, the value of d/D ratio. Nevertheless, it should be noted that there is often a presence

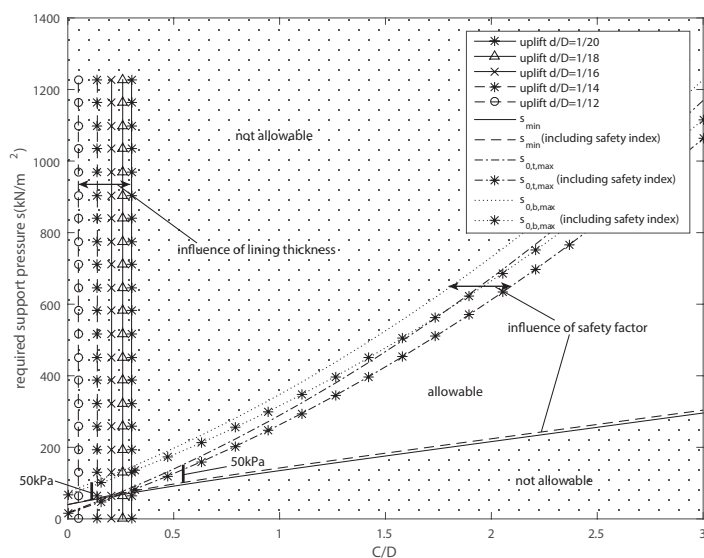
(a) with the 1st centrifuge test(b) with the 2nd centrifuge test(c) with the 3rd centrifuge testFigure 2.31: In comparison with the centrifuge tests in [Bezuijen and Brassinga \(2006\)](#)

of sewage systems and other small infrastructure in the range up to about 4 meters below the surface. Therefore, for metro tunnels with a diameter in the order of 6 to 7 m, a C/D ratio in the range of 0.5 to 1 is the most shallow practical possibility. In practice, however, there needs to be a difference between the maximum and minimum pressures for safety reasons and to be practically workable. Based on Kanayasu et al. (1995) a 50 kPa safety margin seems sufficient, which still allows tunnels with shallow cover in more competent layers. In Figure 2.32, a vertical bar of 50 kPa is included to indicate where the 50 kPa margin is first available (both for the case of safety factors are included and without). It can be seen in this figure that when tunnelling in sand, clayey sand, clay and organic clay with a C/D ratio in the range of 0.5 to 1, this condition of a 50 kPa safety margin is satisfied. In the case of a tunnel in peat, Figure 2.32e shows that the tunnel can be designed theoretically at a very shallow level as the above cases. This would require increasing the weight of the lining (d/D in the order of 1/10 or a similar amount of ballast in the tunnel) but would leave a small margin only between maximum and minimum support pressures. This implies that the tunnel cannot be designed with a low C/D ratio (and should probably not be less than 6) in peat layers if a safety margin is required.

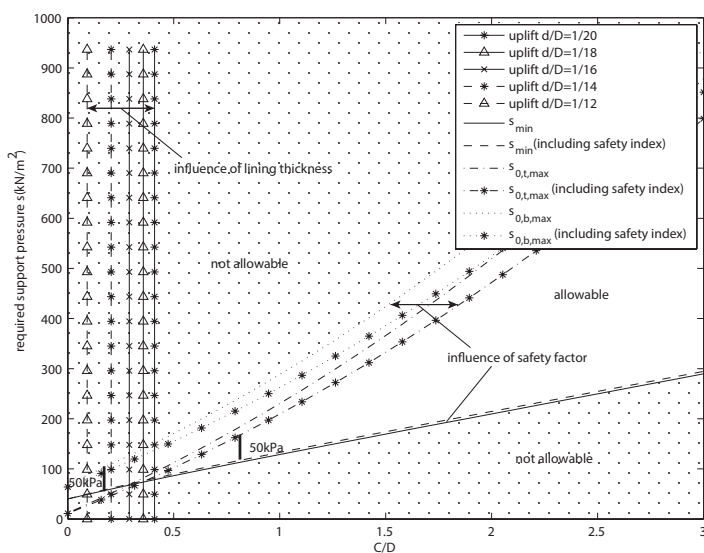
2.6. CONCLUSION

It is concluded that in the case of a tunnel in saturated sand and clay, the ratio of C/D can be reduced by changing the thickness of the tunnel in order to compensate for the uplift or by adding ballast weight. However, the design depth of the tunnel should take into account the existence of utilities and other infrastructure systems. It should also be noted that in practice, there must be a difference between the maximum support pressure s_{max} and the minimum support pressure s_{min} to guarantee a safe operation of the TBM. Therefore, in the case of a tunnel in peat and a 50 kPa safety margin, only d/D ratio larger than 1/12 would allow a stable tunnel construction.

Based on the C/D ratio, the range of workable support pressure can be estimated with the caveat that the results in Figure 2.32 are primarily suitable for tunnelling. With slurry shields, the infiltration of the support medium may lead to excess pore pressure in front of the tunnel face and reduce the effective of the support (Broere, 2001; Hoefsloot, 2001). Therefore, the area of possible support pressure in the case of slurry shields may be smaller than suggested by Figure 2.32, limiting the range of low C/D ratios that are feasible.

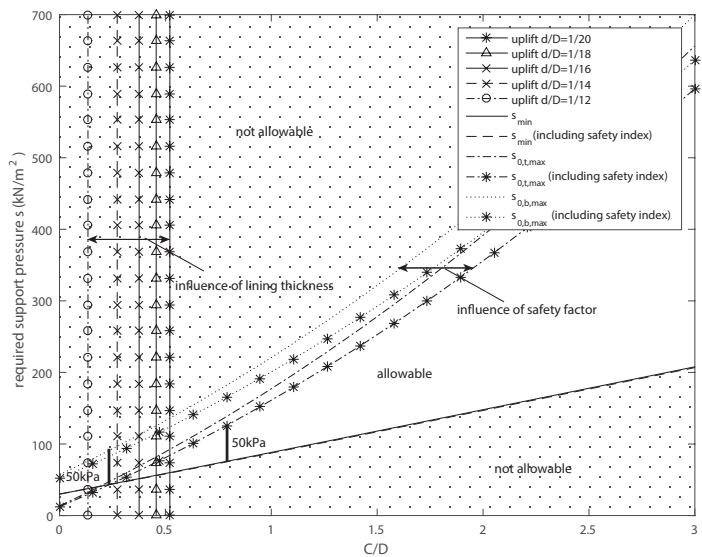


(a) in sand

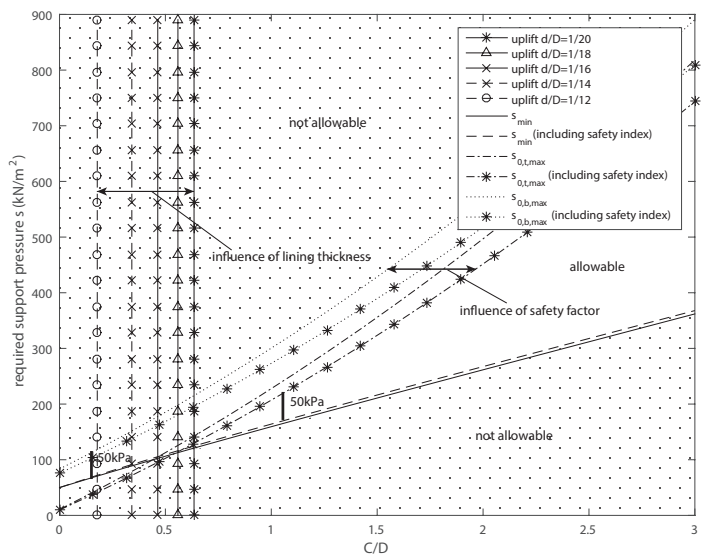


(b) in clayey sand

Figure 2.32: Relation between the C/D ratio and the required support pressures for a tunnel with $D = 10m$ (continue in next page)

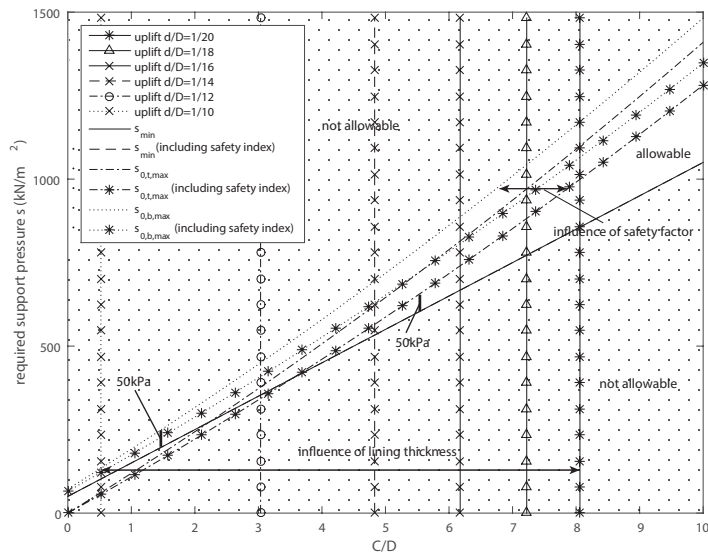


(c) in clay



(d) in organic clay

Figure 2.32: Relation between the C/D ratio and the required support pressures for a tunnel with $D = 10m$ (continue in next page)



(e) in peat

Figure 2.32: Relation between the C/D ratio and the required support pressures for a tunnel with $D = 10m$

3

STRUCTURAL ANALYSIS OF SHALLOW TUNNELS

Step by step and the thing is done.

Charles Atlas

In general, studies on structural design for bored tunnels focus on moderate to deep tunnels (cover-to-diameter ratio $C/D \geq 2$). Such tunnel design methods cannot be used for shallow situated bored tunnels because the influence of buoyancy is discounted and actual loads on the tunnel lining are not taken into account properly. This chapter proposes a new model which has more accurate loads on the tunnel lining combined with finite element analysis for shallow tunnels. Internal forces and deformations of various shallow bored tunnels are investigated. The relation between optimal thickness-to-diameter ratio d/D of tunnel cross-section and cover-to-diameter ratio C/D is also studied.

This chapter is based on a paper under review in International Journal of Geomechanics [Vu et al. \(2015e\)](#). Table 3.2 and Figure 3.11 to 3.20 have been expanded.

3.1. INTRODUCTION

The large diameter driven shield with concrete segments has been common in construction practice in cities due to the ability to limit settlements and damage to existing buildings. The previous chapter indicated the estimate of the C/D ratio in stability analysis for shallow tunnelling. However, in the next stages, the deformations of the tunnel lining has a large influence on the settlement on the surface. The structural analysis of the tunnel lining, therefore, not only estimates the internal forces and deformations of segment lining but also investigates the impact of the overburden on the tunnel lining. With these conditions in mind, this chapter takes a look at the structural design of tunnel linings for shallow tunnels in soft soils.

Many calculation models have been proposed and developed since 1926 for the tunnel design. Schmid (1926) proposed the first analysis method for an elastic continuum. Schulze and Duddeck (1964) presented a bedded ring model for shallow tunnels with limited covers. Morgan (1961) proposed an analytical solution using continuum models which takes into account the elliptical deformation of the tunnel lining. Windels (1966) further developed the method of Schulze and Duddeck to take into account the second order of the series expansion of the analytical solution and the displacement of the tunnel lining in the construction process. Windels (1967) published a model for a circular tunnel in an elastic continuum with geometrical non-linearity. Muir Wood (1975) corrected Morgan (1961) by including the tangential stresses on the model but the radial deformations due to these stresses were ignored, then this problem was solved by Muir Wood (1976).

The common method used in practical tunnel design was proposed by Duddeck and Erdmann (1985). A continuum model (Figure 3.1) and a model without a reduction of ground pressure at the crown (Figure 3.2) were proposed for shallow tunnels with a depth $H \leq 2.5D$. The continuum model includes the interaction between the soil and the structure automatically. In the bedded-beam model, the interaction between the soil and the structure is captured by bedding springs with a suitable applied stiffness. Duddeck (1988) indicated that the bedded-beam model is suitable to calculate the internal forces in a shallow tunnel in soft soil. Blom (2002) included effects of longitudinal joints and soil reaction to estimate the deformations of the tunnel lining.

Based on the models of Duddeck and Erdmann (1985), Oreste (2007) proposed a hyperstatic reaction method to estimate the internal forces in the tunnel lining by using a Finite Element Method (FEM) framework in the case of tunnels in rock. Although this model simulates interactions between tunnel lining and surrounding ground through Winkler springs, only radial pressures are taken into account. A further developed model presented by Do et al. (2014) includes the tangential pressures. This model also takes into account the influence of segmental joints, which is indicated in Groeneweg (2007).

Although many models have been studied and developed, most of them focus on moderate and deep tunnels (cover-to-diameter ratio $C/D \geq 2$). In the case of shallow tunnels, especially very shallow tunnels which have a C/D ratio from 0 to 0.5, there has been little research. This chapter looks into effects of overburden on internal forces and deformations of the tunnel lining and seeks the optimal C/D ratio when tunnelling in soft (Holocene) layers. Firstly, Section 3.2 introduces a new model for structural design for tunnel lining. In the Section 3.3, the impact of overburden on tunnel lining is investi-

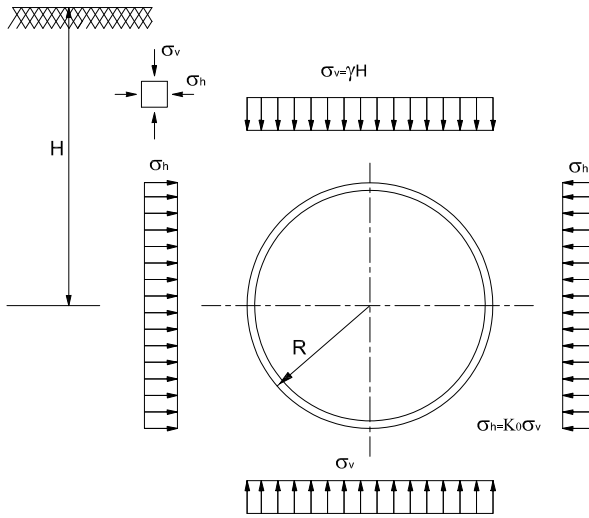


Figure 3.1: Plane strain continuum model (Duddeck and Erdmann, 1985)

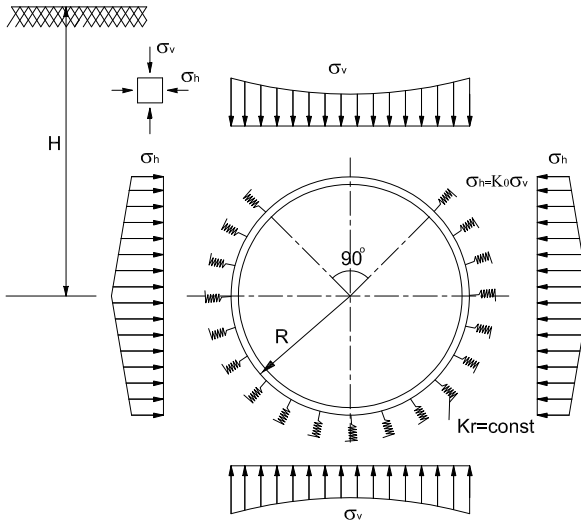


Figure 3.2: Bedded-beam model for shallow tunnels (Duddeck and Erdmann, 1985)

gated when tunnelling in various soils. Conclusions of structural analysis for shallow tunnel lining are presented in Section 3.4.

3.2. STRUCTURAL LINING DESIGN

When designing a tunnel in soft soil, the following assumptions are applied in most common design models (Duddeck and Erdmann, 1985):

- The stress-strain deformations of a cross-section are in plane strain conditions for both the tunnel lining and the ground;
- The active soil pressures on the tunnel lining are equal to the primary stresses in the undisturbed ground before tunnelling;
- At the final stage of tunnelling and in the long-term period, the ground will return to the conditions prior to tunnelling;
- The interaction between ground and tunnel lining is limited to radial and tangential or only radial springs;
- Ground and tunnel lining are elastic materials.

These assumptions, which these models are based on, are also used in guidelines for the design of shield tunnel lining (ITA-Group2, 2000) and considered common practice. However, as e.g. Hashimoto et al. (2002) show the pressures exerted by the soil on the lining after construction can differ significantly from the primary stresses prior to tunnelling, and do not need to revert to this initial state over time, as the weight of the tunnel is generally less than the weight of the excavated soil. Duddeck and Erdmann (1985) already stated that these assumptions are conservative. Nevertheless, these load conditions have become common practice (ITA-Group2, 2000) and experience shows that with these assumptions a safe lining design is possible. Therefore, in this study, these assumptions are applied to the proposed model and a further review of these assumptions is outside the scope of this thesis.

3.2.1. INFLUENCE OF LOAD AND OVERBURDEN ON LINING MODELS

For the shallow tunnel, according to Duddeck (1988), a continuum model or a bedded-beam model without a reduction of ground pressure at the crown should be used in design. Most of these models in studies of Muir Wood (1975), Einstein and Schwartz (1979), Duddeck and Erdmann (1985), Möller (2006), Plizzari and Tiberti (2006), and Do et al. (2014) use a uniform load of vertical pressure on the tunnel lining at upper and lower parts of the tunnel, which is equal to the overburden pressure (Figure 3.1) as:

$$\sigma_v = \gamma H \quad (3.1)$$

where γ is the volumetric weight of soil and H is the depth of the tunnel (at spring line location).

The horizontal pressure on the sides of the tunnel is constant and is given by:

$$\sigma_h = K \sigma_v \quad (3.2)$$

where K is the earth pressure coefficient.

In shallow tunnels with the C/D ratio less than 2, the pressures at the top and the bottom of the tunnel lining are significantly different. The loading used in Duddeck's methods,

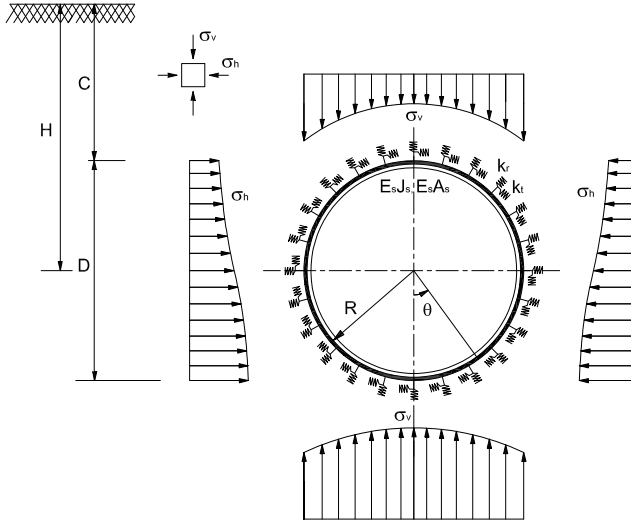


Figure 3.3: Soil pressures on the tunnel lining

therefore, is not applicable in the case of shallow tunnels. To be more accurate, in this study, the vertical pressures should be calculated at every particular point of the tunnel cross section.

In the new model proposed in Figure 3.3 for a shallow tunnel with radius R at the depth H , the vertical soil pressure on the tunnel lining can be estimated as:

$$\sigma_v = \gamma(H + R \cos \theta) \quad (3.3)$$

where θ is the angle between the element axis and the vertical axis of a tunnel section.

The horizontal soil pressure on the tunnel lining is given by:

$$\sigma_h = K\gamma(H + R \cos \theta) \quad (3.4)$$

Figure 3.3 only shows the soil pressures on the tunnel lining. When considering the total vertical soil pressures, without taking into account the interaction between the tunnel lining and surrounding soil, the equilibrium seems not satisfied. In this model, the interaction between surrounding soil and the tunnel lining is presented via radial and tangential springs. The radial and tangential interaction forces on the tunnel lining are not included in this figure. When these forces are taken into account, the equilibrium condition is satisfied.

Unlike the method of [Duddeck and Erdmann \(1985\)](#) and [Blom \(2002\)](#) for the reduction of vertical pressures at the lower part of the tunnel, the above assumptions indicate that the active soil pressures on the tunnel lining are equal to the primary stresses in the undisturbed ground before tunnelling. Therefore, there is no reduction of vertical pressures in the case of a shallow tunnel in this model.

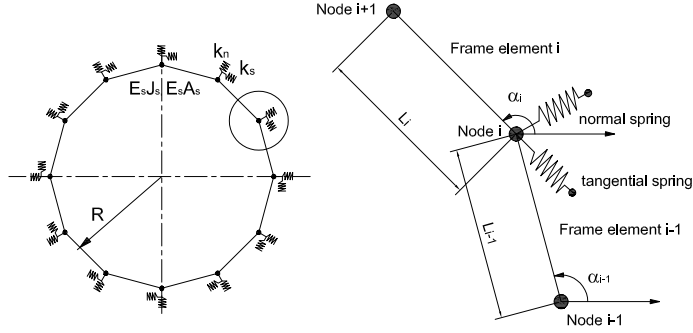


Figure 3.4: Radial and tangential Winkler springs in FEM analysis (Do et al., 2014)

3.2.2. INFLUENCE OF GROUND-LINING INTERACTION

The interaction between soil and the tunnel lining is presented via spring stiffness in this model. According to the hypothesis of Winkler (1867), the spring stiffness is estimated as:

$$p = k \cdot S \quad (3.5)$$

where p is the ground bedding pressure, S is the radial displacement of the tunnel lining, and k the ground reaction modulus.

In Duddeck's bedded-beam models (Duddeck and Erdmann, 1985), the stiffness of radial spring k_r is given by:

$$k_r = E_s / R \quad (3.6)$$

where the stiffness modulus of the ground E_s is estimated as:

$$E_s = E_c \frac{1 - \nu}{(1 + \nu)(1 - 2\nu)} \quad (3.7)$$

where E_c is the elasticity modulus of the ground, and ν is Poisson's ratio.

These methods use a constant spring stiffness for every point on the tunnel lining based on the stiffness modulus of the ground and Poisson's ratio ν . This is not appropriate as the spring stiffness of each point on the tunnel lining is different due to the stress state of the soil and the change of the deformation pattern of the tunnel lining.

Oreste (2007) and Do et al. (2014) use a nonlinear relationship between the reaction pressure of the ground p and the deformation of the tunnel lining δ in Duddeck's model to calculate internal forces in the tunnel lining. The apparent stiffness of the ground η^* is estimated as:

$$\eta^* = \frac{p_{lim}}{\delta} \left(1 - \frac{p_{lim}}{p_{lim} + \eta_0 \delta} \right) \quad (3.8)$$

where p_{lim} is the maximum reaction pressure that the ground can offer and η_0 is the initial stiffness of the ground (for the δ value close to 0).

For the circular tunnel in elastic ground, the interaction between ground and the tunnel

lining depends on the radius of the tunnel and the ground parameters. The initial radial ground reaction stiffness $\eta_{r,0}$ is estimated as the following empirical formula (Möller, 2006):

$$\eta_{r,0} = \beta \frac{1}{1 + \nu} \frac{E}{R} \quad (3.9)$$

where E is Young's modulus of the ground and β is a dimensionless factor.

The value of β depends on soil and structural parameters, therefore, it is difficult to determine the exact β value. In conventional studies of Mashimo and Ishimura (2005), Möller (2006), Plizzari and Tiberti (2006) and Molins and Arnau (2011), the value of β is taken equal to 1. In Do et al. (2014), the value of β is taken equal to 2 by comparing to Einstein and Schwart's method. In this study, the value of $\beta = 2$ is used in this analysis to estimate the impact of the depth of cover on internal forces of the tunnel.

According to Mashimo and Ishimura (2005), Möller (2006), Plizzari and Tiberti (2006), and Molins and Arnau (2011), the simple relationship between tangential spring stiffness η_s and normal spring stiffness η_n is:

$$\eta_s = \frac{1}{3} \eta_n \quad (3.10)$$

The maximum radial reaction pressure $p_{n,lim}$ in Equation 3.8 can be calculated as:

$$p_{n,lim} = \frac{2ccos\phi}{1 - sin\phi} + \frac{1 + sin\phi}{1 - sin\phi} \Delta\sigma_{conf} \quad (3.11)$$

where $\Delta\sigma_{conf}$ is the confining pressure on the tunnel perimeter estimated as:

$$\Delta\sigma_{conf} = \frac{\sigma_h + \sigma_v}{2} \frac{\nu}{1 - \nu} \quad (3.12)$$

Similar as in Do et al. (2014), the maximum shear reaction pressure on the tunnel lining in Equation 3.8 can be estimated as:

$$p_{s,lim} = \frac{\sigma_h + \sigma_v}{2} tan\phi \quad (3.13)$$

The stiffness of the radial and tangential springs in each elements of the frame is:

$$k_{n,i} = \eta_{n,i}^* \left[\frac{L_{i-1} + L_i}{2} \right] = \frac{p_{n,lim}}{\delta_{n,i}} \left(1 - \frac{p_{n,lim}}{p_{n,lim} + \eta_{n,0}\delta_{n,i}} \right) \frac{L_{i-1} + L_i}{2} \quad (3.14)$$

$$k_{s,i} = \eta_{s,i}^* \left[\frac{L_{i-1} + L_i}{2} \right] = \frac{p_{s,lim}}{\delta_{s,i}} \left(1 - \frac{p_{s,lim}}{p_{s,lim} + \eta_{s,0}\delta_{s,i}} \right) \frac{L_{i-1} + L_i}{2} \quad (3.15)$$

where L_i is the distance between node i^{th} and node $(i + 1)^{th}$ (see Figure 3.4).

The radial springs are only active in the compression condition. It means that in the area where the tunnel moves away from the soil, the radial springs are inactive.

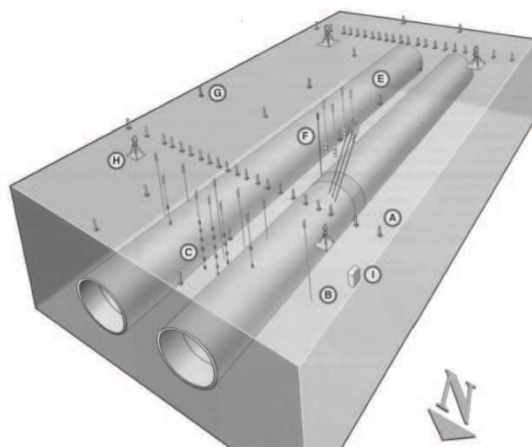


Figure 3.5: Measuring field at Second Heinenoord Tunnel (Broere, 2001)

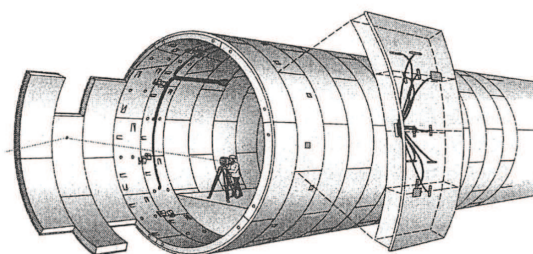


Figure 3.6: Measuring ring and instrumentation (Bakker, 2003)

3.2.3. A CASE STUDY OF SECOND HEINENOORD TUNNEL

The validation of the new model is carried out with the case study of Second Heinenoord Tunnel which is presented in Section 2.4. In this project, there were two measurement locations, one on the North Bank and one on the South Bank of the river Oude Maas (Figure 3.5). Measurement instruments were installed in all seven elements of a ring in order to derive the stress distribution in the ring as can be seen in Figure 3.6. Pressure cells were installed on the outer face of segments with two cells per segment on 7 segments. During the construction, bending moments and normal forces in the lining were measured using strain gauges.

On the North Bank, the tunnel axis is located at about $16.25m$ below the surface. Figure 3.7 shows a cross-section at the measuring section in North Bank. With the tunnel diameter of $8.3m$, the C/D ratio at this location is approximately 2. The description of soil layers and soil parameters are shown in Table 3.1.

A back-analysis with 2D FEM Plaxis was carried out as indicated in Bakker (2003). The

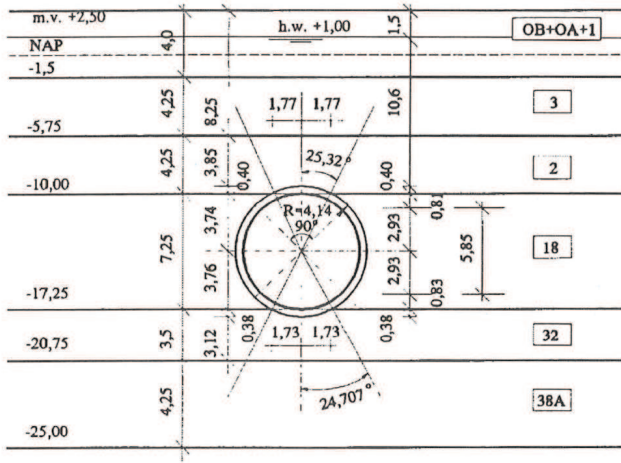


Figure 3.7: Cross-section of the measured location in the North Bank in Second Heinenoord Tunnel (Bakker, 2003)

derived bending moments and normal forces from Plaxis model were compared to the measured data in the North Bank. Moreover, a 3D model with ANSYS FEM software (Figure 3.8) was also analyzed in order to derive bending moments in the tunnel lining in this case (Bakker et al., 2000). In this analysis, the concrete segments were modelled as solid volume segments. Three rings were modelled using 8100 elements. In this model, the interaction between the tunnel lining and the surrounding ground was modelled as linear springs in the radial direction as in Duddeck and Erdmann (1985) with 1418 spring elements in total. The bending moments were derived with 3 rings and were compared with the field data.

In order to validate the new model, calculations for the Second Heinenoord case have been made in order to derive internal forces in the lining. The derived bending moments and normal forces from the new model are compared to the field data after 330 days and the analytical results from Bakker et al. (2000) as shown in Figure 3.9 and 3.10. A comparison between the bending moments derived from the new model and the bending moments from measurement in this project, Duddeck's model, 2D Plaxis model and 3D ANSYS model from Bakker et al. (2000) is shown in Figure 3.9. This figure shows that bending moments derived from these models have the same bending moments trend with the measured data in the field. The bending moment derived from the new model is close to the moments derived from Duddeck's model and Bakker's 3D analysis by ANSYS. In comparison with the field data, the highest bending moment observed in the field data is close to the bending moments in all these models (at the location of 166° on the cross-section of the tunnel lining). Even though there exists a difference between the measured bending moment at the sides of the tunnel lining, the highest bending moment at the top and the bottom of the tunnel lining shows an agreement between the

Table 3.1: Description of layers and soil parameters for the North Bank in Second Heinenoord Tunnel (Bakker, 2000)

Symbol	Soil type	Top of layer(m) N.A.P	γ_{wet} (γ_{dry}) (kN/m^3)	c_u (kPa)	c' (kPa)	φ' ($deg.$)	ν (-)	E_{oed} (MPa)	K_0 (-)
OA/1/OOB	mixture of sand and clay	+2.50	17.2(16.5)	-	3	27	0.34	5.2	0.58
3	sand, local parts of clay	-1.50	19.5	-	0	35	0.3	26	0.47
2	sand with clay	0-5.75	19	-	0	33	0.31	25	0.47
18	sand, local parts of clay	-10.00	20.5	-	0	36.5	0.3	40	0.45
32	sand, gravel	-17.25	20.5	-	0	36.5	0.3	60	0.5
38A	clay, local parts of sand	-20.75	20.0	140	7	31	0.32	16	0.55
38F	sand	-25	21	-	0	37.5	0.3	80	0.55
38A	clay, local parts of sand	-26.5	20.0	140	7	31	0.32	16	0.55

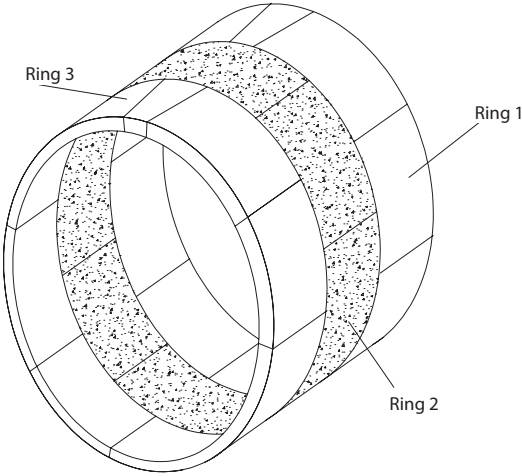


Figure 3.8: 3D model of segmental lining in ANSYS FEM analysis in Bakker et al. (2000)

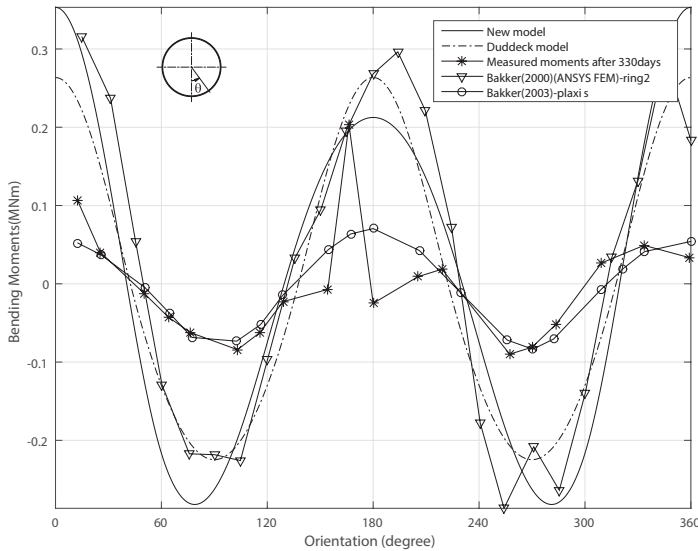


Figure 3.9: Validation of bending moments in Second Heinenoord Tunnel

field data and the analytical models.

Figure 3.10 shows a comparison of normal forces between field data and normal forces derived from Duddeck's model, Bakker's 2D Plaxis model and the new model. Overall, normal forces calculated from these models have the same trend with measured normal forces in field data. From this figure, it can be seen that the normal force from the new model is closer to the field data than the results from Duddeck's model and Bakker's 2D Plaxis model, especially at locations at the sides of the tunnel lining, although there still exists a difference between the analytical results and measured normal forces. It was explained in Bakker (2003) that the accuracy of the soil pressure gauges on the segments was unclear and the influence of the grout injection pressure was not taken into account at the measured time of 330 days. This might also explain the strong variability in the measurement.

On the basis of this analysis, it is shown that the results derived from the new model have the same trend as the analysis results from previous numerical models and have a better agreement with the field data. In this case study with $C/D = 2$, the difference between these models is not very large, but for tunnels at shallower locations, the difference are expected to be larger. Unfortunately, detailed field measurements at shallow overburden are launching.

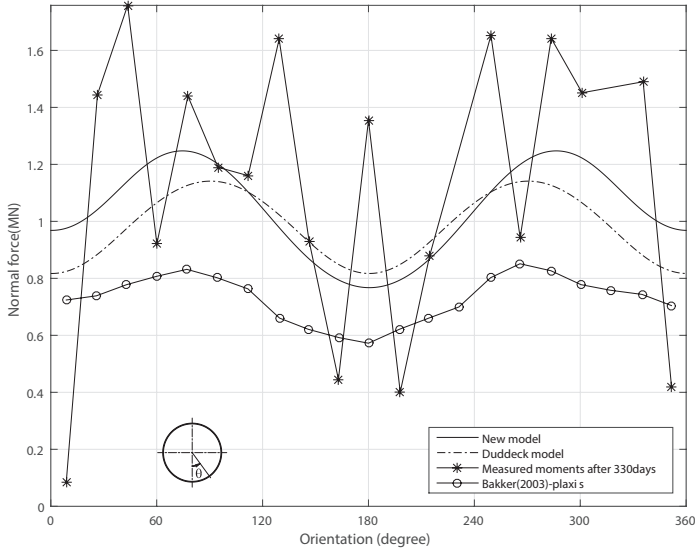


Figure 3.10: Validation of normal forces in Second Heinenoord Tunnel

3

3.3. IMPACTS OF OVERBURDEN ON TUNNEL LINING

Structural analysis is carried out with Duddeck's bedded-beam model without a reduction of ground pressure at the crown and the new model with and without buoyancy conditions in the model, as can be seen in Figure 3.3. A circular tunnel with radius $D = 6.3m$ in various soil conditions with parameters as indicated in Table 2.1 in order to compare to results in [Duddeck and Erdmann \(1985\)](#).

In comparing the internal forces derived from other methods of [Ahrens et al. \(1982\)](#), [Windels \(1967\)](#), [Muir Wood \(1976\)](#) and [Einstein and Schwartz \(1979\)](#), [Duddeck and Erdmann \(1985\)](#) used the following relative stiffness to investigate the effect of soil properties on the internal forces in the tunnel lining:

$$\alpha_D = \frac{ER^3}{E_l I_l} \quad (3.16)$$

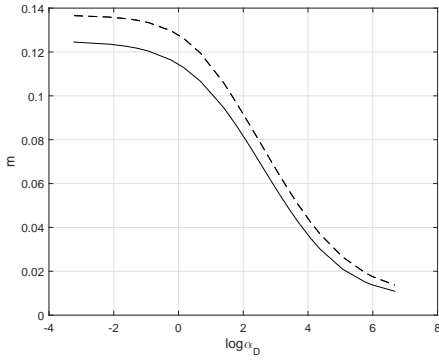
where $E_l I_l$ is the bending stiffness of the tunnel lining. This relative stiffness is also used in analysis results from the new model and the Duddeck's model.

In Figures 3.11 and 3.12, the maximum bending moments are presented as a function of relative stiffness α_D with the value of m determined by:

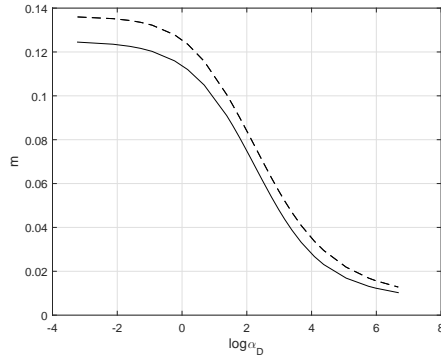
$$maxM = m\sigma_v R^2 \quad (3.17)$$

where σ_v is the vertical soil pressure at the tunnel spring line.

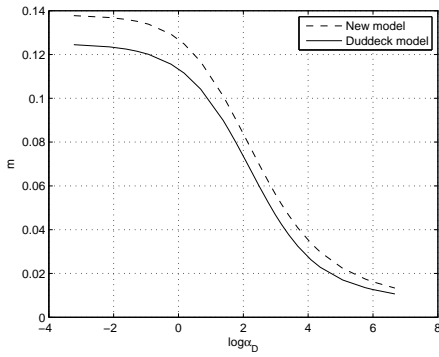
Figure 3.11 shows a comparison between the normalized maximum moments m derived



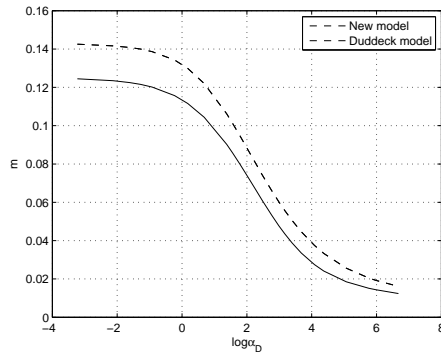
(a) in sand



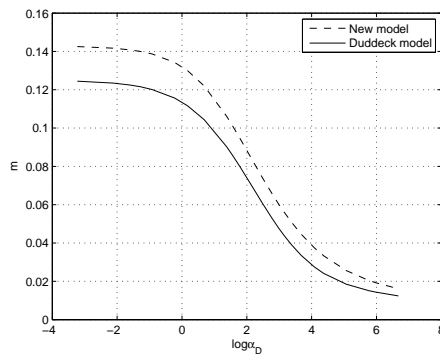
(b) in clayey sand



(c) in clay



(d) in organic clay



(e) in peat

Figure 3.11: Normalized maximum bending moments in models with varied relative stiffness α_D values

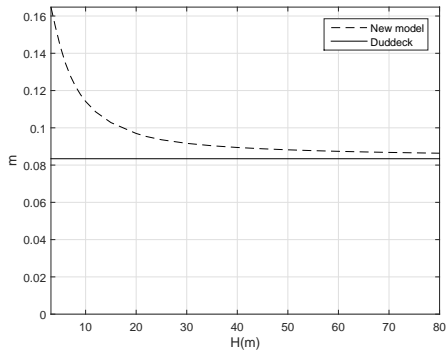
from the new model and Duddeck's model in varied relative stiffness α_D of soil and the tunnel lining. Overall, the normalized maximum bending moments of the new model show the same trend as Duddeck's model but are larger in the values. With the large α_D value corresponding with stiffer ground or more flexible tunnel linings, the normalized maximum moments m derived from the new model are closer to these moments from Duddeck's model.

Figure 3.12 shows the changes of the normalized maximum bending moments m derived from these models with the depth of the tunnel H for tunnelling in sand, clay, organic clay and peat. With Duddeck's method, the m value does not change with the varied depths of the tunnel (m is equal to 0.083 for sand, 0.09 for clayey sand, 0.093 for clay, 0.107 for organic clay and 0.117 for peat). Meanwhile, the m value in the new model is greater than in Duddeck's model and becomes constant when the tunnel is at great depth and close to the m value of Duddeck's model. In the range of H from 3.15 to 15.75m or C/D from 0 to 2 in the case of shallow tunnels, the m value in the new model is much higher than the m value in Duddeck's model. Especially, when tunnels are close to the surface (at tunnel depth $H \approx 3.15m$), the m value in the new model is double that in Duddeck's model. This stems from the above analysis of the loading in the tunnel lining models. In Duddeck's model, the loading on the tunnel lining is assumed to be symmetric loading in both the vertical and horizontal axes of the tunnel. This leads to the maximum bending moments that appear at the top and bottom of the tunnel cross section and have the same value. In the new model, the loading on the tunnel lining changes with the depth of a particular point of the tunnel cross-section. Therefore, the bending moments at the top and at the bottom of the tunnel cross-section are different. In shallow tunnels, the loading at the bottom of the tunnel lining is significantly greater than the overburden loadings at the top and the spring line of the tunnel lining. Therefore, the normalized maximum bending moment in the new model is much greater than in Duddeck's model.

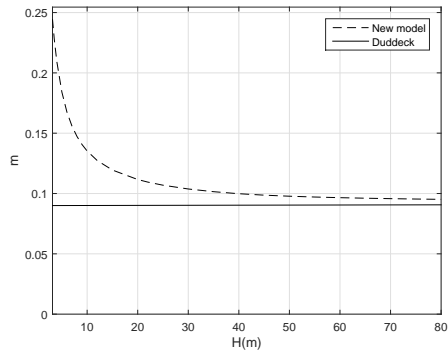
One of the most important considerations in tunnel design is the deformation of the tunnel lining. Figures 3.13 and 3.14 show the changes in maximum radial displacements in these models at various depths of the tunnel for various types of soil. In Figure 3.13, in the analysis results obtained from Duddeck's model, the maximum radial displacement of the tunnel lining increases linearly with the increase of the tunnel depth. This trend also appears in the new model with and without buoyancy for moderate and deep tunnels ($H \geq 15.75m$ or $C/D \geq 2$). Maximum radial displacement in the new model with buoyancy is higher than this in Duddeck's model due to the higher maximum bending moments as indicated in the above analysis.

Figure 3.14 shows the change in the maximum radial displacement in the case of shallow tunnels ($C/D \leq 2$). Maximum radial displacements in the new model with and without buoyancy are higher than the maximum radial displacement in Duddeck's model. In the analysis results from Duddeck's model, the maximum radial displacement decreases linearly to nearly 0 when the tunnel is close to the surface. Clearly, this is not appropriate in practical cases. Therefore, it might be risky when applying Duddeck's model to design very shallow tunnels.

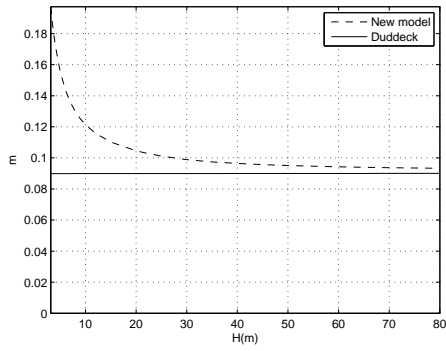
For very shallow tunnels in sand with $C/D = 0 \div 1$ or $H = 3.15 \div 6.3m$, the maximum radial displacement increases sharply in the buoyancy model and significantly in the



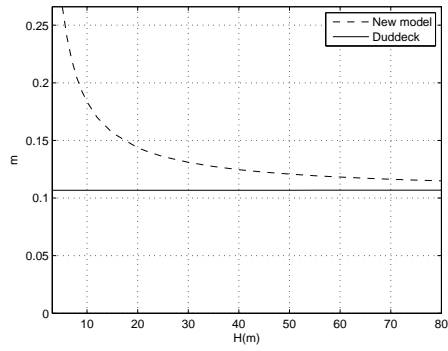
(a) in sand



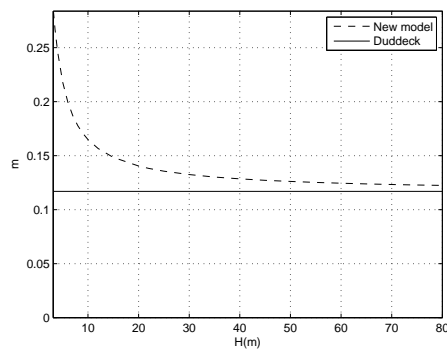
(b) in clayey sand



(c) in clay



(d) in organic clay



(e) in peat

Figure 3.12: Normalized maximum bending moments in models with varied values of tunnel depth H

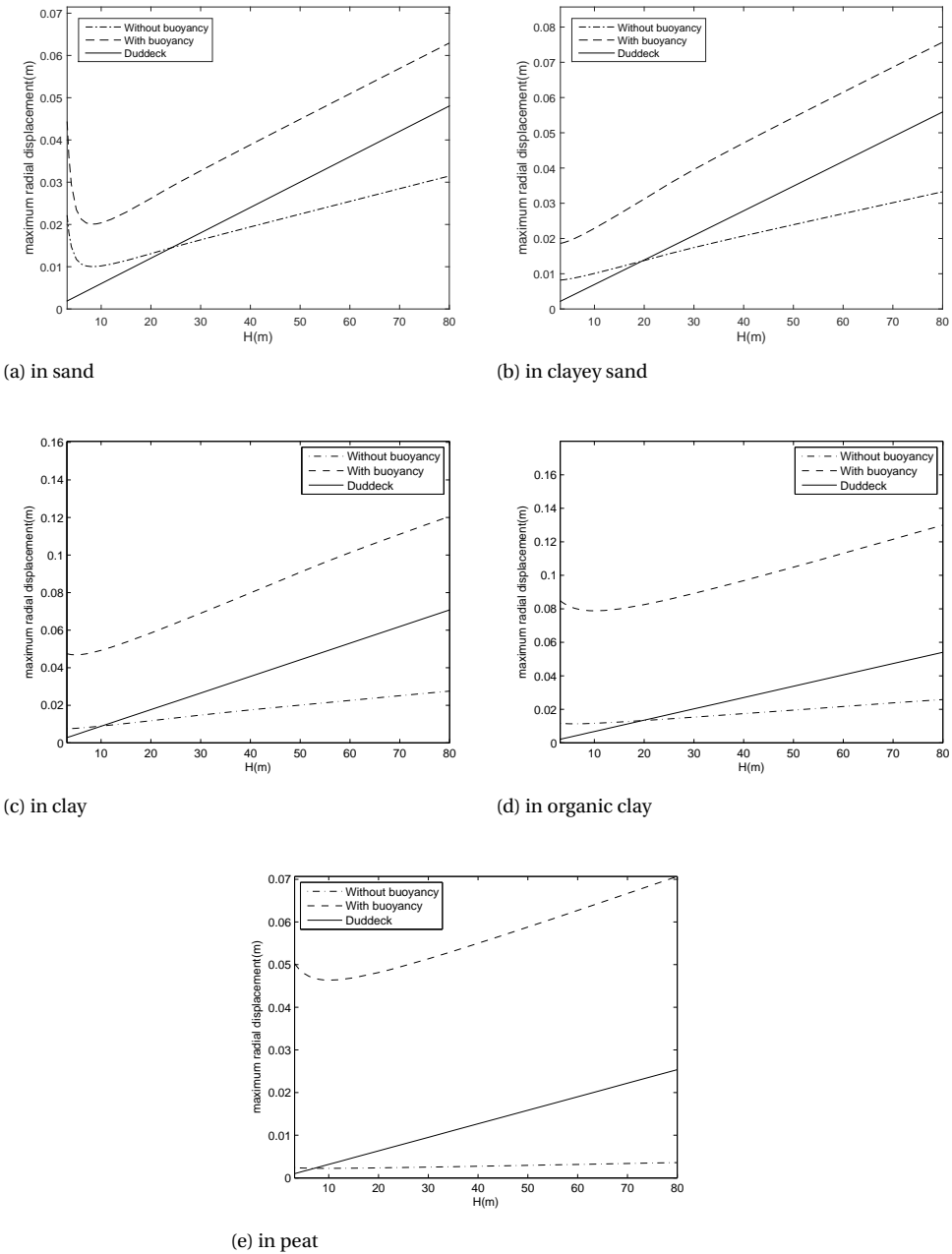


Figure 3.13: Maximum radial displacements in models with varied values of tunnel depth H

Table 3.2: Optimal C/D ratios for minimum of maximum lining deformations

Soil type	d/D									
	1/10	1/12	1/14	1/16	1/18	1/20	1/25	1/30	1/35	1/40
Sand	2.05	1.58	1.27	1.07	0.90	0.8	0.66	0.57	0.53	0.48
Clayey sand	0.68	0.35	0.20	0.00	0.00	0.00	0.00	0.00	0.00	0.00
Clay	0.85	0.53	0.32	0.17	0.00	0.00	0.00	0.00	0.00	0.00
Organic clay	2.39	1.67	1.27	0.95	0.68	0.50	0.22	0.00	0.00	0.00
Peat	4.08	3.02	2.32	1.80	1.42	1.14	0.69	0.36	0.18	0.00

model without buoyancy when the tunnel is near the surface. If one compares the two the maximum radial displacements in the buoyancy model are 2 to 3 times higher than displacements in the model without buoyancy for tunnelling in sand and clayey sand. For very shallow tunnels in clay, organic clay and peat, the maximum radial displacements in the buoyancy model are significantly larger compared to these displacements in the model without buoyancy and in Duddeck's model. It can be seen that deformation in cases without buoyancy is closer to Duddeck's calculation when tunnelling in clay, organic clay and peat while the deformations in the case with buoyancy are much higher. The reason for this is that when the tunnel is close to the surface, the relative difference in the loading on the upper and lower parts of the tunnel lining increases more both for soil loading and pore pressure.

From the maximum radial displacement lines of the new model given in Figure 3.14, it can be observed that there are lowest points in both the cases with and without buoyancy. This indicates the existence of an optimal depth for a particular tunnel where maximum deformation is minimal both with and without buoyancy. For example, in Figure 3.14a, the optimal depth is estimated at the depth of the tunnel $H = 8.5m$ where the minimum values of maximum displacements in models with and without buoyancy are $0.02m$ and $0.01m$, respectively.

Analysing for varied tunnel radii R and the d/D ratio of cross-sections in the new model with and without buoyancy, Figures 3.15, 3.16, 3.17, 3.18 and 3.19 show the relationship between maximum radial displacements and the C/D ratio. At a particular value of the C/D ratio, the thinner tunnel cross-section is, and/or the larger the tunnel radius is, the larger maximum the radial displacement is.

It is interesting to note the existence of a value of the C/D ratio where the maximum radial displacement is minimum for a particular d/D ratio with varied tunnel radii R in both cases of with and without buoyancy. For example, in Figure 3.15a for the tunnel with cross-section $d/D = 1/10$, the maximum displacement of the tunnel lining reaches the minimum value when $C/D = 2.05$ for the models without and with buoyancy. These optimal values are 1.58 for the tunnel with cross-section $d/D = 1/12$ in Figure 3.15b, and 0.8 for the tunnel with cross-section $d/D = 1/20$ in Figure 3.15f.

Based on these analysis results, Table 3.2 summarizes the values of the C/D ratio when the maximum displacement of the tunnel lining reaches the minimum value for the models without and with buoyancy with various d/D ratios of the tunnel cross-section in the case of tunnelling in sand, clay, organic clay and peat.

On the basis of this structural analysis for shallow tunnels in various soils, for varied geometry of cross-section of the tunnel d/D , an optimal C/D value can be found that gives

a minimum value of the maximum deformation of the tunnel lining. Moreover, uplift analysis for shallow tunnels in Chapter 2 provides the minimum C/D ratio where ballast should be used for varied values of d/D . From Table 3.2, the optimal C/D value based on the structural analysis and uplift analysis for shallow tunnels with or without buoyancy can be determined. In Figures 3.20a, 3.20b, 3.20c, 3.20d and 3.20e, the intersection between the optimal values of the C/D ratio from structural analysis and uplift analysis shows the situation of a designed shallow tunnel where ballast layers are required or which value of the d/D ratio should be minimally used in a particular depth of the tunnel.

3.4. CONCLUSION

Structural design for tunnels has been previously focused on moderate to deep tunnels (with $C/D \geq 2$). The loading on tunnel linings in recent models does not include the difference of loadings at the top and at the bottom of shallow tunnels. By calculating the soil pressure at particular points on the cross-section of the tunnel combined with finite element method for structural analysis, the new model in this study becomes appropriate for tunnels at shallow depths. Structural analysis from the new model shows that the normalized internal forces and the deformations of the tunnel lining increase significantly when the tunnel is designed at shallow location with and without taking buoyancy into account. From the analysis results it follows there is a minimum value of maximum deformation of the tunnel lining when changing the depth H of the tunnel. From combined structural analysis with uplift analysis, an optimal C/D ratio for a particular cross-section d/D ratio in tunnelling without ballast can be derived.

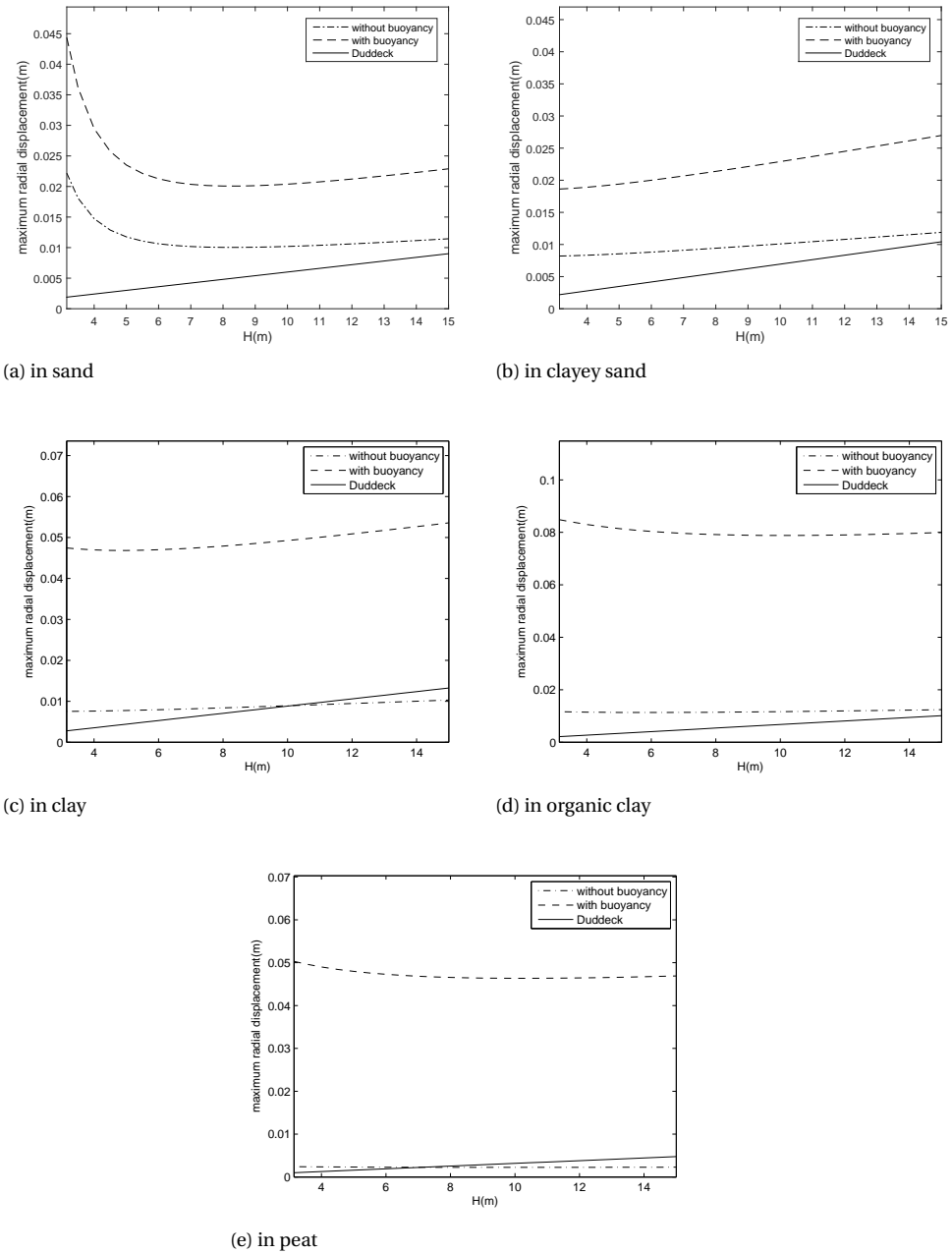


Figure 3.14: Maximum radial displacements in models in shallow tunnels

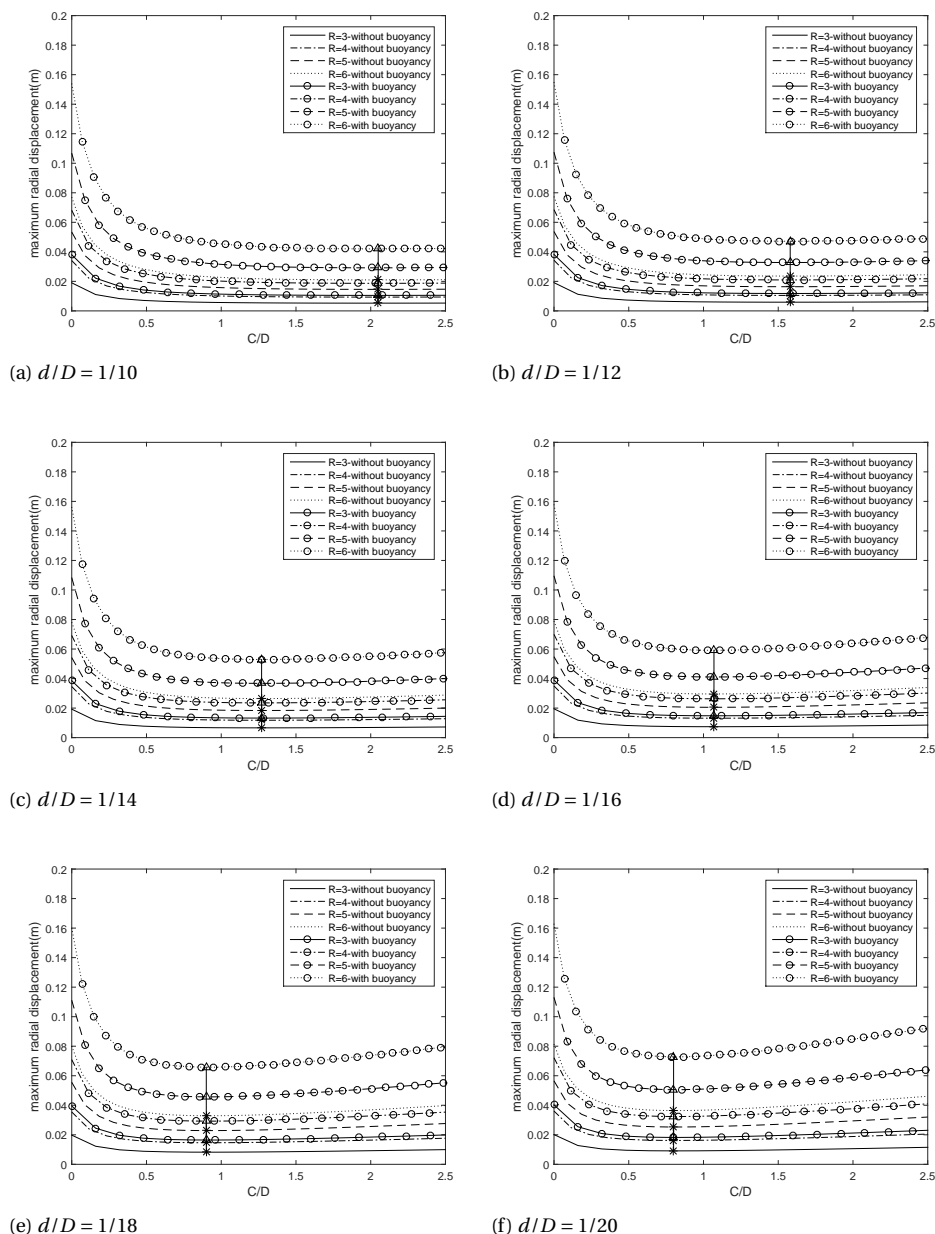


Figure 3.15: Relationship between maximum radial displacements and cover-to-diameter C/D values for models in with and without buoyancy in varied thickness-to-diameter ratio d/D of the tunnel cross-section in sand. Vertical lines include the optimal C/D where radial displacement is minimal (continue in next page).

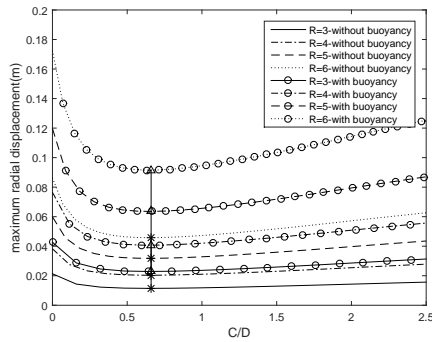
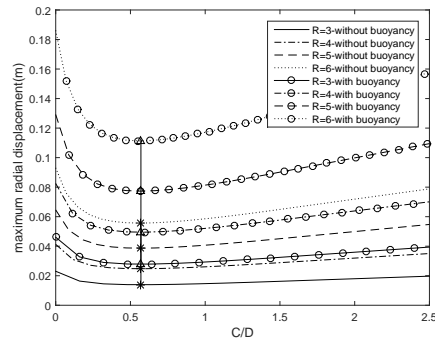
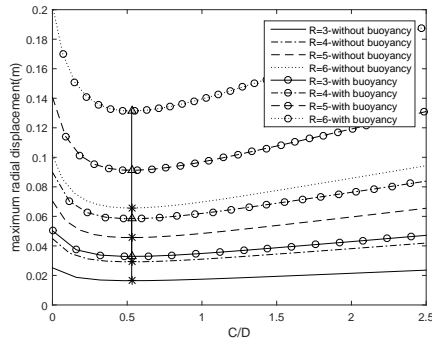
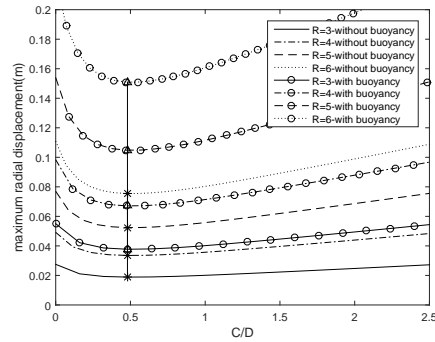
(g) $d/D = 1/25$ (h) $d/D = 1/30$ (i) $d/D = 1/35$ (j) $d/D = 1/40$

Figure 3.15: Relationship between maximum radial displacements and cover-to-diameter C/D values for models in with and without buoyancy in varied thickness-to-diameter ratio d/D of the tunnel cross-section in sand. Vertical lines include the optimal C/D where radial displacement is minimal.

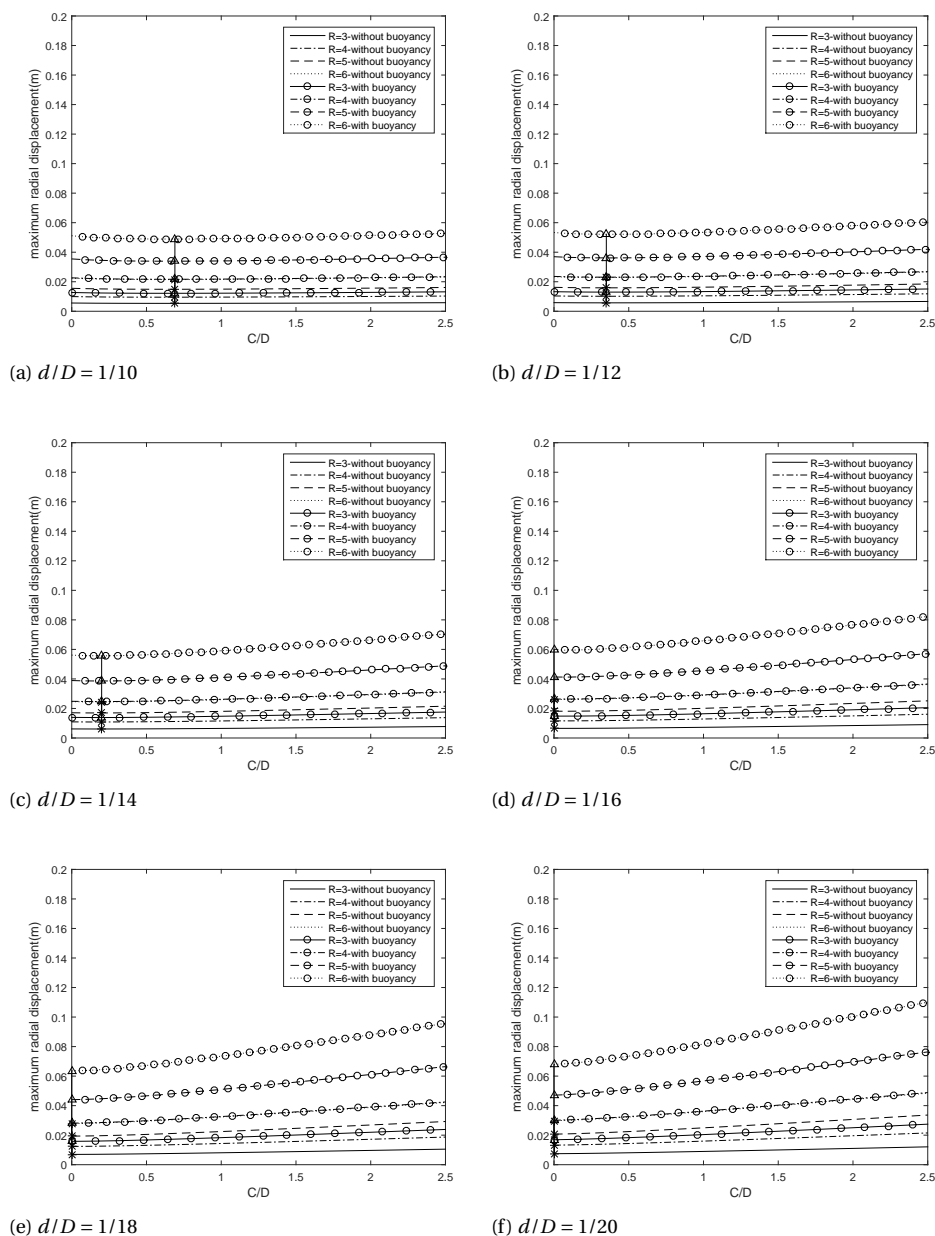


Figure 3.16: Relationship between maximum radial displacements and cover-to-diameter C/D values for models in with and without buoyancy in varied thickness-to-diameter ratio d/D of the tunnel cross-section in clayey sand. Vertical lines include the optimal C/D where radial displacement is minimal (continue in next page).

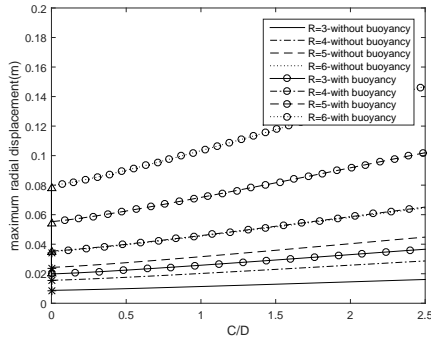
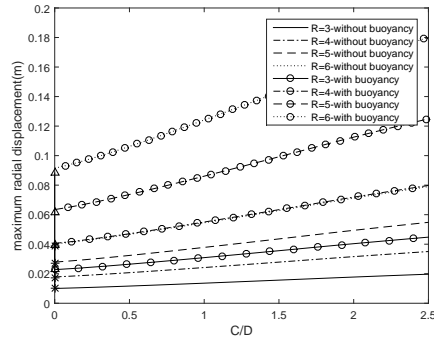
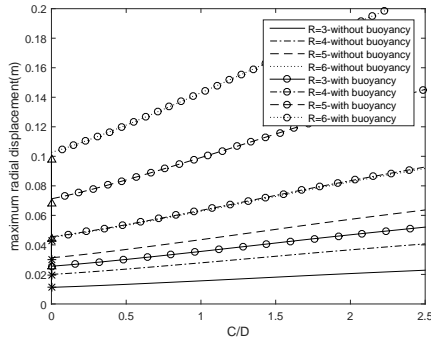
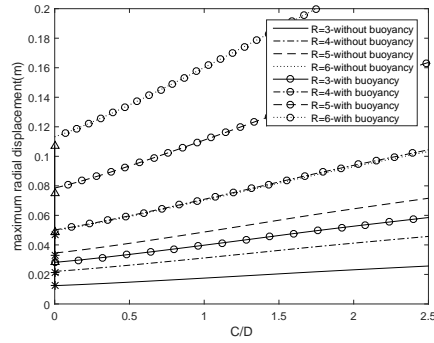
(g) $d/D = 1/25$ (h) $d/D = 1/30$ (i) $d/D = 1/35$ (j) $d/D = 1/40$

Figure 3.16: Relationship between maximum radial displacements and cover-to-diameter C/D values for models in with and without buoyancy in varied thickness-to-diameter ratio d/D of the tunnel cross-section in clayey sand. Vertical lines include the optimal C/D where radial displacement is minimal.

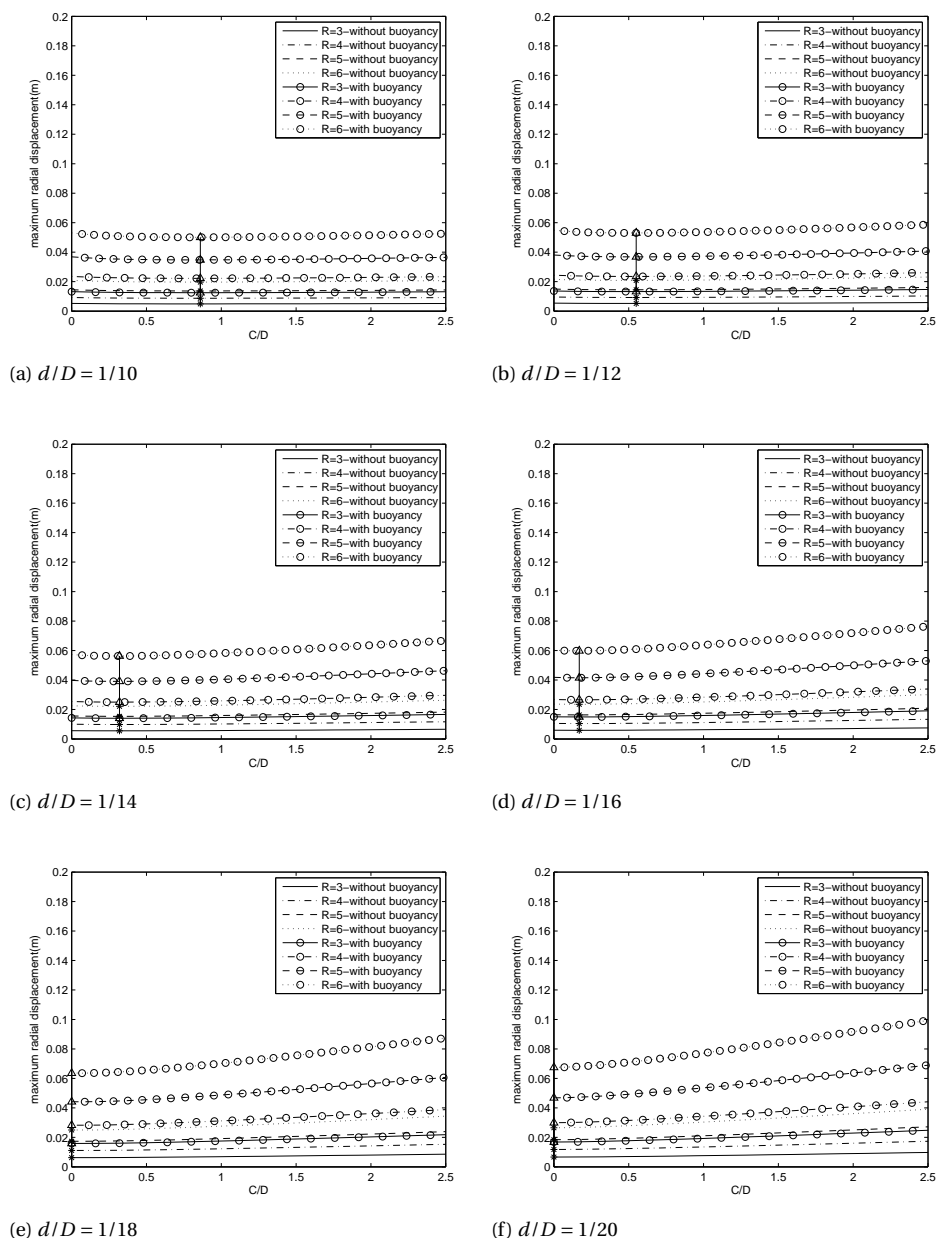


Figure 3.17: Relationship between maximum radial displacements and cover-to-diameter C/D values for models in with and without buoyancy in varied thickness-to-diameter ratio d/D of the tunnel cross-section in clay. Vertical lines include the optimal C/D where radial displacement is minimal(continue in next page).

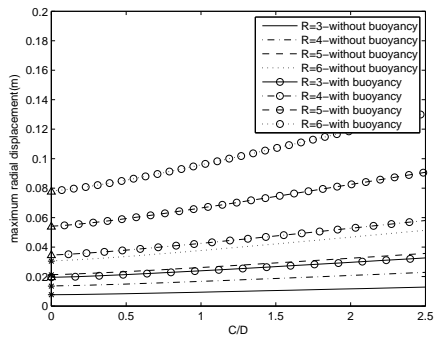
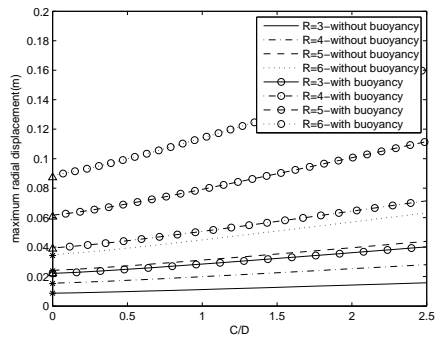
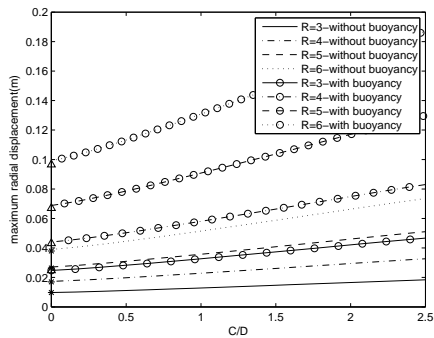
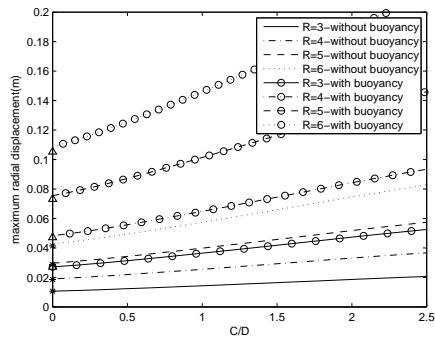
(g) $d/D = 1/25$ (h) $d/D = 1/30$ (i) $d/D = 1/35$ (j) $d/D = 1/40$

Figure 3.17: Relationship between maximum radial displacements and cover-to-diameter C/D values for models in with and without buoyancy in varied thickness-to-diameter ratio d/D of the tunnel cross-section in clay. Vertical lines include the optimal C/D where radial displacement is minimal.

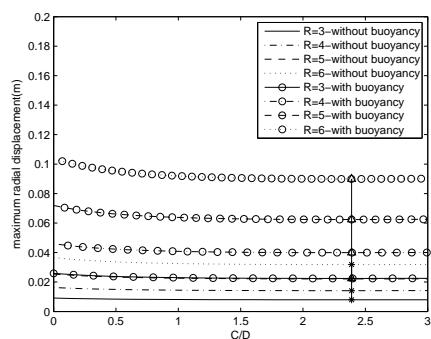
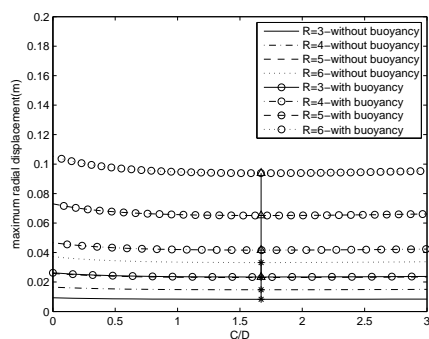
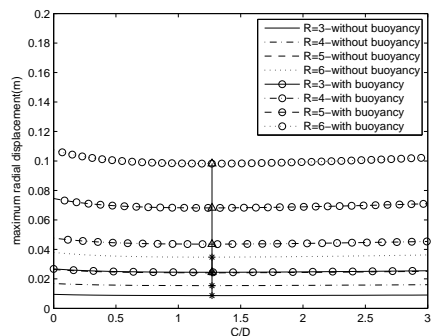
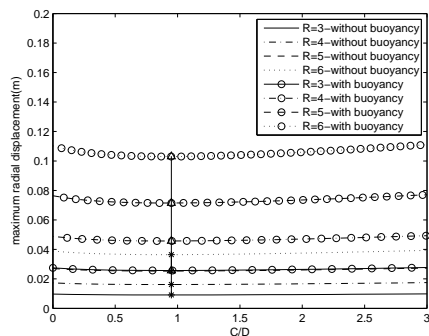
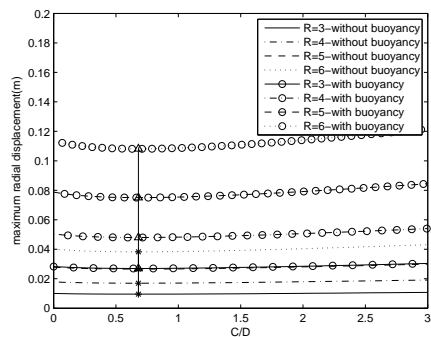
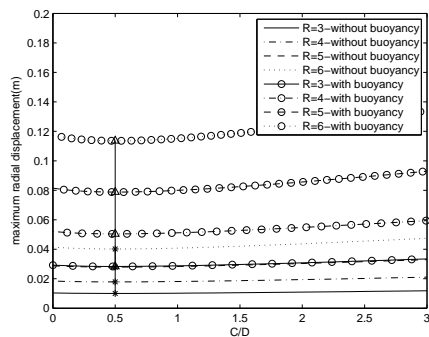
(a) $d/D = 1/10$ (b) $d/D = 1/12$ (c) $d/D = 1/14$ (d) $d/D = 1/16$ (e) $d/D = 1/18$ (f) $d/D = 1/20$

Figure 3.18: Relationship between maximum radial displacements and cover-to-diameter C/D values for models in with and without buoyancy in varied thickness-to-diameter ratio d/D of the tunnel cross-section in organic clay. Vertical lines include the optimal C/D where radial displacement is minimal(continue in next page).

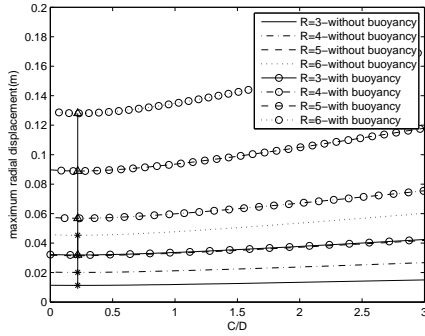
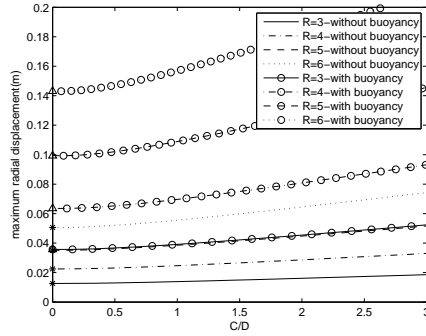
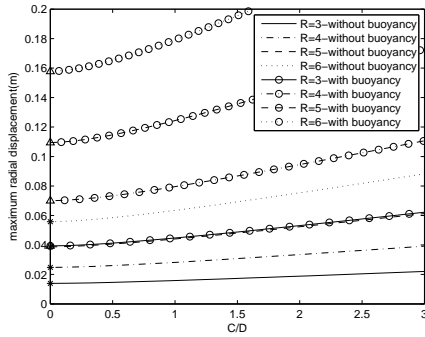
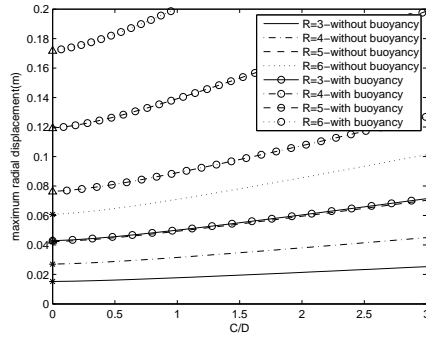
(g) $d/D = 1/25$ (h) $d/D = 1/30$ (i) $d/D = 1/35$ (j) $d/D = 1/40$

Figure 3.18: Relationship between maximum radial displacements and cover-to-diameter C/D values for models in with and without buoyancy in varied thickness-to-diameter ratio d/D of the tunnel cross-section in organic clay. Vertical lines include the optimal C/D where radial displacement is minimal.

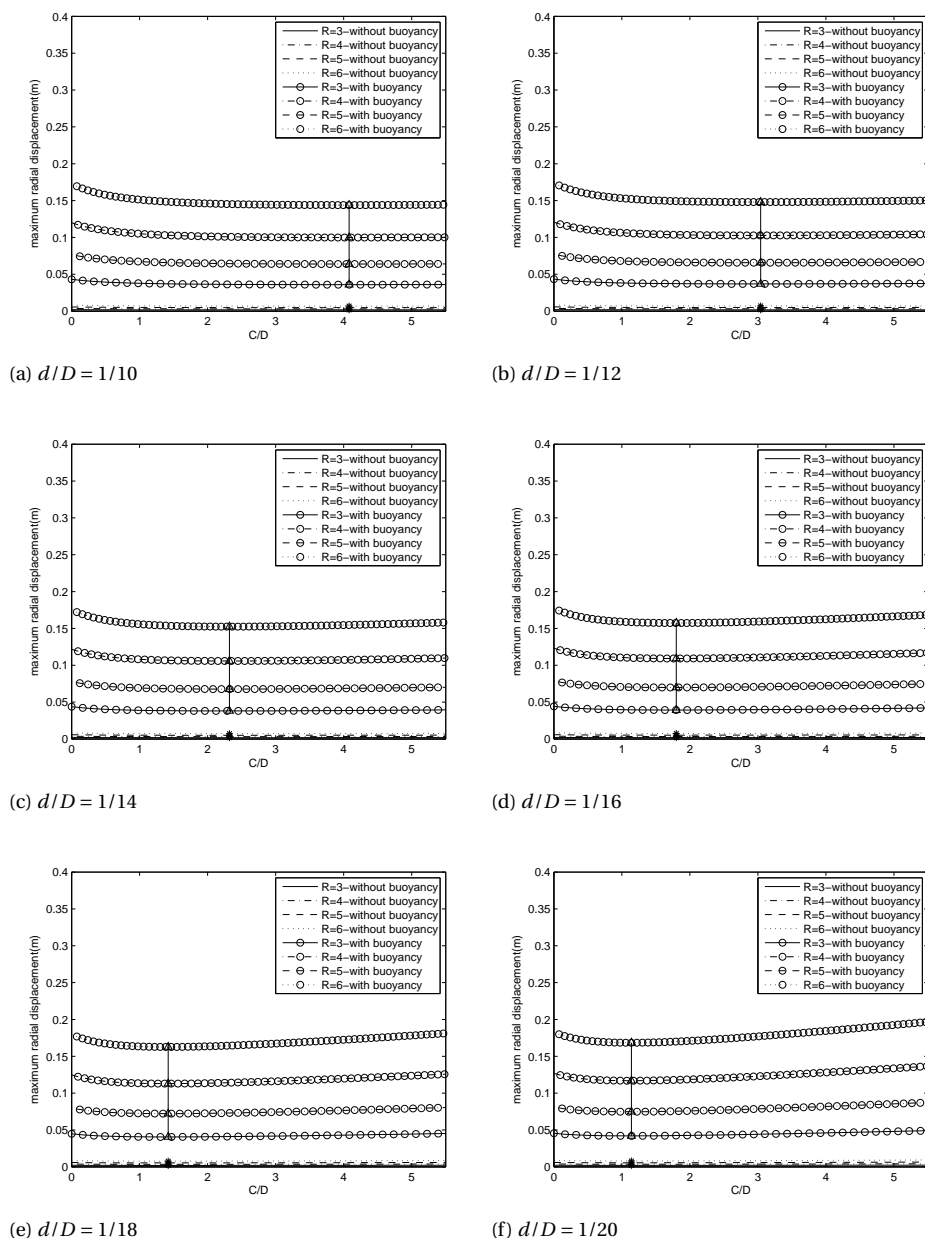


Figure 3.19: Relationship between maximum radial displacements and cover-to-diameter C/D values for models in with and without buoyancy in varied thickness-to-diameter ratio d/D of the tunnel cross-section in peat. Vertical lines include the optimal C/D where radial displacement is minimal(continue in next page).

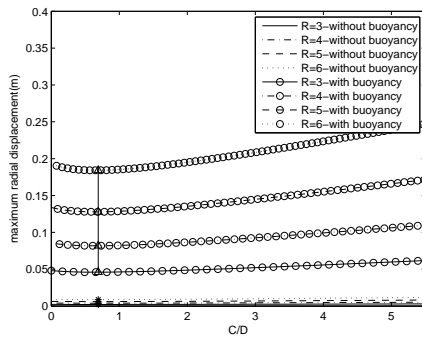
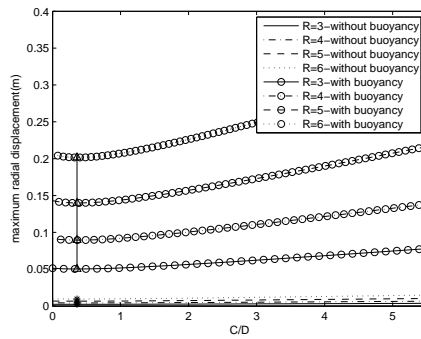
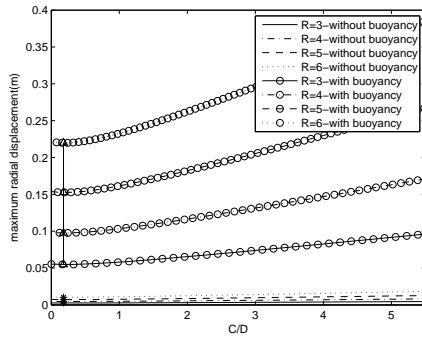
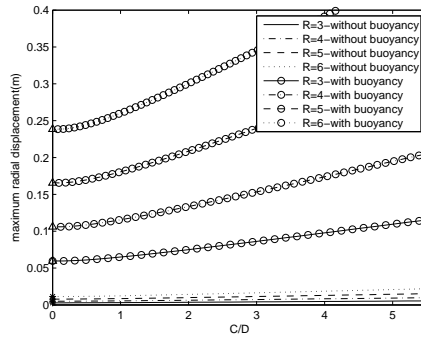
(g) $d/D = 1/25$ (h) $d/D = 1/30$ (i) $d/D = 1/35$ (j) $d/D = 1/40$

Figure 3.19: Relationship between maximum radial displacements and cover-to-diameter C/D values for models in with and without buoyancy in varied thickness-to-diameter ratio d/D of the tunnel cross-section in peat. Vertical lines include the optimal C/D where radial displacement is minimal.

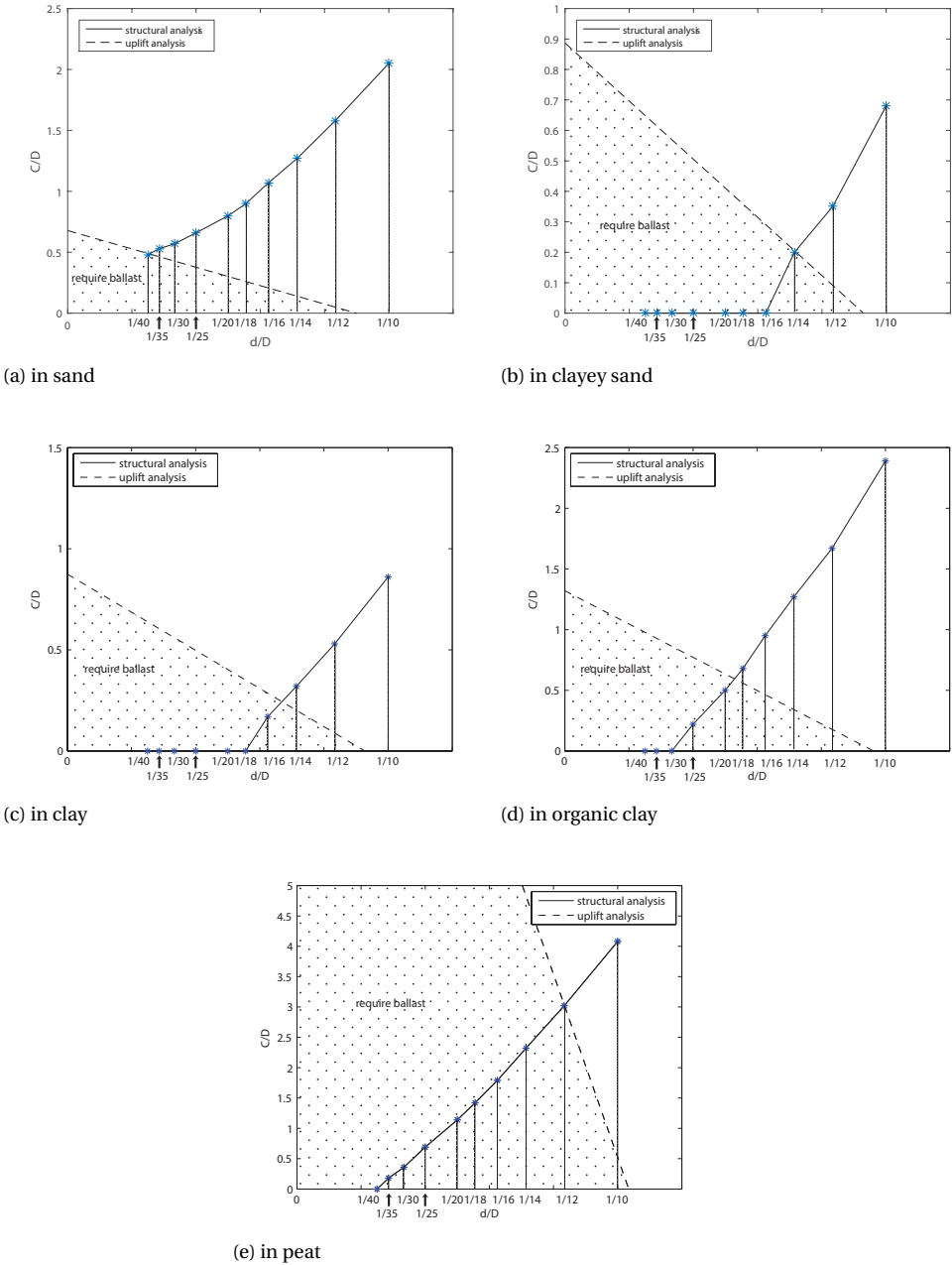


Figure 3.20: Optimal cover-to-diameter ratio C/D values for shallow tunnels

4

GROUND MOVEMENTS AND EFFECTS ON BUILDINGS

Ideas can come from anywhere and at any time. The problem with making mental notes is that the ink fades very rapidly.

Rolf Smith

Assessing the impact of underground construction on existing structures in urban areas is an important topic during design. In this chapter, the extent of the zones affected by tunnelling is estimated, where existing foundations are influenced based on the investigation of surface and subsurface settlements. The extent of the areas where building deformation exceeds allowable settlements is presented, which will provide a preliminary assessment during design on the risk on existing structures, based on allowable settlement u_{max} and slope ω_{max} . A more accurate impact area of shield tunnelling on nearby pile foundations is proposed.

This chapter is based on papers that have been published in ITA WTC 2016 Congress and 42nd General Assembly [Vu et al. \(2016a\)](#) and Tunnelling and Underground Space Technology [Vu et al. \(2015a\)](#). Section 4.2 has been expanded

4.1. INTRODUCTION

Shield tunnelling is often used in constructing underground infrastructure in cities due to the ability to limit settlements and damage to existing buildings. However, in an urban environment with soft soil overburden and buildings on pile foundations such as the North-South Line project in Amsterdam, there is a tendency to design the tunnel well below the surface and below the pile tip level in order to reduce interaction between tunnelling process and piles. This results in deep tunnels and deep station boxes. When the tunnels are located close to the surface and above the pile tip level, this would reduce the required depth of the station boxes and the construction cost. Moreover, other benefits of shallow tunnels are the low operational cost in the long-term and shorter traveling time from the surface to the platforms. Still, the tunnels should be constructed in such a manner that existing buildings are not structurally damaged, which results in a minimum required distance between tunnelling process and existing buildings.

The previous chapters studied the effects of the C/D ratio on the stability when tunnelling and the structural deformations of the tunnel linings. These stability and deformations lead to ground movements around the tunnel and settlements on the surface when tunnelling and have influence on existing buildings. In this chapter, the extent of the area that is influenced by tunnelling will be investigated with the allowable settlement and slope which are derived from the preliminary risk assessment in order to determine the limit distance from tunnelling to existing foundations without inducing too large building deformation. This study takes a look at the ground movements both at the surface and subsurface when tunnelling in soft soils with deep foundations with the following targets:

- Define the areas where ground movements remain below the acceptable limits for the buildings.
- Estimate the effects of the C/D ratio on the extent of this limited ground movement area.

In this chapter, Section 4.2 introduces background definitions of ground movements and assessments of risk of building damage induced by bored tunnelling. Section 4.3 estimates the effects of the C/D ratio on surface settlement. The dependence of subsurface settlements on the C/D ratio is shown in Section 4.4. Conclusions of the impact of shallow tunnelling on ground movements and existing buildings are presented in Section 4.5.

4.2. GROUND MOVEMENT DEFINITIONS AND RISK ASSESSMENT

4.2.1. GROUND MOVEMENT DEFINITIONS

SURFACE SETTLEMENTS

According to [Mair and Taylor \(1999\)](#), the components of ground movements due to tunnelling are: soil movements at the tunnelling face, ground displacements along the shield due to the overcutting and the shape of TBM machines, ground movements at the tail behind the shield and consolidation settlements. Figure 4.1 shows the three dimensional settlement trough on the surface in green field conditions.

From analyzing empirical data of many shield tunnels, [Peck \(1969\)](#) firstly presented the settlement trough on the surface induced by tunnelling in soft soil as a Gaussian distribution. This is also confirmed by other authors ([Cording and Hansmire, 1975](#); [Mair et al.,](#)

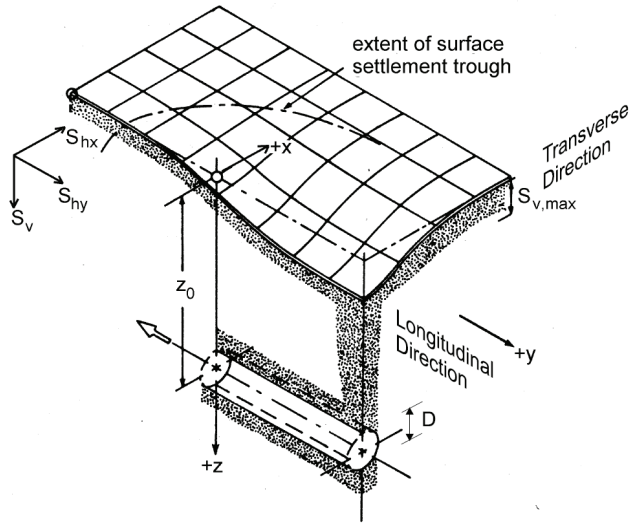


Figure 4.1: Surface settlement trough induced by tunnelling (Franzius, 2004)

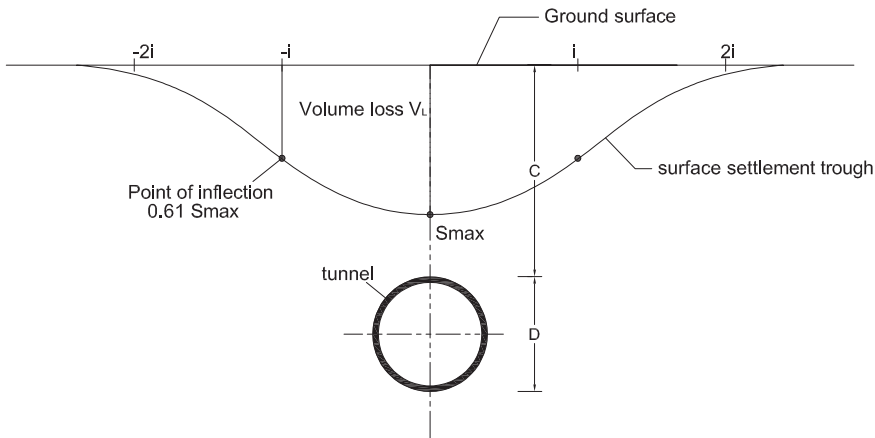


Figure 4.2: Transverse settlement trough due to tunnelling (Peck, 1969)

1993; Ahmed and Iskander, 2010). Even though some studies show that there are some deviations of the Gaussian distribution in some particular cases (Celestino et al., 2000; Jacobsz, 2003; Vorster, 2006; Farrell et al., 2012) and in Japan (JSSMFE, 1993), the Gaussian curve is still used widely in research and practical design, especially in the Anglo-Saxon countries. In this study, the Gaussian curve is used to investigate the ground movement when tunnelling in order to find the effects on existing structures.

The transverse settlement shape of the ground surface shown in Figure 4.2 as a Gaussian distribution (Peck, 1969) can be estimated from the maximum settlement $S_{v,max}$ at the surface directly above the tunnel location and the trough width i as follows:

$$s_v = S_{v,max} \exp\left(\frac{-x^2}{2i^2}\right) \quad (4.1)$$

The shape of curve is determined by the position of the inflection point i . The width of the settlement trough depends on the depth of the tunnel z_0 and the soil parameters. O'Reilly and New (1982) gave the relationship:

for cohesive soils:

$$i = 0.43z_0 + 1.1 \quad (4.2)$$

and for granular soils:

$$i = 0.28z_0 - 0.1 \quad (4.3)$$

This relationship was also compared by Mair and Taylor (1999) to the relations for settlement trough width and depth of tunnel axis from many authors and recommended for practical purposes.

The volume of settlement trough per unit tunnel length can be estimated by:

$$V_s = \sqrt{2\pi} i S_{v,max} \simeq 2.5 i S_{v,max} \quad (4.4)$$

For a circular tunnel, V_s is often calculated via the volume loss V_L as the percentage of the notional excavated tunnel volume (Mair et al., 1993):

$$V_s = V_L \frac{\pi D^2}{4} \quad (4.5)$$

According to Cording and Hansmire (1975), when tunnelling in drained conditions, V_s is less than the volume loss around the tunnel due to dilation and when tunnelling in undrained conditions, V_s equals volume loss around the tunnel. In calculation, V_s is often assumed equal to the volume loss around the tunnel. The volume loss around tunnel includes volume loss caused by deformations due to face support, passage of the tunnelling machine and the annular gap grouting (Maidl, 2012). The detailed calculation of volume loss is presented in Chapter 5.

From Equations 4.4 and 4.5, the maximum transverse settlement can be calculated as:

$$S_{v,max} = \sqrt{\frac{\pi}{2}} \frac{V_L D^2}{4i} \quad (4.6)$$

Therefore, the transverse settlement trough can be described as:

$$s_v = \sqrt{\frac{\pi}{2}} \frac{V_L D^2}{4i} \exp\left(\frac{-x^2}{2i^2}\right) \quad (4.7)$$

The horizontal component of the displacement can damage buildings on the surface when tunnels are constructed in the urban area. O'Reilly and New (1982) proposed the following to estimate the horizontal displacement for tunnelling in clays:

$$s_h = \frac{x}{z_0} s_v \quad (4.8)$$

According to Attewell and Woodman (1982), the vertical settlement in the longitudinal direction on the surface induced by tunnelling can be described as:

$$s_v(y)_{(x=0)} = S_{v,max} \phi(y) \quad (4.9)$$

where y is the longitudinal coordinate and $\phi(y)$ is the cumulative probability function, estimated as:

$$\phi(y) = \frac{1}{i_y \sqrt{2\pi}} \int_{-\infty}^y e^{-\frac{y^2}{2i_y^2}} dy \quad (4.10)$$

where i_y is the trough width parameter of the longitudinal settlement. It is often assumed that $i_x = i_y$.

Attewell and Woodman (1982) also showed the horizontal displacement in the longitudinal direction as:

$$s_h(y)_{(x=0)} = \frac{V_L D^2}{8z_0} e^{-\frac{y^2}{2i_y^2}} \quad (4.11)$$

Another important assessment in tunnelling design is the slope, which can be estimated as the first derivative of the settlement trough as:

$$\omega \approx \tan \omega = s'_v = -\frac{S_{v,max}}{i^2} x \exp\left(\frac{-x^2}{2i^2}\right) = -\sqrt{\frac{\pi}{2}} \frac{V_L D^2}{4i^3} x \exp\left(\frac{-x^2}{2i^2}\right) \quad (4.12)$$

Figure 4.3 presents the relationship between maximum settlement $S_{v,max}$ with the C/D ratio in cohesive and granular soil for a tunnel with diameter $D = 6m$ and $V_L = 0.5\%$. This figure shows that the deeper the tunnel is, the smaller the maximum settlement $S_{v,max}$ at surface is. From Equation 4.2 and 4.3, it then follows that settlements are spread over a larger surface area for a fixed volume loss.

Figure 4.4 shows the transverse settlement, horizontal displacement and the slope on the surface in the case of tunnel with diameter $D = 6m$, at the depth $z_0 = 6m$ or $C/D = 0.5$ in cohesive soil.

This figure agrees with the conclusion from Mair and Taylor (1999) that $S_{h,max}$ occurs at the position of the inflection points of the settlement trough. And as expected, the maximum slope of surface settlement appears at the position of inflection points of the settlement trough.

SUBSURFACE SETTLEMENT

Based on the results of centrifuge test and empirical data, Mair et al. (1993) showed that the subsurface settlement profile also distributes as the Gaussian curve. The width of settlement trough at the depth z depends on the depth of the tunnel z_0 via a coefficient K depending on depth as:

$$i = K(z_0 - z) \quad (4.13)$$

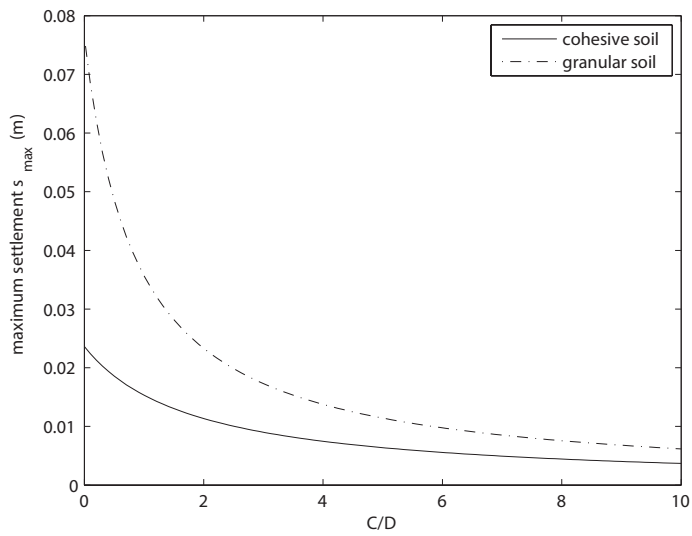


Figure 4.3: Relationship between $S_{v,max}$ and C/D with tunnel diameter $D = 6m$

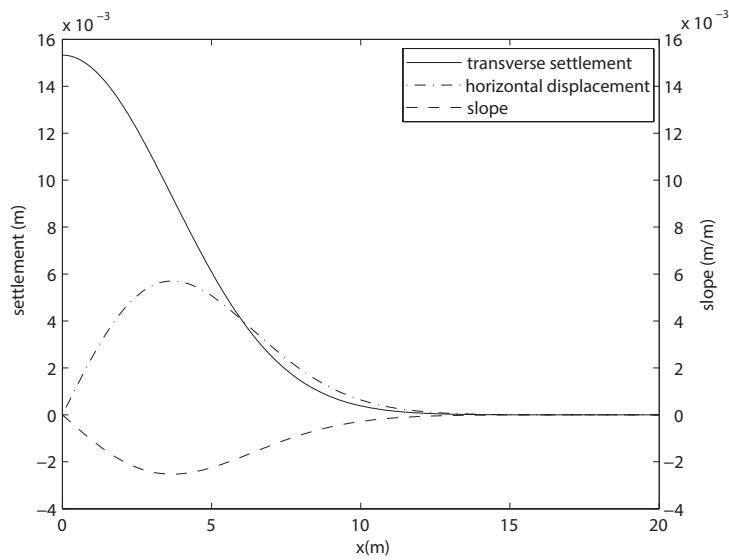


Figure 4.4: Surface settlement troughs and slope curve due to tunnelling

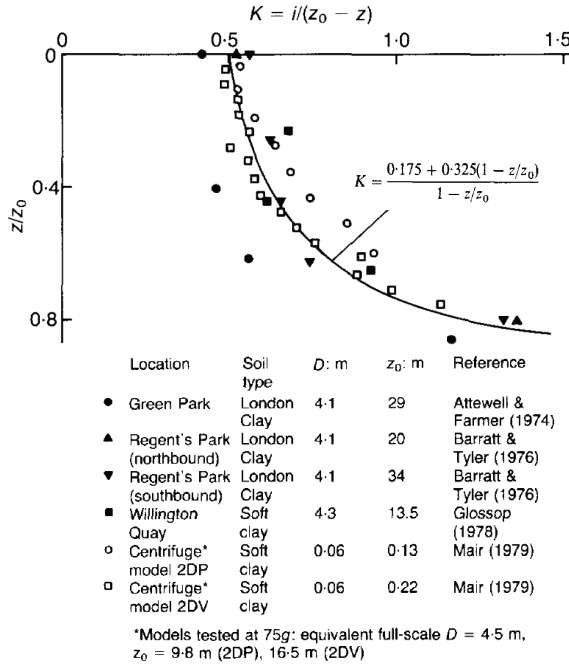


Figure 4.5: The trough width parameter K for the subsurface settlement profiles above the tunnel in clays (Mair et al., 1993)

with the K value is estimated as:

$$K = \frac{0.175 + 0.325(1 - z/z_0)}{1 - z/z_0} \quad (4.14)$$

The trough width parameter K was derived from the analysis of observation data from the Heathrow Express trial tunnel and the Jubilee Line Express project for the subsurface settlements above the tunnel in clays as shown in Figure 4.5.

From Equations 4.6, 4.13 and 4.14, the maximum subsurface settlement can be estimated as:

$$\frac{S_{v,max}}{R} = \sqrt{\frac{\pi}{2}} \frac{V_L}{0.175 + 0.325(1 - z/z_0)} \frac{R}{z_0} \quad (4.15)$$

where R is the tunnel radius.

The normalized maximum settlement against $R/(z_0 - z)$ is shown in Figure 4.6. The curve A is derived from Equation 4.13 with $K=0.5$. Curves B and C are derived from Equation 4.15 with volume loss $V_L = 1.4\%$ and $R/z_0 = 0.1$ and 0.06 , respectively. This graph also includes the field data from tunnels constructed in London clay. The plastic solution given by Taylor (1993) is also used to compare. It shows in this figure that the field data is in agreement with these methods.

Other studies by Moh et al. (1996), Grant and Taylor (2000) and Jacobsz (2003) based on

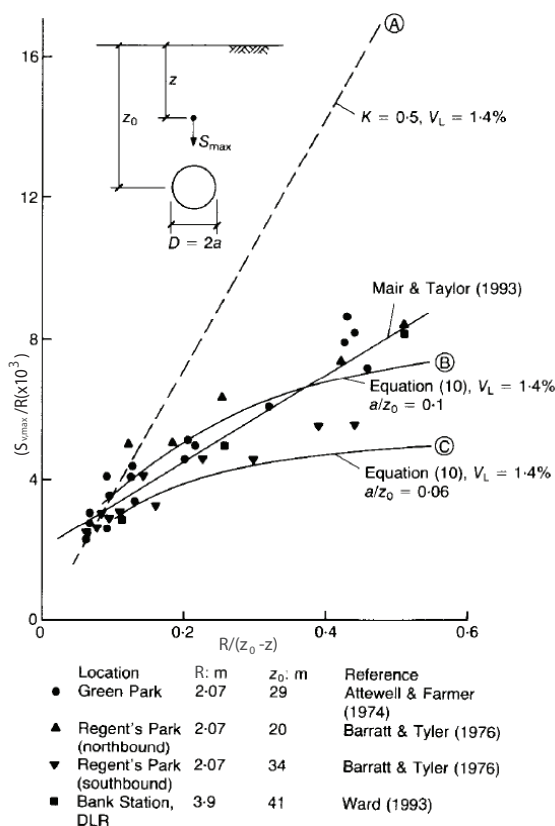


Figure 4.6: Subsurface settlement above the tunnel center line (Mair et al., 1993)

Mair et al. (1993) proposed a limited change of K in various kinds of soil. Ahmed and Iskander (2010) noted that the equation proposed by Mair et al. (1993) to predict subsurface settlement and horizontal displacement in clay yields acceptable results in sand as well from the observation of the displacement inside transparent soil models.

4.2.2. RISK OF BUILDING DAMAGE ASSESSMENT

Assessing the impact of underground construction on existing structures in urban area is important in design. Many studies have focused on the ground movements around tunnelling and the settlement trough on the surface but research focused on the ground movements that affect nearby buildings for a first assessment the stability of the buildings and the effect of tunnelling near existing deep foundation has only recently gained interest in geotechnical studies. The affected area due to tunnelling should be estimated in order to avoid the impact on the existing foundations.

The response of buildings due to tunnelling has been investigated by many authors (Rankin, 1988; Boscardin and Cording, 1989; Mair et al., 1996; Franzius, 2004; Netzel,

Table 4.1: Typical values of maximum building slope and settlement for damage risk assessment (Rankin, 1988)

Risk Category	Maximum slope of building	Maximum settlement of building (mm)	Description of risk
1	Less than 1/500	Less than 10	Negligible; superficial damage unlikely
2	1/500 - 1/200	10-50	Slight; possible superficial damage which is unlikely to have structural significance
3	1/200 - 1/50	50-75	Moderate; expected superficial damage and possible structural damage to buildings, possible damage to relatively rigid pipelines
4	Greater than 1/50	Greater than 75	High; expected structural damage to buildings. Expected damage to rigid pipelines, possible damage to other pipelines

Table 4.2: Relationship between category of damage and limiting tensile strain (after Boscardin and Cording (1989))

Category of damage	Normal degree of severity	Limiting tensile strain (%)
0	Negligible	0-0.05
1	Very slight	0.05-0.075
2	Slight	0.075-0.15
3	Moderate*	0.16-0.3
4 to 5	Severe and very severe	>0.3

*Note: Boscardin and Cording (1989) describe the damage corresponding to the tensile strain in the range 0.015 – 0.3% as moderate to severe. However, none of the cases quoted by them exhibit severe damage for this range of strains. There is therefore no evidence to suggest that tensile strains up to 0.3% will result in severe damage.

2009; Giardina, 2013). Table 4.1 shows the value of maximum slope and settlement for the building with a category damage risk assessment proposed by Rankin (1988). The Limiting Tensile Strain Method proposed by Boscardin and Cording (1989) has been widely used in design. This method has four steps: prediction of the greenfield movement; projection of greenfield ground movement on the building; determination of induced building strains and classification of damage related to strain levels. The category of damage and the relationship with limiting tensile strain are shown in Table 4.2. Burland (1995) presented a damage category chart for horizontal strain and deflection ratio in the case of $L/H = 1$ in line with the damage category in Table 4.2 in Figure 4.7.

Mair et al. (1996) proposed a three stage methodology for the assessment of risk of building damage induced by bored tunnelling as followings:

- Stage 1 - Preliminary Assessment: A building has a negligible risk of damage when its settlement less than 10mm. It can be checked with an additional assessment with slope exceeding 1/500.
- Stage 2 - Second Stage Assessment: The maximum tensile strain is calculated with the green field conditions. Buildings are assumed to have no stiffness and follow the green field settlement trough. The possible damage category is derived.
- Stage 3 - Detailed Evaluation: Detailed evaluation is carried out for buildings classified in Stage 2 at risk of category 3 or greater. The calculation is carried out for structural continuity, foundations and soil-structure interaction. If the building remains in damage category 3 or greater, protective methods will be required.

The Eurocode 7 (NEN-EN 1997-1, 1997) also indicates limiting values for structural de-

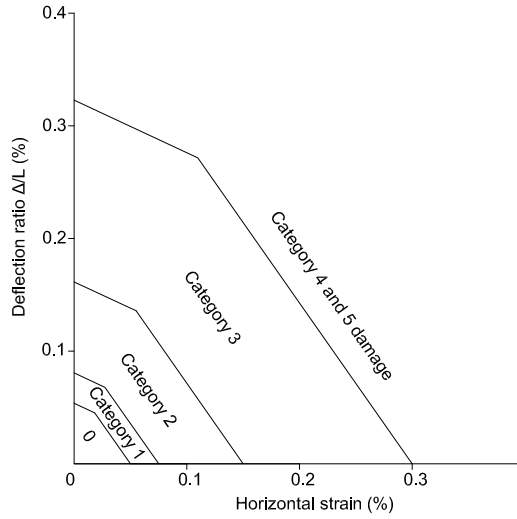


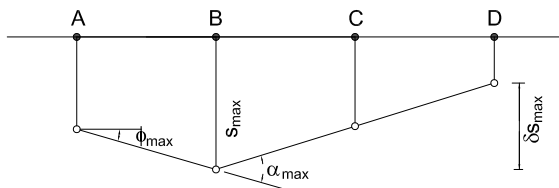
Figure 4.7: Damage category chart for $L/H = 1$, hogging mode (Burland, 1995)

formations and foundation movements. In order to prevent the occurrence of a serviceability limit state in open framed structures, infilled frames and load bearing or continuous brick walls, the maximum acceptable relative rotations are in the range from about $1/2000$ to about $1/300$. For many structures in general, a maximum relative rotation of $1/500$ is acceptable. An ultimate limit state of the relative rotation is about $1/150$. For settlements, the Eurocode 7 indicates that for total settlements up to 50mm are acceptable and larger settlements can be acceptable if the relative rotations remain within acceptable limits.

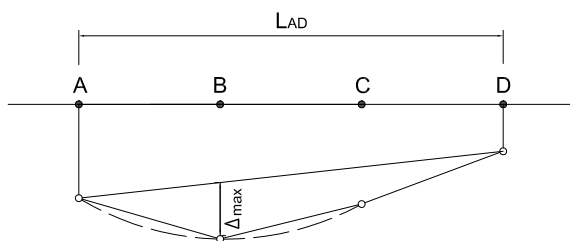
In this study, the value for category 1 in Table 4.1 which is the lowest damage category to the building is used, setting the maximum slope of building $\omega_{max} = 1/500$ and maximum settlement of building $u_{max} = 10\text{mm}$. These allowable values are also applied in the preliminary assessment in the three stage methodology for the assessment of risk of building damage induced by bored tunnelling indicated in Mair et al. (1996) and Burland et al. (2001) and in the acceptable range of the Eurocode 7. The influence of building stiffness and the difference between sagging and hogging zones of the settlement trough in this risk assessment is, therefore, not taken into account in this study.

4.3. EFFECTS OF THE C/D RATIO ON SURFACE SETTLEMENT

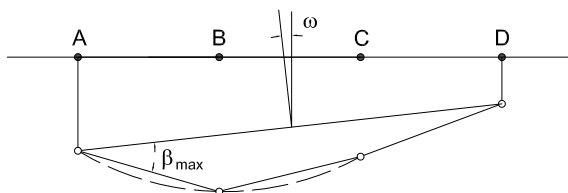
In designing a tunnel under existing structures, it is necessary to determine the extent to which the building is influenced by the tunnel. The theoretical influence zone is often presented via the distance from the surface building with shallow foundation to the tunnel axis. In this study, the relationship between the C/D ratio and this distance is



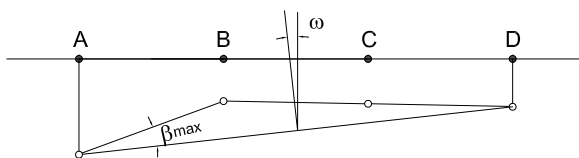
(a) definitions of settlement s , differential settlement δs , rotation ϕ and angular strain α



(b) definitions of relative deflection Δ and deflection ratio Δ/L



(c) definitions of tilt ω and relative rotation β in sagging mode



(d) definitions of tilt ω and relative rotation β in hogging mode

Figure 4.8: Definitions of foundation movement (NEN-EN 1997-1, 1997)

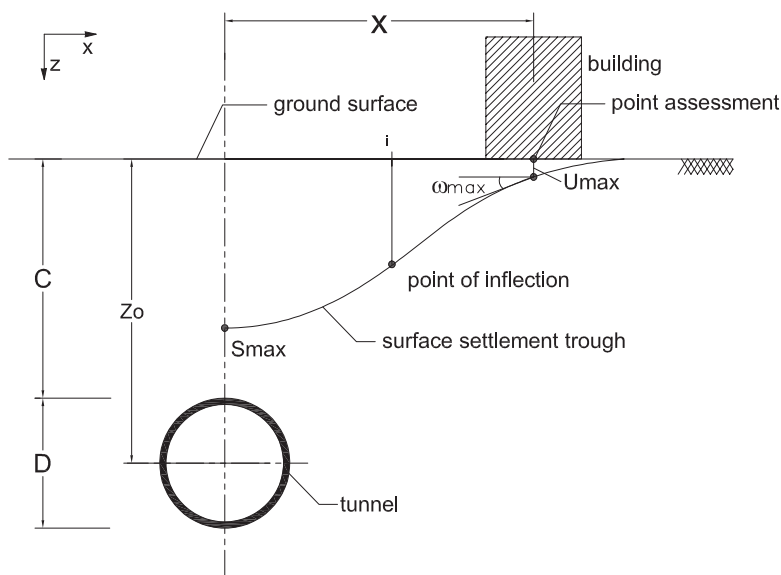


Figure 4.9: Tunnel and existing surface buildings

estimated when the surface settlement reaches the allowable settlement $u_{max} = 10\text{mm}$ and allowable slope $\omega_{max} = 1/500$ corresponding with the risk category 1 in table 4.1. Figure 4.9 illustrates this problem. The relation between the maximum allowable settlement u_{max} and the horizontal distance to the tunnel centre line x is given by:

$$u_{max} = S_{v,max} \exp\left(\frac{-x^2}{2i^2}\right) = \sqrt{\frac{\pi}{2}} \frac{V_L D^2}{4i} \exp\left(\frac{-x^2}{2i^2}\right) \quad (4.16)$$

Solving this equation, the distance x from the building to tunnel axis corresponding with settlement u_{max} is:

$$x = \sqrt{-2i^2 \ln\left(\frac{u_{max}}{S_{v,max}}\right)} = \sqrt{-2i^2 \ln\left(\frac{u_{max} i 4\sqrt{2}}{V_L D^2 \sqrt{\pi}}\right)} \quad (4.17)$$

Figure 4.10 shows the relationship between x/D and C/D ratios in the case of a tunnel with diameter $D = 6\text{m}$ in cohesive soil for various volume loss V_L with the allowable settlement $u_{max} = 10\text{mm}$. The area inside the curve represents the zone where allowable settlements are exceeded and the tunnel is too close to the building. This unsafe area is also determined for particular values of V_L . This figure indicates that for larger volume loss, larger distances x and C/D ratios are required. With C/D and x/D inside the unsafe area for volume loss $V_L = 0.5\%$, the surface settlement is larger than u_{max} . On the boundary of this area, the surface settlement equals u_{max} . In the case of $V_L = 0.5\%$, it also shows that with C/D ratio more than 1.25 the surface settlement is always less than u_{max} . With x/D from 0.522 to 0.57 or x from 3.1 to 3.4m there are two values of C/D ratio

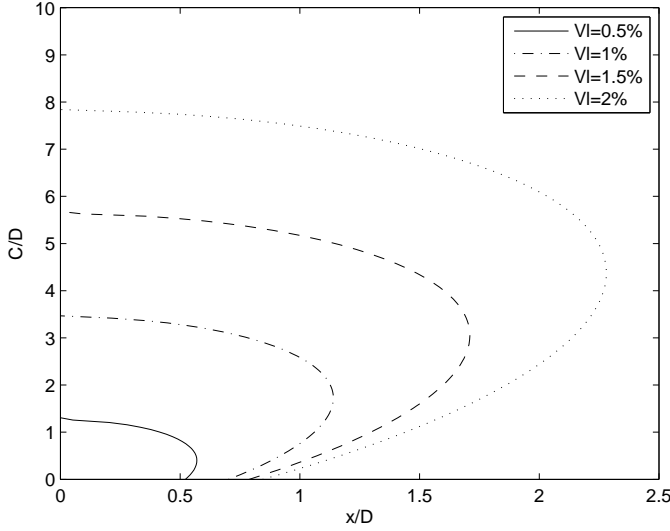


Figure 4.10: Relationship between x/D and C/D ratios in the case of tunnel with $D = 6m$ in cohesive soil and the allowable settlement $u_{max} = 10mm$

or two depths of the tunnel that the settlement of the building equals u_{max} . With x/D more than 0.574 or x larger than $3.4m$, the surface settlement is always less than u_{max} again.

When the slope is considered with $\omega_{max} = 1/500$, the following equation is derived from Equation 4.12:

$$\omega_{max} = -\frac{S_{v,max}}{i^2} x \exp\left(\frac{-x^2}{2i^2}\right) \quad (4.18)$$

Solving this equation, the distance x from the building to tunnel axis corresponding with slope $\omega_{max} = 1/500$ is given by:

$$x = \frac{\omega_{max} i^2}{S_{v,max} \sqrt{-\frac{\omega_{max}^2 i^2}{S_{v,max}^2 \text{Lambert}W\left(-\frac{\omega_{max}^2 i^2}{S_{v,max}^2}\right)}}} \quad (4.19)$$

or

$$x = \frac{\omega_{max} i^3 \sqrt{2}}{\sqrt{\pi} V_L D^2 \sqrt{-\frac{2\omega_{max}^2 i^4}{\pi V_L^2 D^4 \text{Lambert}W\left(-\frac{32\omega_{max}^2 i^4}{\pi V_L^2 D^4}\right)}}} \quad (4.20)$$

where the *Lambert* tW function $W(x)$ is a set of solutions of the equation $x = W(x) \exp W(x)$. Figure 4.11 shows the relationship between x/D and C/D in the case of a tunnel in cohe-

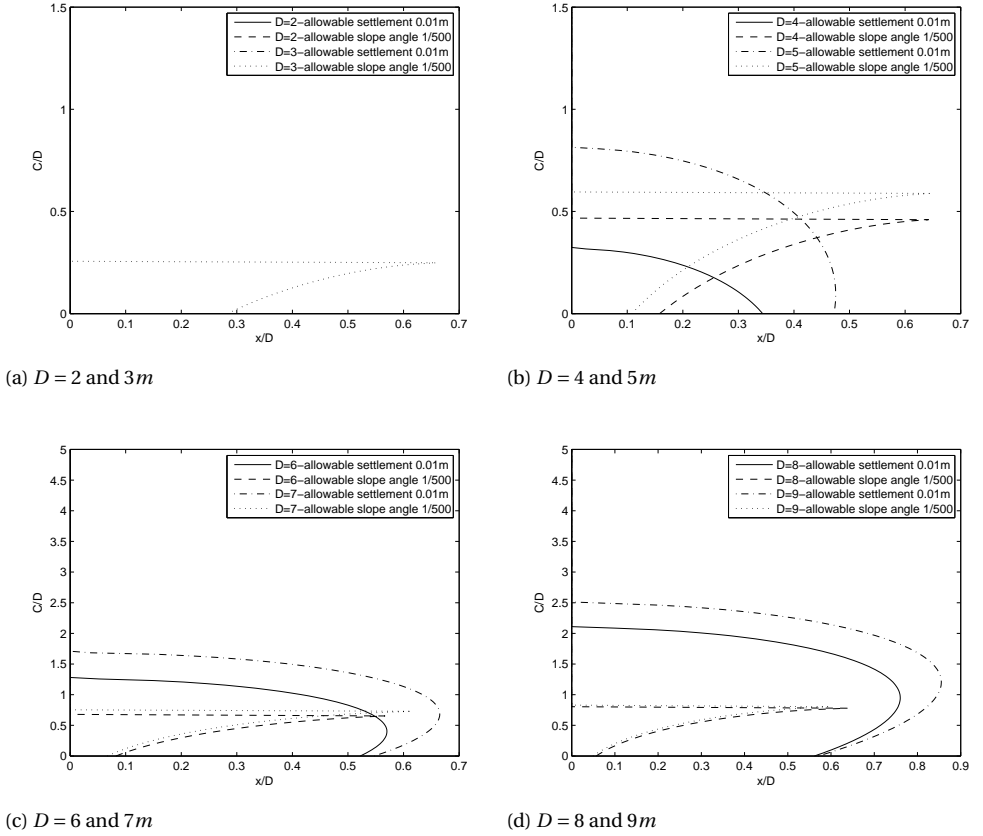


Figure 4.11: Relationship between x/D and C/D with various tunnel diameter D in cohesive soil and $V_L = 0.5\%$

sive soil with allowable settlement of the building $u_{max} = 10mm$ and the allowable slope $\omega_{max} = 1/500$ and $V_L = 0.5\%$ for various tunnel diameters D based on Equations 4.17 and 4.19. In this figure, it can be seen that the smaller the tunnel diameter D is, the smaller the unsafe area due to allowable settlement u_{max} is for a given volume loss V_L . In this case when the diameter $D = 2$ and $3m$, the unsafe settlement area due to allowable settlement u_{max} disappears altogether. Therefore, there exists a value of D that $S_{v,max} \leq u_{max}$ for any values of x and C . The settlement is maximum at the location directly above the tunnel axis $x = 0$ and solving Equation 4.6 for $S_{v,max} = u_{max}$ yields the diameter D_0 where the maximum settlement is always less than u_{max} , regardless of the cover. These D_0 values are shown in Table 4.3. This table shows that this phenomenon only occurs for tunnels at the diameters that are more applicable to microtunnelling than TBM bored tunnels. This table also shows that the D_0 value in the case of tunnelling in cohesive soils is significantly larger than in the case of tunnelling in granular soils with the same volume loss V_L .

Table 4.3: Diameter D_0 value

Volume loss V_L (%)	Diameter D_0 (m)	
	Cohesive soil	Granular soil
0.05	17.7	8.15
0.01	10.28	3.58
0.015	7.64	1.79
0.02	6.24	0
0.5	3.42	0
1	2.25	0
2	1.51	0

In Figure 4.11, when the tunnel diameter D is larger than $7m$, the unsafe area where the slope ω_{max} in governing always falls inside the area due to allowable settlement. It means that with $V_L = 0.5\%$, in cohesive soil, and the tunnel diameter larger than $7m$, the allowable slope ω_{max} need not be assessed.

4.4. EFFECTS OF THE C/D RATIO ON SUBSURFACE SETTLEMENT

When tunnelling in urban areas, tunnels are sometimes designed below or near existing deep foundations. Therefore, the impact of subsurface settlement on foundations should be investigated. The previous section takes only surface settlements into account. In the case of deep foundations, the settlement and slope assessments are similar as in the case of surface settlement but assessed at the foundation depth L_p . In pile systems, the most important assessment is the ground movement at the tip of the pile due to its effect on the bearing capacity of the pile (NEN-EN 1997-1, 1997). In general, the assumption here is that the pile settles as much as the soil at the pile tip level. This implies fully end-bearing piles. It is assumed that for piles which are only partially end-bearing, the model presented here is conservative. Figure 4.12 shows the situation that the tunnel is constructed near a pile.

As indicated in Section 4.2.1, the subsurface settlement profile distributes as the Gaussian curve with the trough width as in Equation 4.13 and 4.14. Applying these values in Equations 4.16 and 4.18, the distance x from the building to tunnel axis corresponding with subsurface settlement u_{max} and subsurface slope ω_{max} are determined.

Figure 4.13 shows the safe and unsafe areas in the case of a tunnel with diameter $D = 6m$, and the pile foundation with depth $L_p = 6m$ based on Equation 4.15 with $V_L = 0.5\%$. The unsafe area also includes the zone where the pile tip would geometrically fall inside the tunnel. According to Dias and Bezuijen (2015), the interaction is largest when the tunnel is below the pile tips. This area is also indicated in Figure 4.13 as an area that needs special attention. From Equation 4.17, the $(\frac{C}{D})_0$ value such that settlement at the tip of the pile is always less than u_{max} for any distance to the tunnel centre line x can be estimated as:

$$\left(\frac{C}{D}\right)_0 = \frac{0.65L_p}{D} + \sqrt{\frac{\pi}{8}} \frac{V_L D}{u_{max}} - \frac{1}{2} \quad (4.21)$$

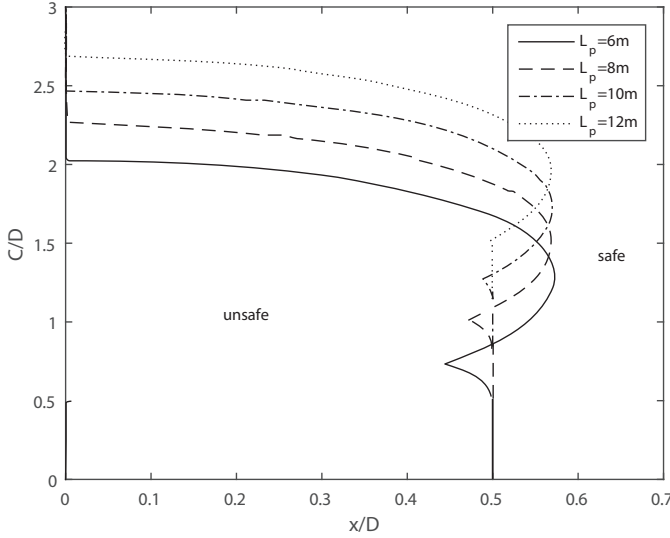


Figure 4.14: Relationship between C/D and x/D in the case of tunnel with $D = 6m$ with various L_p with $V_L = 0.5\%$

In Figure 4.13, the $(\frac{C}{D})_0$ value equals 2.03. It also shows that for x/D from 0.32 to 0.57, there are two values of C/D such that the settlement can reach u_{max} . With x/D more than 0.57, the settlement at the pile tip is always less than u_{max} .

Figure 4.14 presents the safe and unsafe areas for various pile lengths L_p in the case of a tunnel with $D = 6m$ and $V_L = 0.5\%$. It is interesting to note that for various pile length there exists a $(\frac{x}{D})_0$ value such that the settlement of the pile tip is always less than u_{max} , which is independent of the C/D ratio. In this case $(\frac{x}{D})_0 = 0.57$. From Equation 4.17, the value of $(\frac{x}{D})_0$ can be estimated via the distance x_0 from the building to tunnel centre axis as (see Appendix B):

$$x_0 = \frac{V_L D^2 \sqrt{\pi}}{u_{max} 4 \sqrt{2} e} \approx 0.19 \frac{V_L D^2}{u_{max}} \quad (4.22)$$

Figure 4.15 shows the unsafe area of ground movement for the tunnel with $D = 6m$ and various u_{max}/V_L and C/D ratios. With particular values of C/D ratios, the smaller the u_{max}/V_L ratio is, the larger the unsafe area of ground movements is. Meanwhile, when the tunnel becomes deeper with the increase of C/D ratios, the unsafe area is wider.

Figure 4.16 shows unsafe areas for different D with $V_L = 0.5\%$. With the same C/D ratio, the unsafe area increases with increasing tunnel diameter. With a moderate or deep tunnel the surface settlement or settlement near the surface is small. As mentioned above, there is a distance x_0 for a particular tunnel diameter D that the settlement due to tunnelling is always less than u_{max} .

Figure 4.17 compares the safe areas as indicated by Kaalberg et al. (2005) and this study. Kaalberg et al. (2005) carried out a data analysis of a trial test at the Second Heinenoord

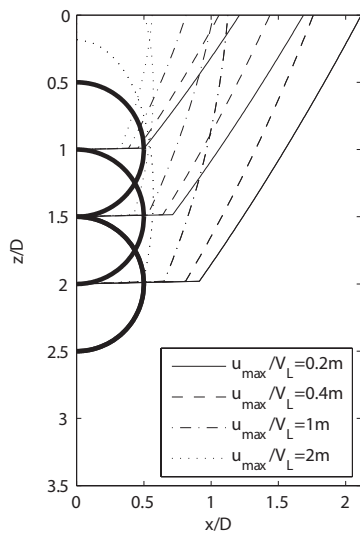


Figure 4.15: Ground movement area for tunnel with $D = 6\text{ m}$ in cohesive soil

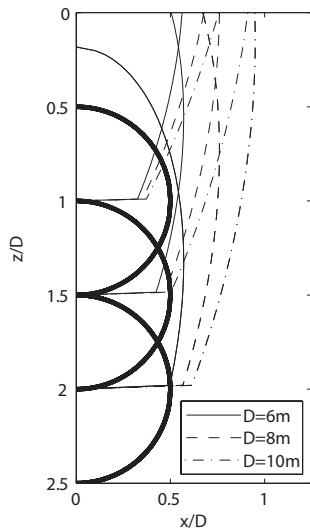


Figure 4.16: Ground movement area for tunnel in cohesive soil with $V_L = 0.5\%$

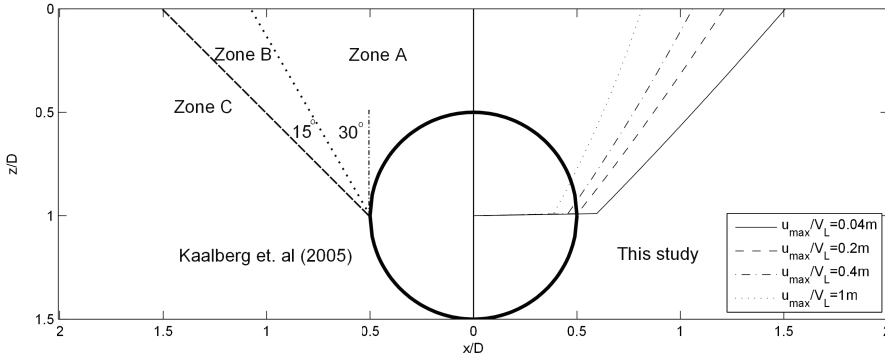


Figure 4.17: Safe zones in comparing with [Kaalberg et al. \(2005\)](#)

tunnel where 63 driven piles, 90 surface settlement points, 29 subsurface points, and 11 inclinometers were measured over a period of 2 years in order to estimate the impact of tunnelling on piles and pile toes. They also concluded that the safe distance between the piles and tunnels should be more than $0.5D$ for varying volume loss. Meanwhile, the safe area derived from this study depends on the distance, volume loss and the designed allowable settlement of the building. This figure shows that the larger the allowable settlement is, the closer the piles can be near the tunnel.

The unsafe zone A, as indicated by [Kaalberg et al. \(2005\)](#), mostly overlaps the zone where $u_{max}/V_L \geq 0.4m$ and the intermediate zone B overlaps the zone where $0.04m \leq u_{max}/V_L \leq 0.4m$. This indicates that the approach followed in this chapter and the results in the Figures 4.14 and 4.15 can be used to estimate the safe zone also for different combinations of tunnel diameter, cover and soil conditions.

4.5. CONCLUSION

Based on the investigation into surface and subsurface settlement, the extent of safe and unsafe areas due to tunnelling are presented, which will provide a preliminary assessment for the design on the risk of damage for existing structures with an allowable settlement u_{max} and slope ω_{max} . For the surface settlement assessment, it shows that the smaller the tunnel diameter D is, the smaller the unsafe area with an allowable settlement u_{max} is for a given volume loss V_L . This study derives a D_0 value such that for D less than D_0 the surface settlement is always less than the allowable settlement u_{max} . It is also found that with large diameter D , the assessment of allowable slope ω_{max} need not be taken into account. For the subsurface settlement, the analysis derives influence zones induced by shallow tunnelling based on allowable settlements u_{max} , volume loss V_L and tunnel diameter D . It is also shown that the unsafe area is larger when the C/D ratio increases. There exists a minimum distance x_0 for a particular D that for larger distances from existing structures the settlement is always less than u_{max} . Depending

on the allowable settlement u_{max} of the building, designers can determine the influence zones of shield tunnelling on surface buildings or on deep or pile foundations.

5

VOLUME LOSS IN SHALLOW TUNNELLING

The best way to have a good idea is to have a lot of ideas.

Linus Pauling

Although volume loss has an important effect in estimating the ground movements due to tunnelling in the design stage, this parameter is often determined by experience. This makes it difficult to estimate the impact on volume loss when changing project parameters like soil conditions, depth of the tunnel or sensitivity of the surroundings. This chapter investigates the relationship between volume loss and cover-to-diameter C/D ratio in shallow tunnelling. Based on a number of (empirical) relations from literature, such as the stability number method and an analysis of the bentonite and grout flows, volume loss at the face, along the shield and at the tail is determined. Long-term volume loss behind the shield is also estimated by means of consolidation. In this way a band width of achievable volume loss for future projects is derived.

This chapter is based on a paper that has been published in Tunnelling and Underground Space Technology [Vu et al. \(2016b\)](#).

5.1. INTRODUCTION

Tunnelling often leads to settlements of the soil surface due to over-excavation, soil relaxation and inefficient tail void filling. The magnitude of volume loss is influenced by tunnelling management, characteristics of the tunnelling machines, and the geotechnical conditions. In predictions of surface settlement (Peck, 1969) and subsurface settlement (Mair et al., 1993), the volume loss is often determined by engineering experience and data from previous cases. This makes it difficult to correctly assess the volume loss for a future project under radically different conditions like a shallow depth of the tunnel and/or very different soil parameters. A ground movement analysis in Chapter 4 shows the important role of volume loss for settlement calculations and in predicting the effects on existing buildings induced by tunnelling. Especially for (very) shallow tunnels near building foundations, the impact of changes in volume loss is large. This chapter aims to estimate the volume loss when tunnelling with limited C/D ratios (i.e. less than 1) in various soils with a focus on slurry shield tunnelling.

On the basis of the studies by Attewell and Farmer (1974), Cording and Hansmire (1975) and Mair and Taylor (1999), the volume loss in the tunnelling progress can be estimated by the sum of the following components as shown in Figure 5.1:

- Volume loss at the tunnelling face (in Section 5.2): soil movement towards the excavation chamber as a result of movement and relaxation ahead of the face, depending on the applied support pressures at the tunnelling face;
- Volume loss along the shield (in Section 5.3): the radial ground loss around the tunnel shield due to the moving soil into the gap between the shield and surrounding soil, which can be caused by overcutting and shield shape. The bentonite used in the tunnelling face flows into the gap, while the grout used in the shield tail also flows in the opposite direction. Due to the drop of bentonite and grout flow pressures in a constrained gap, soil can still move into the cavity when the soil pressure is larger than the bentonite pressure or grout pressure;
- Volume loss at the tail (in Section 5.4): when precast segments are placed, the advance of the shield results an annular cavity between the segments and surrounding soil. Grout is used in order to prevent surrounding soil moving into the gap. Volume loss at the tail depends on applied grouting pressure at the tail and proper volume control, where high grout volume and pressure may lead to local heave and low volume to increase settlements as indicated in Figure 5.1;
- Volume loss behind the shield tail due to consolidation (in Section 5.4): in this void along the tunnel lining, grout consolidates and forms a grout cake, and the stress changes induced in the soil may lead to long-term consolidation settlements in soil volume above the tunnel. Other causes of volume loss are shrinkage of grout and long-term lining deformations. However, their contributions to the total volume loss are small comparing to the above factors.

The total volume loss V_L in tunnelling progress can be given as:

$$V_L = V_{L,f} + V_{L,s} + V_{L,t} + V_{L,c} \quad (5.1)$$

where $V_{L,f}$ is volume loss at the tunnelling face, $V_{L,s}$ is volume loss along the shield, $V_{L,t}$ is volume loss at the tail, and $V_{L,c}$ is volume loss due to consolidation.

To illustrate the impact of the different contributions in different soil conditions, esti-

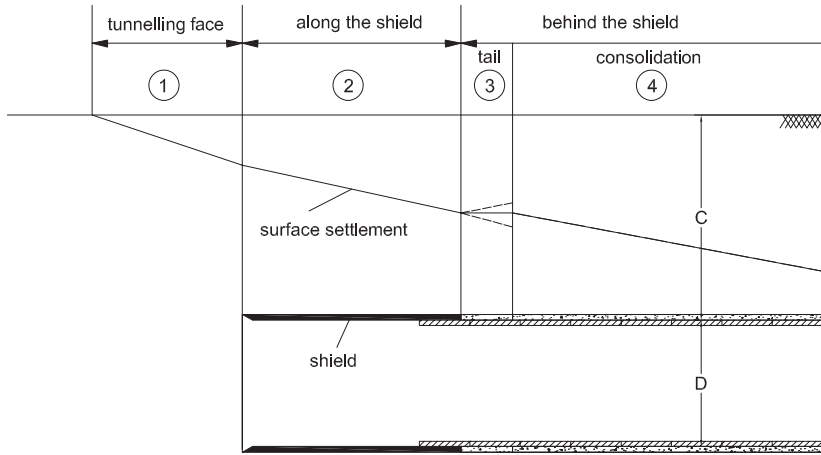


Figure 5.1: Volume loss components

mates are made for a number of ideal soil profiles consisting of a single soil type with most important properties as defined in Table 2.1.

5.2. VOLUME LOSS AT THE TUNNELLING FACE

When tunnelling, the soil ahead of the excavation chamber generally has the trend to move into the cavity which is created by the tunnelling machine. The soil volume moving towards the face depends on the applied support pressures and can be controlled by adjusting the support pressures. In the stability analysis for tunnelling in undrained cohesive soil, the stability number N proposed by Broms and Bennermark (1967) is widely used. By studying the relationship between this stability number N and volume loss at tunnelling face, Attewell et al. (1986), Mair et al. (1982), Mair (1989), Macklin (1999) and Dimmock and Mair (2007) presented a method to determine the expected volume loss based on observed data.

The stability number N is given by Equation 2.9 with $q_s = 0(kN/m)$ in the case of green field:

$$N = \frac{\gamma(C + D/2) - s}{c_u}$$

In shallow tunnelling, the support pressure at the tunnelling face should be high enough to avoid the collapse to the excavation chamber but also limited to prevent blow-out and fracturing. Firstly, the required support pressure must be higher than or at least equal to the total of water pressure and horizontal effective soil pressure taking into account three dimensional arching effects. The wedge model, which was studied by Anagnostou and Kovári (1994), Jancsecz and Steiner (1994) and Broere (2001), is commonly applied

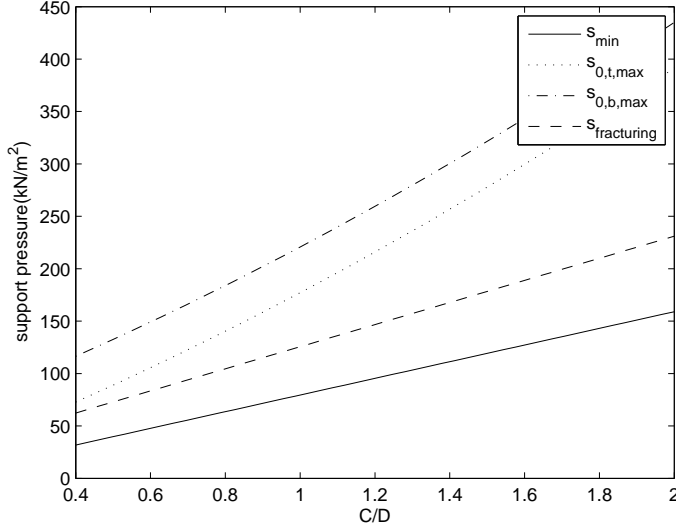


Figure 5.2: The range of support pressures at the tunnelling face of a tunnel with a diameter $D = 6\text{ m}$ in clay

to determine the minimum support pressure s_{min} . In the case of shallow tunnelling, from Equation 2.18 the minimum support pressure s_{min} can be derived from the wedge model, as follows:

$$s_{min} = \sigma'_h + p = \sigma'_v K_{A3} + p = \gamma' z K_{A3} + p \quad (5.2)$$

where p is pore pressure.

Secondly, the maximum support pressures are often estimated as to avoid blow-out with the maximum support pressure at the top of the tunnel $s_{0,t,max}$ and the maximum support pressure at the bottom of the tunnel $s_{0,b,max}$ and fracturing. According to Vu et al. (2015d), the maximum support pressures in the case of blow-out are given by Equations 2.32 and 2.35 in Chapter 2.

In normally consolidated soil, according to Mori et al. (1991), the maximum pressure in the case of fracturing is presented as:

$$s_f = \sigma'_v K + p + c_u \quad (5.3)$$

However, field data show that the higher allowable support pressures are often applied in the tunnelling face, according to NEN-3650 (2012) and reports by BTL (Boren van Tunnels en Leidingen), in the Netherlands. Therefore, the support pressures boundaries are determined with the minimum support pressure and the maximum support pressure in the case of blow-out as indicated in Equations 2.32 and 2.35 above.

Figure 5.2 shows the relationship between the required support pressures and the C/D ratio with the tunnel diameter $D = 6\text{ m}$ in clay. We will elaborate the calculation method for these conditions and present overall results for different diameters and soil conditions later in Figure 5.10. Only C/D ratios larger than 0.4 are studied, as less cover would

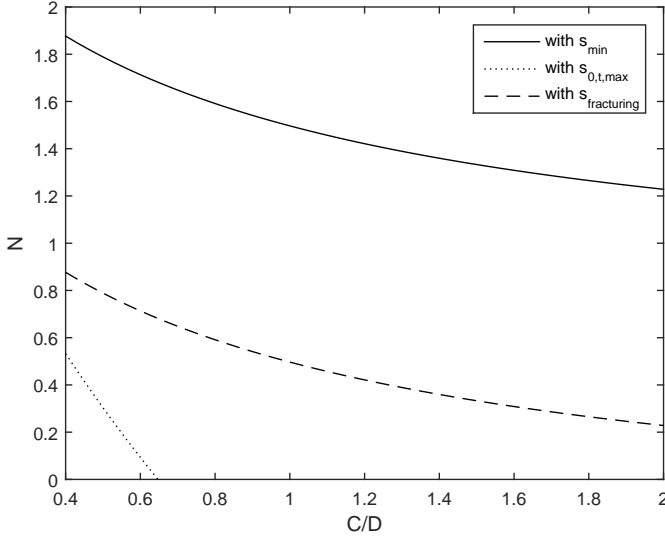


Figure 5.3: The range of stability number N for a tunnel with a diameter $D = 6m$ in clay

lead to unreasonable large volume loss, and the upper 3 to 4 meter of soil in urban areas are often taken up by various utilities and therefore would not be available for tunnelling. The support pressures calculated here are the minimum support pressure from a wedge model and the maximum support pressures for fracturing and blow-out at the top and the bottom of the tunnel.

Figure 5.3 shows the calculated stability number N for these support pressures. Since the applied support pressures are derived from the wedge stability model, fracturing and blow-out conditions, N values in this figure are smaller than 2. It means that the tunnelling face is stable with these support pressures.

O'Reilly (1988) indicated that a relation exists between the volume loss at tunnelling face $V_{L,f}$ and the load factor LF , which is estimated by the ratio of working stability number N and the stability number at collapse N_{TC} , as follows:

$$LF = \frac{N}{N_{TC}} \quad (5.4)$$

where N_{TC} is estimated from Equations 2.11 and 2.12 as:

For $0 \leq C/D \leq 1$:

$$N_{TC} = 2 + 2 \ln \left(\frac{2C}{D} + 1 \right)$$

For $1 \leq C/D \leq 1.8$:

$$N_{TC} = 4 \ln \left(\frac{2C}{D} + 1 \right)$$

Figure 5.4 shows the relationship between the load factor LF and the C/D ratio. The load

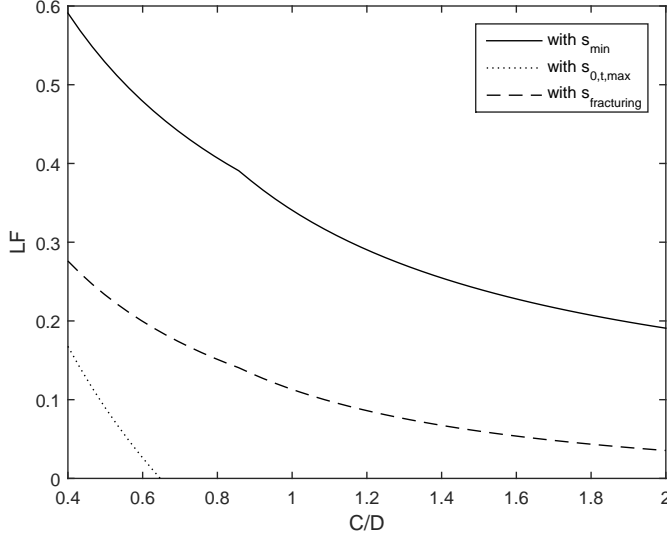


Figure 5.4: Relationship between load factor LF and C/D ratio for a tunnel with diameter $D = 6m$ in clay

factor is less than 0.6 for the minimum support pressure and has the trend of reducing when the C/D ratio increases. This means that the tunnel becomes safer with regards to estimating the support pressures when the C/D ratio becomes larger.

From the analysis of case history data of the load factor LF and the volume loss at the tunnelling face (Figure 5.5), Macklin (1999) presented a formula to calculate the volume loss at the tunnelling face $V_{L,f}$ as:

$$V_{L,f}(\%) = 0.23e^{4.4LF} \quad (5.5)$$

Equation 5.5 can be used to convert the load factor LF to the volume loss $V_{L,f}$ estimates, which leads to Figure 5.6. This shows the range of volume loss at the tunnelling face $V_{L,f}$ with various C/D ratios for a tunnel with $D = 6m$ in clay. In shallow tunnels with $0.4 \leq C/D \leq 1$ the range of possible volume loss $V_{L,f}$ is large, ranging from 0.12% to 3.1%. This means that if tunnelling uses the minimum pressure in the excavation chambers, the volume loss $V_{L,f}$ will increase significantly. Meanwhile, the volume loss $V_{L,f}$ in the case of $1 \leq C/D \leq 2$ ranges from 0.27% to 1.05%. The difference in volume loss $V_{L,f}$ between the minimum pressure and maximum pressures due to blow-out and fracturing is clearly reduced. Therefore, in the case of very shallow tunnels ($C/D \leq 1$) the support pressures applied at the tunnelling face should be kept near to the maximum pressure in order to avoid increasing the volume loss.

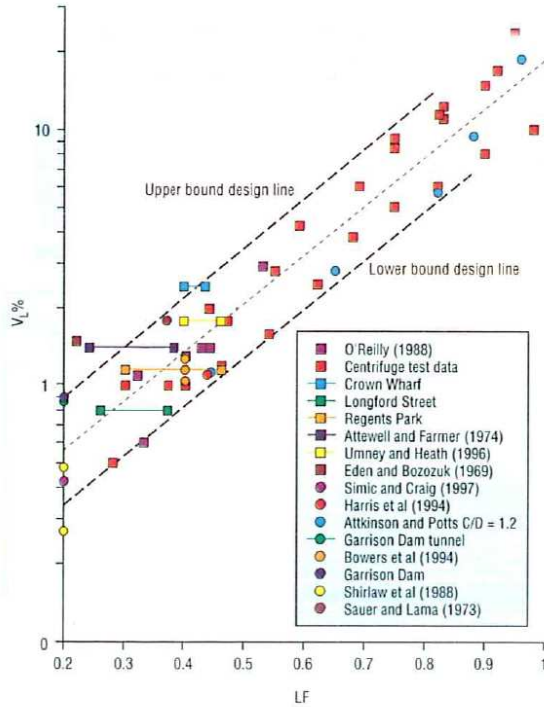


Figure 5.5: Volume loss V_L and load factor LF (Macklin, 1999)

5.3. VOLUME LOSS ALONG THE SHIELD

The diameter of the cutting wheel in front of the TBM is often larger than the diameter of the shield. This leads to an overcut when tunnelling (Figure 5.7). Also, the TBM is often tapered, which creates a gap between the shield skin and the surrounding soil. Additional gapping can also occur when the TBM moves in curves as indicated in Festa et al. (2015). In this study, the effect of curves is not included. This gap is often filled by bentonite, which flows from the tunnelling face and/or grout which comes from the shield tail. In practice, the grout and bentonite pressures are often larger than the vertical soil pressure at the tunnelling face and tail. From the observation of Bezuijen (2007), there are three possible bentonite and grout flows that can occur along the shield when tunnelling. Firstly, the bentonite flows from the tunnelling face to the tail and pushes the grout at the joint between the tail and the TBM. Secondly, the grout flows from the tail to the tunnelling face and pushes the bentonite away. Thirdly, the grout flows from the tail to the tunnelling face and the bentonite also flows in the opposite direction. The flows of bentonite and grout are also simulated in Nagel and Meschke (2011). In shallow tunnelling, due to the possibility of blow-out and fracturing, there is a limitation of applied grout and bentonite pressures at the tunnelling face and the tail.

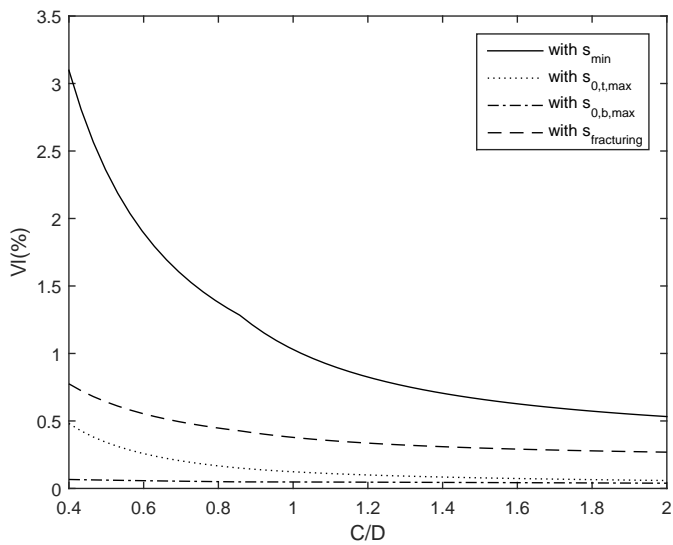


Figure 5.6: Volume loss at tunnelling face for a tunnel with diameter $D = 6m$ in clay

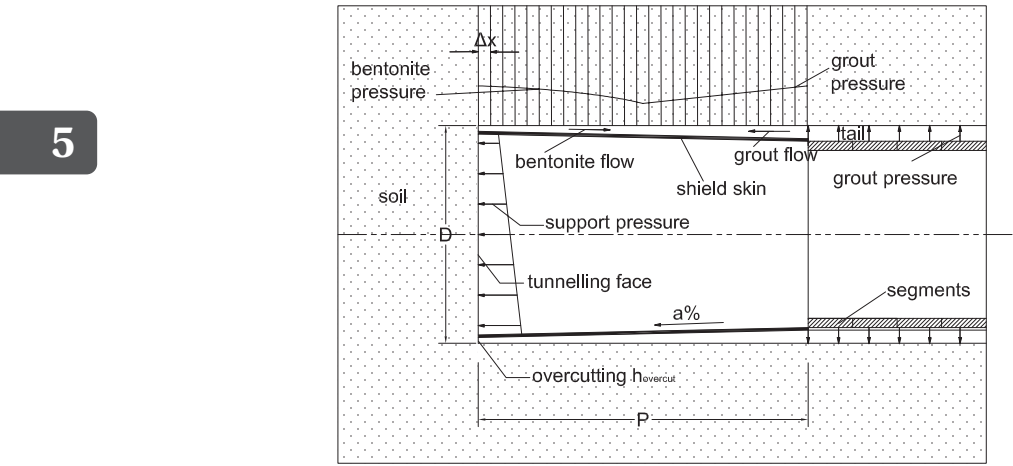


Figure 5.7: Bentonite and grout flows along the shield and lining segments

Table 5.1: Input parameters of tunnel boring machine

Diameters of shield D	6, 8 and 10m
Length-to-diameter P/D ratio of the shield	1
Reduction of shield diameter a	0.2%
Overcutting $h_{overcut}$	0.015m
Shear strength of grout τ_y^{grout}	1.6kPa
Shear strength of bentonite $\tau_y^{bentonite}$	0.8kPa

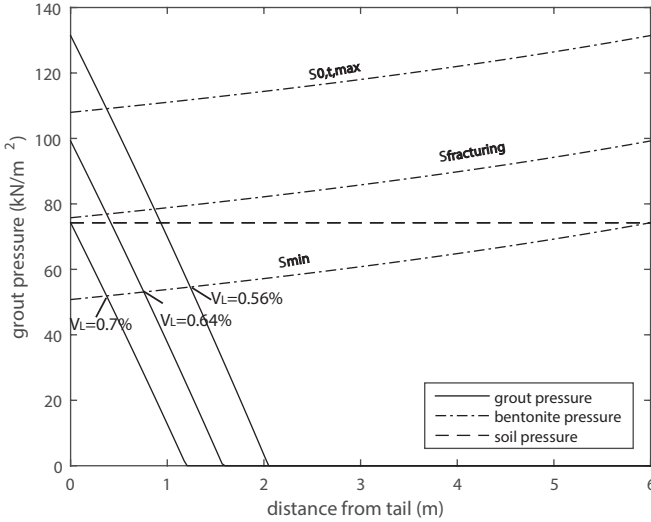


Figure 5.8: Bentonite and grout pressures along a shield with $D = 6m$ in clay

According to [Bezuijen \(2007\)](#), both liquids, the grout in the shield tail and the bentonite applied at the tunnelling face are assumed to behave as the Bingham liquids, such that the yield stress is governing in the flow behaviour. The flow pressures in grout and bentonite reduce along the shield as in Figure 5.7. The reduction of grout pressure along the shield is given by:

$$\Delta p = \frac{\Delta x}{w_j} \tau_y \quad (5.6)$$

where Δp is the change of the pressure due to flow, Δx is a length increment along the TBM, w_j is the joint width between the tunnel and the surrounding soil and τ_y is a shear strength of the grout around the TBM.

In this section, the volume loss along the shield is calculated with input parameters as indicated in Table 5.1 with the following approach. As an example, the calculation is carried out case of tunnel with $D = 6m$ and $C/D = 0.75$ in clay. Figure 5.8 shows the change of grout pressure and bentonite pressure along the shield. It is assumed that when the grout pressure and bentonite pressure are less than the vertical soil pressure, the soil is moving into the cavity. The volume loss is estimated as the void volume that is filled by

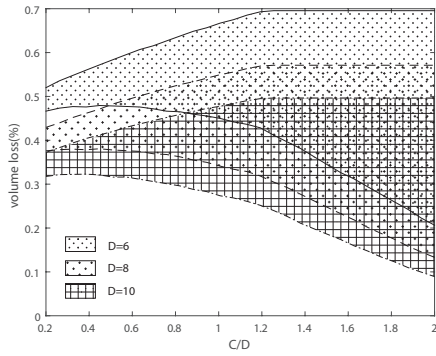
soil. The volume loss will not occur if the grout pressure and the bentonite pressure are larger than the vertical soil pressure. In that case, the gap along the shield is assumed to be completely filled by grout and bentonite. From this figure, the volume loss along the shield depends on the bentonite pressure, which is applied at the tunnelling face and the grout pressure at the tail. When the bentonite and grout pressures are equal to the minimum required pressure as calculated in previous section, the volume loss will be maximal. On the other hand, when the maximum allowable pressures are applied, there is no volume loss along the shield under these assumptions.

In order to investigate the effect of grout pressure on the shield in different soils, we assume the bentonite pressure applied at the tunnelling face is the average of the minimum support pressure and the maximum support pressure for fracturing. Figure 5.9 shows the change of volume loss with different tunnel diameters in various soils. When the C/D ratio increases, the range of the volume loss along the shield $V_{L,s}$ is larger. With a particular C/D ratio of the tunnel, the larger the tunnel diameter is, the smaller the volume loss $V_{L,s}$ is with the constant overcut parameter of the shield. In the case of tunnelling in sand, the upper boundary of the volume loss $V_{L,s}$ increases nearly linearly with the C/D ratio from 0.4 to 0.8, then becomes almost constant when the C/D ratio increases whereas the lower boundary reduces linearly when the C/D ratio increases. This also appears in the cases of tunnelling in clay and organic clay. At this point, basically, the entire annulus is filled by the surrounding soil, leading to a maximum attainable volume loss along the tail. In the case of tunnelling in peat, in the range of this analysis with $0.4 \leq C/D \leq 2$, the upper boundary of the volume loss $V_{L,s}$ lightly rises and the lower boundary linearly decreases. It is noted that the maximum upper boundary volume loss along the shield $V_{L,s}$ is the same for a given tunnel diameter. Regardless of soil conditions, for a tunnel with $D = 6m$, it follows that $V_{L,s,max} = 0.7\%$, with $D = 8m$, $V_{L,s,max} = 0.57\%$ and with $D = 10m$, $V_{L,s,max} = 0.5\%$.

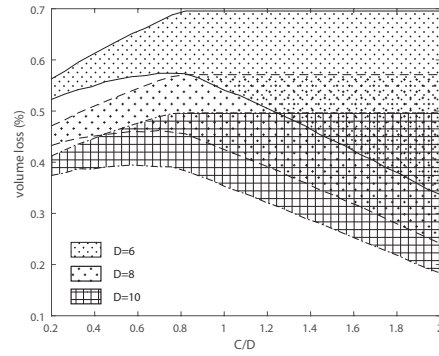
Figure 5.10 shows the boundary of the volume loss along the shield $V_{L,s}$ in relationship with C/D ratios for different tunnel diameters in different soils. The upper boundary for $0.4 \leq C/D \leq 0.6$ corresponds to the case of tunnelling in peat in all three tunnel diameters. When tunnelling with $0.6 \leq C/D \leq 1$, the upper boundary is given by tunnelling in organic clay and when tunnelling with the C/D ratio larger than 1, the upper boundary becomes constant and depends on the tunnel diameter D . The maximum volume loss along the shield $V_{L,s}$ is about 0.7% for $D = 6m$, $V_{L,s,max} = 0.57\%$ for $D = 8m$ and $V_{L,s,max} = 0.5\%$ for $D = 10m$. For the lower boundary, there is a decreasing trend of the minimum volume loss along the shield $V_{L,s}$ when the C/D ratio increases. In the case of $D = 6m$ the maximum $V_{L,s}$ of the lower boundary is about 0.47% when $C/D = 0.5$. The maximum volume loss along the shield $V_{L,s}$ of the lower boundary is about 0.38% with $D = 8m$ and 0.32% with $D = 10m$ when $C/D = 0.5$. When $C/D = 2$, $V_{L,s,max} = 0.2\%$ for $D = 6m$, $V_{L,s,max} = 0.13\%$ for $D = 8m$ and $V_{L,s,max} = 0.09\%$ for $D = 10m$.

5.4. VOLUME LOSS BEHIND THE SHIELD

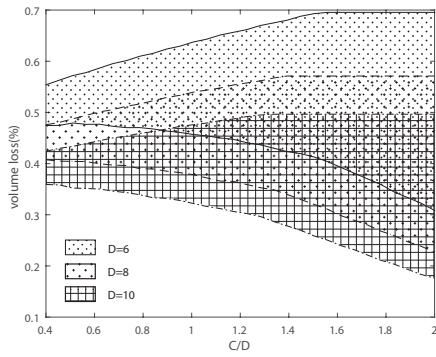
When precast segments are placed, the advance of the shield results in an annular cavity between the segments and the surrounding soil due to the shape of the TBM and the overcut as discussed above. Grout is injected rapidly in order to prevent the sur-



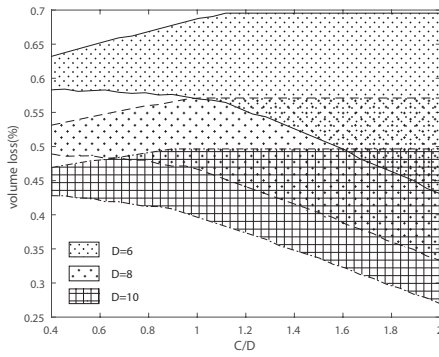
(a) in sand



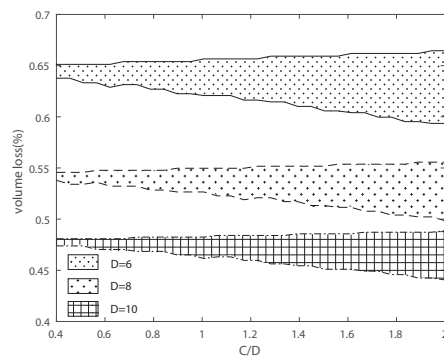
(b) in clayey sand



(c) in clay



(d) in organic clay



(e) in peat

Figure 5.9: Volume loss along the shield in various soils

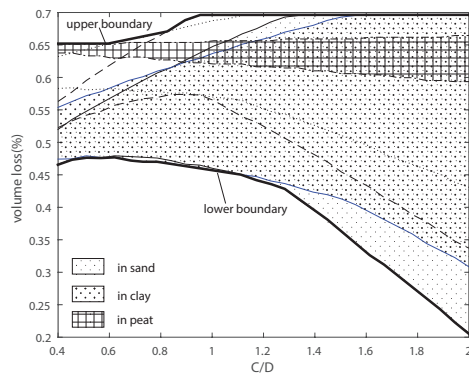
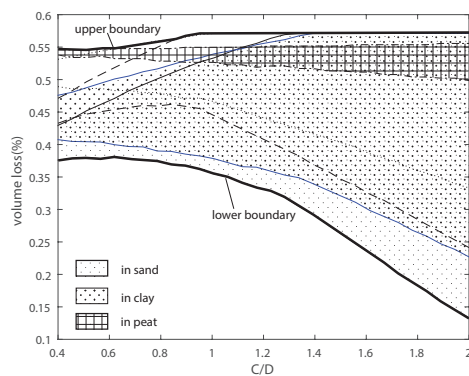
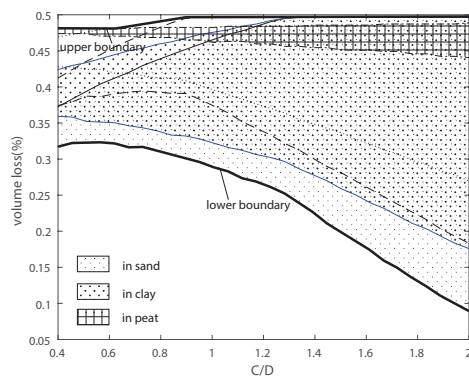
(a) $D = 6m$ (b) $D = 8m$ (c) $D = 10m$

Figure 5.10: Volume loss along the shield with different tunnel diameters

rounding soil to move into the gap. It is assumed that the void is filled by the grout. The injected grout pressure induces the loading on the soil around the tunnel lining. This might lead to immediate displacements and long-term consolidation of the soil. These are two components of the volume loss behind the shield: the volume loss at the tail and the volume loss due to consolidation.

5.4.1. VOLUME LOSS AT THE TAIL

When the grout is injected with high pressures at the tail, the ground around the tunnel will be deformed. In order to estimate the surface settlement induced by tunnelling, there are some analytical solutions proposed by Sagaseta (1988); Verruijt (1997); Strack (2002) based on cavity expansion and taking the influence of a free surface into account. However, the effect of the range of support pressures has not taken into account in these methods and resulting solutions, for instance expressed as a Laurent series expansion in the case of Verruijt (1997), require an increasing number of terms for a stable numerical integration if the distance between free surface and tunnel reduces. On the other hand, the cavity expansion developed for the case of a cavity in infinite medium has been implemented in tunnelling studies by Taylor (1993); Yu (2013) and results in far more elegant and practical solution for a first estimate of the effect of grout pressures on soil stresses and deformations around the TBM. To determine the effect of grouting at the tail on volume loss at the tail and consolidation, in this study, the cavity expansion method for tunnelling, which is proposed by Yu (2013), is therefore applied as a simplified method. In this cavity-expansion theory, it is assumed that the soil around the tunnel is a Tresca medium. The stresses in the soil and the settlement at the surface can be calculated by the cavity-expansion theory. According to Yu (2013), the plastic zone will deform around the tunnel wall, as can be seen in Figure 5.11, with the radius R_p of the plastic zone estimated from the following equation:

$$R_p = \frac{D}{2} \exp \left(\frac{p_0 - s}{Y} - \frac{k}{1+k} \right) \quad (5.7)$$

where p_0 is the pre-tunnelling pressure; $k = 1$ or 2 corresponding to cylindrical or spherical cavity models; $Y = 2c_u$ or $-2c_u$ corresponding to the case of contraction or expansion of the tunnel.

Similar to Yu (2013) and Taylor (1993), the pre-tunnelling pressure p_0 can be estimated as:

$$p_0 = \gamma \left(C + \frac{D}{2} \right) \quad (5.8)$$

The soil displacement u_s in the elastic zone is given by:

$$u_s = -\frac{Yr}{2(k+1)G} \left(\frac{R_p}{r} \right)^{1+k} \quad (5.9)$$

where r is the distance from the calculated point to the tunnel centre and $G = E/2(1 + \nu)$ is the shear modulus of soil.

The soil displacement u_s in the plastic zone is given by:

$$u_s = -\frac{Y}{2(k+1)G} \left(\frac{D}{2r} \right)^k \frac{D}{2} \exp \left(\frac{(1+k)(p_0 - s)}{kY} - 1 \right) \quad (5.10)$$

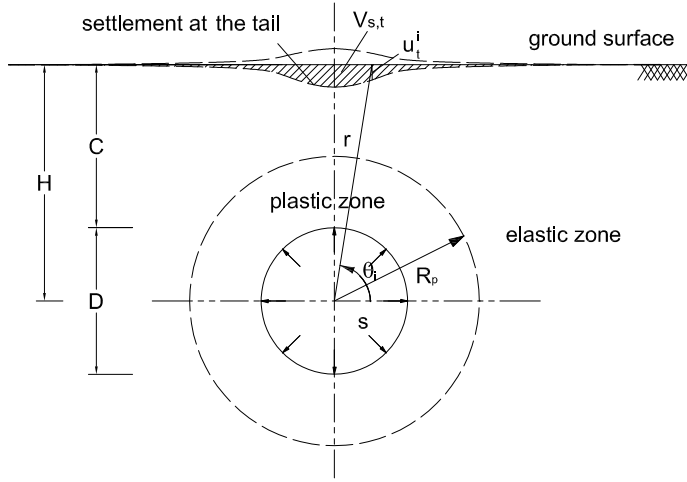


Figure 5.11: Deformations around a shallow tunnel at the tail

In this case, the effect of grouting pressures at the tail is analysed with a cylindrical cavity model and is calculated with the minimum and maximum support pressures. Thus, in Equation 5.7, k equals 1.

It can be assumed that the volume loss around the tunnel due to grouting at the tail equals the volume of ground settlement at the surface. In order to identify the contribution of soil deformation at the tail on the total volume loss, the displacement of the ground surface is estimated. According to assumptions in Yu (2013), the tunnel will collapse when the plastic zone expands to the ground surface. It means that when the tunnel is stable, the radial displacement of ground u_s at the surface is in the elastic zone and can be calculated with Equation 5.9. It should be noted that the risk of fracturing is not taken into account in this theory.

The surface settlement at the tail can be estimated from:

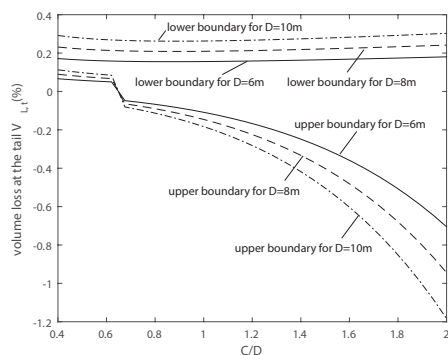
$$u_t = u_s \sin \theta \quad (5.11)$$

where θ is the angle between the calculated point to the tunnel centre and the horizontal axis (see Figure 5.11).

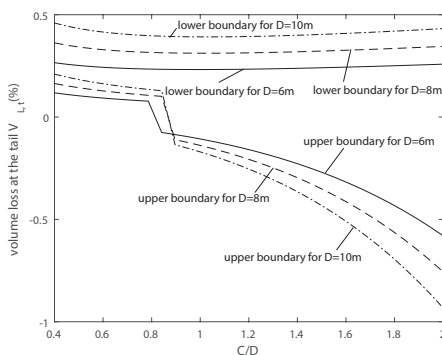
The volume loss at the tail $V_{L,t}$ can be estimated as:

$$V_{L,t} = \frac{V_{s,t}}{\pi(D/2)^2} \quad (5.12)$$

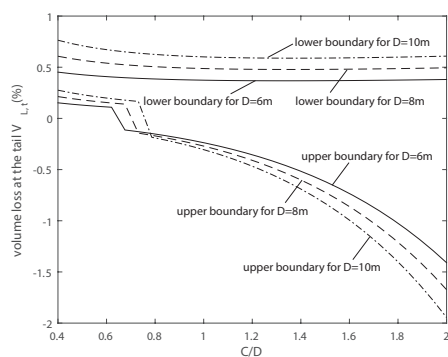
where $V_{s,t}$ is the volume of the surface settlement due to grouting pressures at the tail (see Figure 5.11).



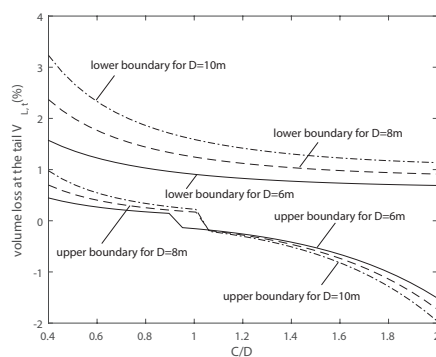
(a) in sand



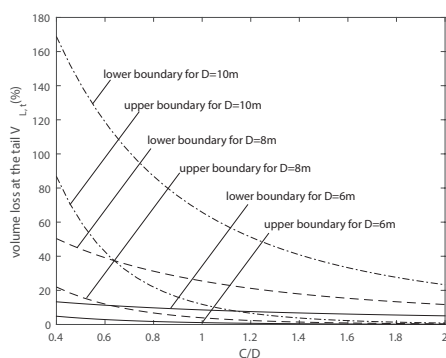
(b) in clayey sand



(c) in clay



(d) in organic clay



(e) in peat

Figure 5.12: Volume loss at the tail with different tunnel diameters in various soils

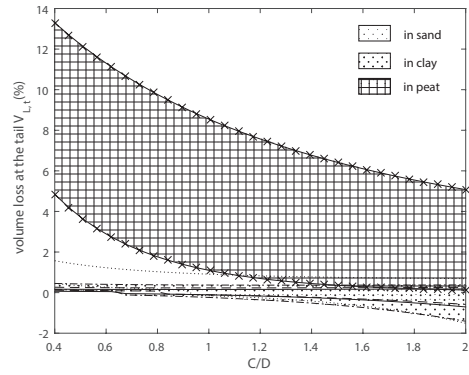
Figure 5.12 shows the boundaries of the volume loss at the tail $V_{L,t}$ in various soils for tunnels with $D = 6, 8$ and 10m with the range of the support pressures from the vertical soil stress to the maximum support pressure at the top of the tunnel derived from Equation 2.32. The figure shows that the larger the tunnel diameter is, the larger the range of volume loss $V_{L,t}$ is. When the support pressure equals the vertical soil stress at the top of the tunnel lining, there is a contraction in the cavity and this leads to positive values of the lower boundary of volume loss at the tail. When a high support pressure is used, the cavity will expand. The negative volume loss $V_{L,t}$ values indicate that the soil above the tunnel lining is pushed upward and there might be heave at the ground surface. In practice, this heave might not be observed because the settlement due to volume loss at the tunnelling face and along the shield could be larger. When a high support pressure is applied at the tail, a heave can occur in order to compensate the volume loss at the tunnelling face and along the TBM as can be seen in Figures 5.12a, 5.12b, 5.12c and 5.12d. However, in the case of very shallow tunnelling, there is no heave due to the small margin in the range of allowable support pressures as indicated in Figure 2.32. In Figure 5.12e, when tunnelling in peat, the volume loss at the tail is positive with a high value, especially in the case of a tunnel diameter $D = 10\text{m}$. It means that shallow tunnelling with a large diameter in peat might be difficult due to the large expected volume loss. This conclusion coincides with the conclusion indicated in Section 2.5 for the range of support pressure for shallow tunnelling in peat with low C/D ratios.

Figure 5.13 shows the dependence of $V_{L,t}$ values on soils in various tunnel diameters. When tunnelling in peat, the range of $V_{L,t}$ values is significantly large compared to tunnelling in sand, clay and organic clay, especially in the case of tunnels with large diameters as indicated above.

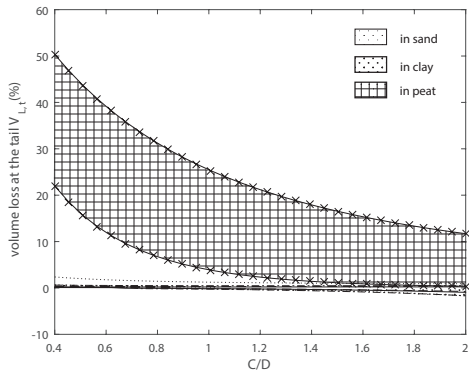
5.4.2. VOLUME LOSS DUE TO CONSOLIDATION

For the volume loss due to consolidation, in the cavity behind the tail, two consolidation processes occur along the tunnel lining. Firstly, the newly injected grout is consolidating and forms a consolidated grout cake in the cavity along the tunnel lining (Talmon and Bezuijen, 2009). In the case of tunnelling in clay, the consolidation in grout might not occur (Bezuijen and AM, 2005) and the length of liquid grout on the lining is much longer. Although the grout pressure decreases along the lining, the injected grout may flow along 2 to 3 following segments and the appearance of the grout cake will prevent the movement of the soil above. It is often assumed that there is no volume loss in the grout consolidating. The other volume loss is due to the subsequent shrinkage of grout, which is estimated at about 0.06 to 0.1 percent of the grout volume (NEN-EN 1992-1-1, 1992; ACI-506R-05, 2005; Han et al., 2007). However, the contribution of this volume loss to the total volume loss is small comparing to the other volume losses. This volume loss, therefore, is not taken into account in this study.

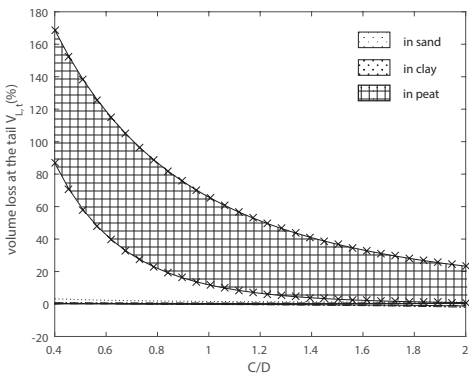
The second process is the consolidation of the soil volume above the tunnel behind the tail. When grout is applied at the tail, the soil stress in the above soil volume will change. This will induce consolidation in the long term behind the tail. The volume loss due to consolidation $V_{L,c}$ is derived from the consolidation settlement of the soil volume above tunnel lining. In the case of tunnelling in sand, consolidation of soil will probably not occur or be minimal. For tunnels in clay or peat, this may be a notable contribution.



(a) $D = 6m$



(b) $D = 8m$



(c) $D = 10m$

Figure 5.13: Volume loss at the tail with different tunnel diameters

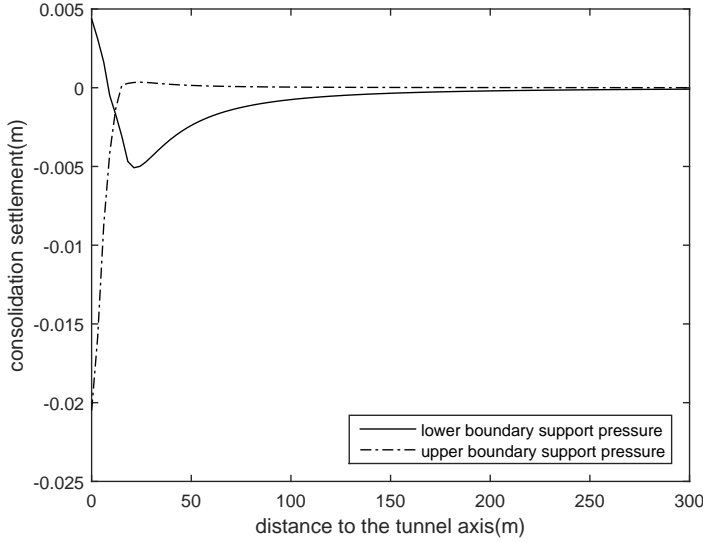


Figure 5.15: Consolidation settlement troughs when tunnelling in clay with $D = 10m$ and $C/D = 1$

where σ_r and σ_θ are the radial and tangential stresses as shown in Figure 5.14. In the plastic zone, the stresses are given by:

$$\sigma_r = -p_0 + \frac{kY}{1+k} + kY \ln \frac{R_p}{r} \quad (5.17)$$

$$\sigma_\theta = -p_0 - \frac{Y}{1+k} + kY \ln \frac{R_p}{r} \quad (5.18)$$

In order to estimate the consolidation settlement, the soil volume above the tunnel lining is divided into n layers. The final consolidation settlement is derived by summing deformations of these layers, which are calculated by Equations 5.13 and 5.14.

The final consolidation settlement is given by:

$$u_c^j = \sum_{i=1}^n u_c^{(j,i)} \Delta z \quad (5.19)$$

where $u_c^{(j,i)}$ and $\Delta z^{(i)}$ are the deformation due to consolidation and the depth of the i^{th} layer at the j^{th} location along the surface.

Figure 5.15 shows settlement troughs in the case of tunnelling in clay with a diameter $D = 10m$ and the ratio of $C/D = 1$, as an example. It can be seen that a heave and a settlement can occur depending on what particular support pressure is applied.

By integrating the final consolidation settlements over the surface, the volume of consolidation settlement at the surface V_{cons} can be estimated as:

$$V_{cons} = \sum_{j=1}^m u_c^{(j)} \Delta x \quad (5.20)$$

where Δx is a length increment along the surface consolidation settlement and m is the increment number.

The volume loss due to consolidation settlement is then estimated as:

$$V_{L,c} = \frac{V_{cons}}{\pi(D/2)^2} \quad (5.21)$$

Figure 5.16 shows the relationship between the consolidation volume loss $V_{L,c}$ and the C/D ratio for tunnels with different diameters in clay, organic clay and peat. With $0.4 \leq C/D \leq 1.3$ in the case of tunnelling in clay and $0.4 \leq C/D \leq 1.7$ in the case of tunnelling in organic clay, it can be seen that the maximum support pressure applied at the tail can lead to a heave on the surface. The volume loss due to consolidation $V_{L,c}$ when maximum support pressure is applied becomes smaller than when minimum support pressure is applied. An example shown in Figure 5.15 shows that the volume of consolidation settlement V_{cons} when applying lower boundary of support pressure is smaller than the value of V_{cons} when applying the maximum support pressure. When the tunnel is located at a deeper level, the volume loss $V_{L,c}$ when applying the maximum support pressure is higher than the volume loss $V_{L,c}$ in the case of applying minimum support pressure.

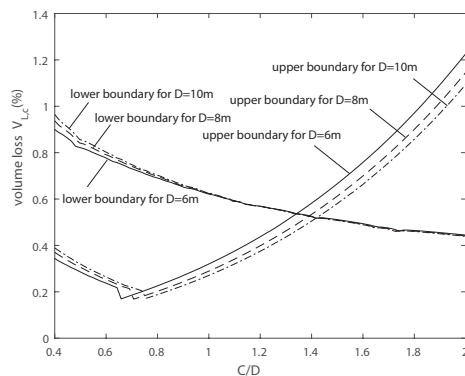
The dependence of the volume loss due to consolidation $V_{L,c}$ on soil type is shown in Figure 5.17 for tunnels with diameters $D = 6, 8$, and 10m . It can be seen that the volume loss $V_{L,c}$ in the case of tunnelling in peat is much higher compared to tunnelling in clay and organic clay.

5.5. TOTAL VOLUME LOSS AND CASE STUDIES

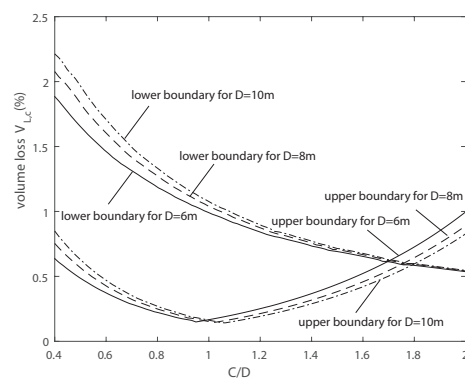
5.5.1. TOTAL VOLUME LOSS

From Equation 5.1, the total volume loss is derived by summing the volume loss of tunnelling face, along the shield, at the tail and due to consolidation. Figures 5.18 and 5.19 show the total volume loss in the case of shallow tunnelling in sand and clayey sand. It can be seen that the range of the total volume loss decreases with the increase of the C/D ratio and the tunnel diameter D . In the case of a C/D ratio from 0.4 to 1, a volume loss in shallow tunnelling of less than 0.5% can be achieved with the condition of careful monitoring. The highest expected volume loss in this range of the C/D ratio is about 3.7% for tunnelling in sand and 5% for tunnelling in clayey sand when less optimal but still stable support and grout pressures are applied. When the C/D ratio larger than 1, the maximum volume loss is less than 1.5% with the range of support pressures in this study. These figures also show that a result of no volume loss can be achieved when tunnelling with $C/D \geq 2$.

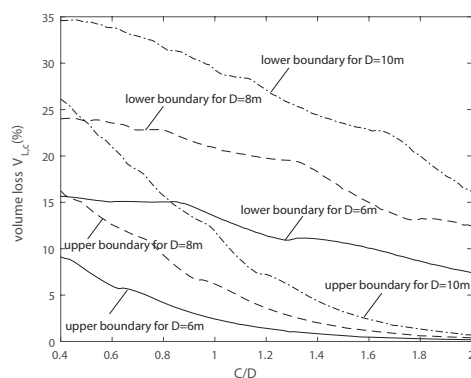
Figure 5.20 shows the relationship between the total volume loss V_L and C/D ratios when tunnelling in clay. The total volume loss V_L when tunnelling has just finished (not taking into account the consolidation) is shown in Figure 5.20a. It can be seen that a total volume loss V_L less than 0.5% after tunnelling is feasible even with $C/D \leq 1$. This figure also shows that for very shallow tunnelling with $C/D \leq 0.6$, a tunnel with a large diameter has a larger range of expected volume loss. With deeper tunnelling when $1 \leq C/D \leq 2$, the maximum value of the total volume loss reduces and becomes less than 2%.



(a) in clay

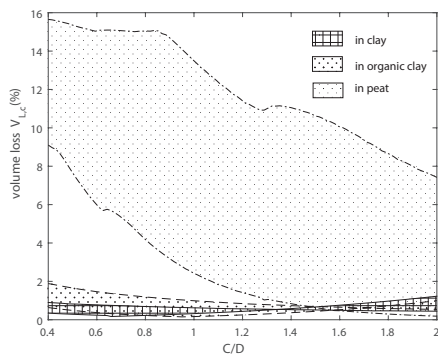
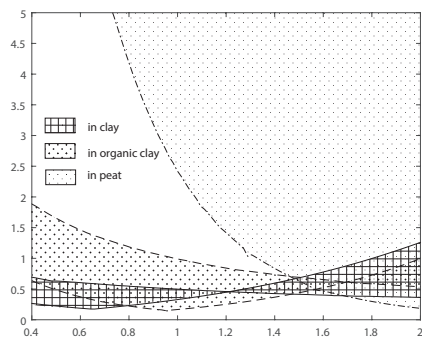
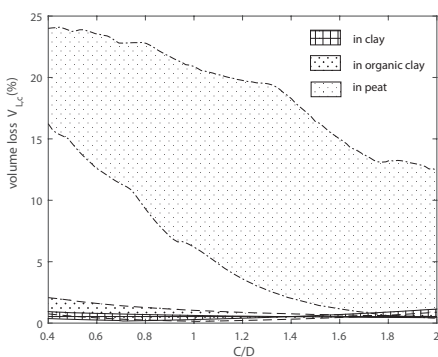
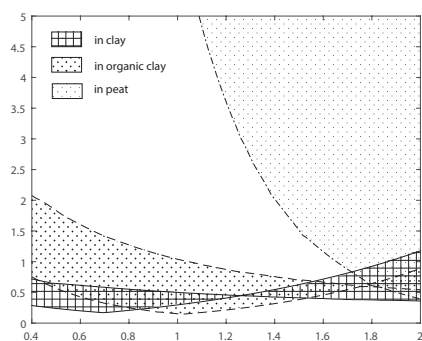
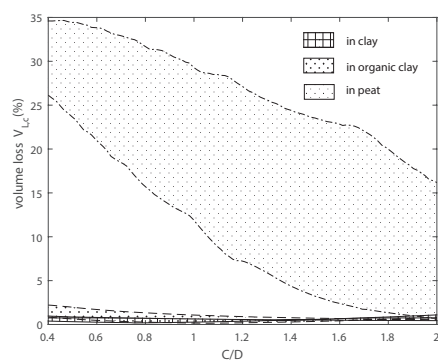
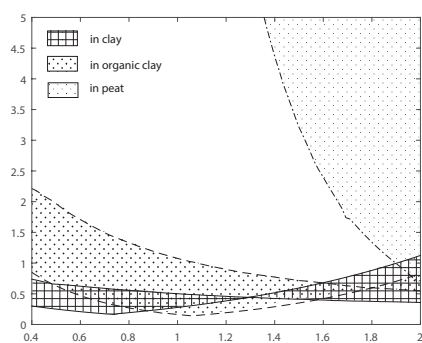


(b) in organic clay



(c) in peat

Figure 5.16: Volume loss due to consolidation $V_{L,c}$ with different tunnel diameters in various soils

(a) $D = 6m$ (b) $D = 6m$ (in detailed)(c) $D = 8m$ (d) $D = 8m$ (in detailed)(e) $D = 10m$ (f) $D = 10m$ (in detailed)Figure 5.17: Volume loss due to consolidation $V_{L,c}$ with various tunnel diameters

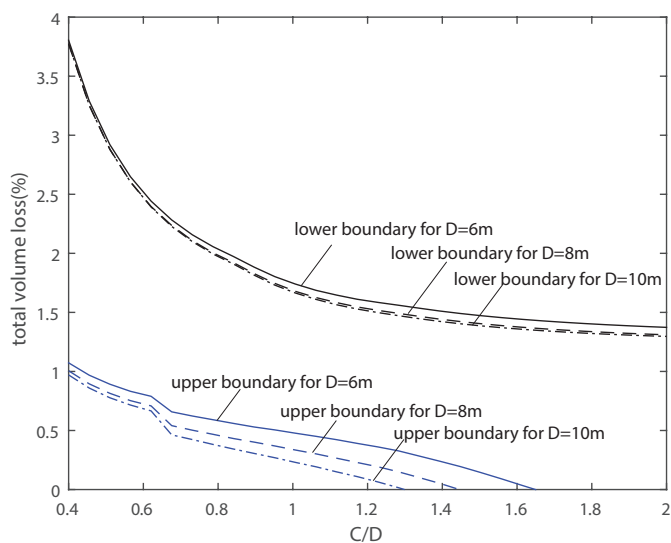


Figure 5.18: Total volume loss for tunnelling in sand with various diameter D

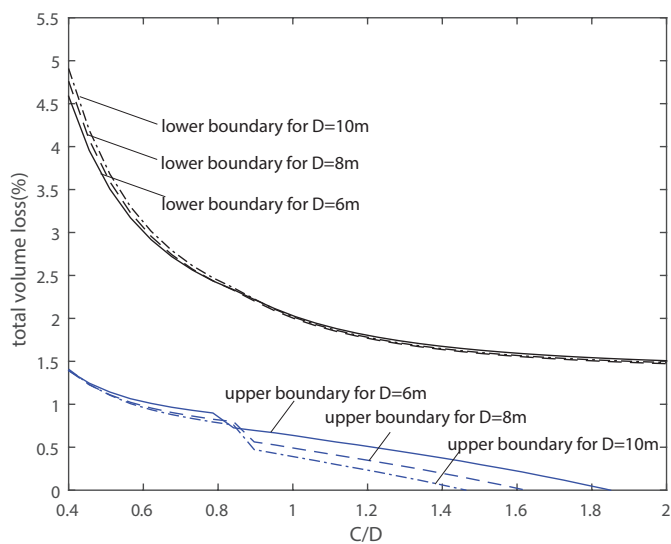
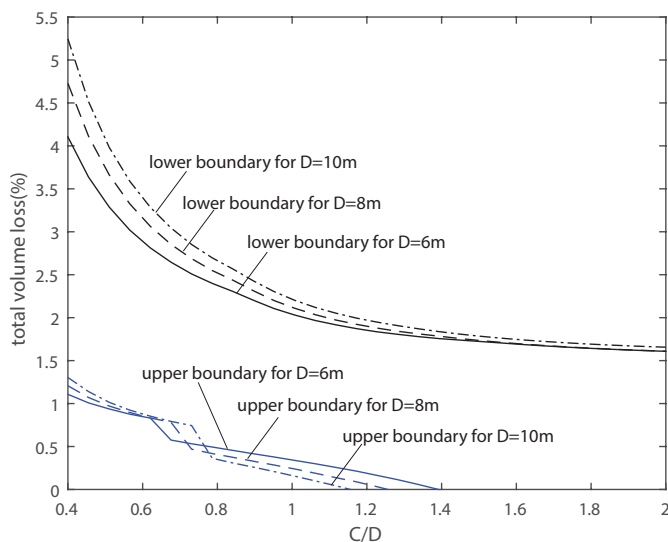
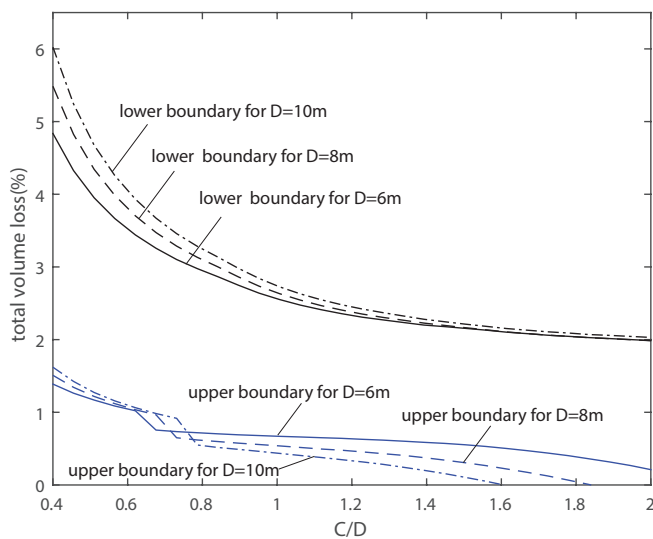


Figure 5.19: Total volume loss for tunnelling in clayey sand with various diameter D



(a) not including consolidation of soil layers above the tunnel



(b) including consolidation of soil layers above the tunnel

Figure 5.20: Total volume loss for tunnelling in clay with various diameter D

Figure 5.20b shows the total volume loss V_L for tunnelling with various diameters $D = 6, 8$ and 10m in clay including consolidation of soil layers above the tunnel. It also follows that the lower the C/D ratio is, the larger the range of volume loss is. The total volume loss of tunnelling in clay would be at maximum about 6% with $D = 10\text{m}$, 5.5% with $D = 8\text{m}$ and 5% with $D = 6\text{m}$ when $C/D = 0.4$. The lower boundary corresponding with the minimum support pressure applied has a reducing trend when the C/D ratio increases. This means there might be a larger volume loss when the tunnel becomes shallower. At the upper boundary of the total volume loss, corresponding with the maximum support pressure applied, the final volume loss of tunnelling with $D = 6\text{m}$ can reach just over 0% after consolidation has been taken into account.

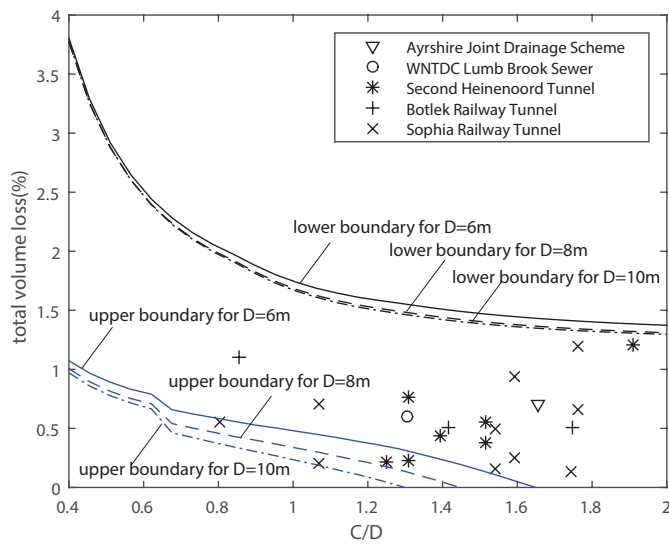
5.5.2. CASE STUDIES

Tables 5.2 and 5.3 show a summary of volume loss in case histories for tunnelling in sand and clay with the C/D ratio less than 2. In Table 5.2, there are two case studies the Ayrshire Joint Drainage Scheme and WNTDC Lumb Brook Sewer, derived from the study of O'Reilly and New (1982) and three case studies Second Heinenoord Tunnel, Botlek Railway Tunnel and Sophia Railway Tunnel, derived from Netzel (2009). Table 5.3 shows volume loss data from various projects all over the world including Madrid Metro Extension, Heathrow Express Trail Tunnel, Waterloo, Garrison Dam test tunnel, Baulos 25, Barcelona Subway and London Transport Experimental Tunnel.

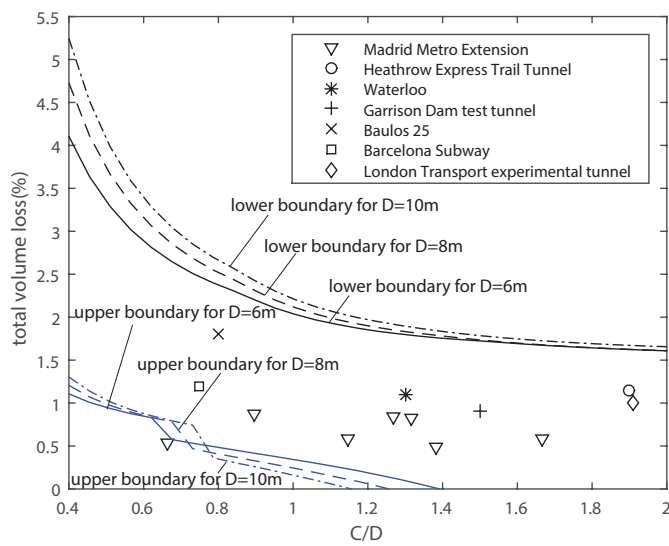
The data in Table 5.2 are plotted in Figure 5.21a in order to compare the volume loss derived from this analysis to field data in the case of shallow to medium deep tunnelling in sand. It can be seen that most of field data falls in the boundaries of volume loss in Figure 5.21a.

Figure 5.21b shows the validation of the calculated volume loss to the field data in Table 5.3 in the case of shallow tunnelling in clay. It also shows that all the field data is in agreement with the boundaries of volume loss derived in this study. Only the Madrid Metro Extension which is known as a successful tunnelling project has one data point below the lower boundary of volume loss for a low C/D ratio.

The agreement between derived boundaries of volume loss in sand and clay and field data shows that the approach of estimating volume loss in this study can successfully predict volume loss in shallow tunnelling.



(a) in sand



(b) in clay

Figure 5.21: Validation for volume loss in shallow tunnelling

Case	H(m)	C(m)	D(m)	C/D	V_L (%)	Soil conditions	Reference
Ayrshire Joint Drainage Scheme	6.25	4.8	2.9	1.66	0.7	fine to medium slightly silty sand; loose and medium density	O'Reilly and New (1982)
WNTDC Lumb Brook Sewer	6.5	4.7	3.6	1.31	0.5	medium/dense sands and gravel with a little clay	O'Reilly and New (1982)
Second Heinenoord Tunnel	14.5	10.37	8.3	1.25	0.21	dense sand	Netzel (2009)
	15.0	10.8	8.3	1.31	0.22		
	15.0	10.8	8.3	1.31	0.7		
	15.7	11.6	8.3	1.39	0.44		
	16.7	12.6	8.3	1.51	0.38		
	16.7	12.6	8.3	1.51	0.55		
Botlek Railway Tunnel	20.0	15.8	8.3	1.91	1.2	Holocene and Pleistocene sand	Netzel (2009)
	13.1	8.3	9.65	0.86	1.11		
	18.5	13.7	9.65	1.42	0.5		
	21.7	16.9	9.65	1.75	0.5		
Sophia Railway Tunnel	12.4	7.6	9.5	0.8	0.55	Pleistocene sand	Netzel (2009)
	14.9	10.1	9.5	1.1	0.21		
	14.9	10.1	9.5	1.1	0.7		
	19.4	14.7	9.5	1.5	0.15		
	19.4	14.7	9.5	1.5	0.5		
	19.9	15.1	9.5	1.6	0.25		
	19.9	15.1	9.5	1.6	0.94		
	21.3	16.6	9.5	1.7	0.14		
	21.5	16.75	9.5	1.8	0.65		
	21.5	16.75	9.5	1.8	1.2		

Table 5.2: Volume loss of tunnelling in sand projects

Case	H(m)	C(m)	D(m)	C/D	V_L (%)	Soil conditions	Reference
Madrid Metro Extension	10.3	5.9	8.88	0.66	0.54	stiff clay	Melis et al. (2002)
	12.43	8	8.88	0.9	0.87		
	14.61	10.17	8.88	1.15	0.6		
	15.7	11.26	8.88	1.27	0.84		
	16.12	11.68	8.88	1.32	0.83		
	16.7	12.27	8.88	1.38	0.5		
	19.23	14.79	8.88	1.67	0.58		
Heathrow Express Trail Tunnel	21	16.67	8.66	1.9	1.15	London clay	Bowers et al. (1996)
Waterloo	11.7	8.45	6.5	1.3	1.1	London clay	Harris et al. (1994)
Garrison Dam Test Tunnel	11	8.25	5.5	1.5	0.9	clay-shale and lignite	Peck (1969)
Baulos 25	8.45	5.2	6.5	0.8	1.8	Frankfurt clay	Macklin (1999)
Barcelona Subway	10	6	8	0.75	1.2	red and brown clay with some gravel	Ledesma and Romero (1997)
London Transport Experimental Tunnel	10	7.9	4.15	1.91	1	dense sandy gravel overlain with made ground of soft clay with sand and gravel	O'Reilly and New (1982)

Table 5.3: Volume loss of tunnelling in clay projects

5.6. CONCLUSION

Volume loss is a major parameter in the calculation of ground movement by tunnelling. The range of attainable volume loss can be estimated by combining stability analysis at tunnelling face, along and behind the shield. In this theoretical study, it is found that in the case of tunnelling with $C/D \leq 1$, the volume loss at the tunnelling face has a major impact in total volume loss.

The volume loss along the shield can be optimized by selecting optimal bentonite and grout pressures applied at tunnelling face and tail. The proposed calculation method estimates attainable upper and lower boundaries of volume loss along the shield for a particular tunnel.

This paper also presents methods to identify the volume loss behind the shield. The volume loss at the tail when tunnelling in peat has a large impact, especially in the case of shallow tunnels ($C/D \leq 1$). The volume loss behind the tail was estimated by the volume loss due to shrinkage of grout and consolidation of above soil volume. The volume loss due to consolidation depends on the surrounding soil and the C/D ratio.

The total volume losses for tunnelling in sand, clayey sand and clay are derived and have a good agreement with case studies. Overall, the range of volume loss increases when tunnelling with shallower overburden. By controlling the applied support pressure at the tunnelling face and tail, the volume loss can be minimized. Still, a direct volume loss around 1% is a reasonable minimum for very shallow tunnels ($C/D = 0.4$) where for deeper tunnels no volume loss should be attainable. If pressure control is less optimal but still controlled, a direct volume loss up to 5.5% is not unreasonable to expect for very shallow tunnels.

Analysis also shows that consolidation after the TBM has passed can contribute considerably to the final surface settlements and can be of this same order as direct volume loss effects in clay and even larger in very soft soils like peat. This effect, however, is more pronounced in deeper tunnels, where it could easily double the direct volume loss.

6

IMPACT FACTORS OF INFLUENCE ZONES

Now this is not the end. It is not even the beginning of the end. But it is, perhaps, the end of the beginning.

Winston Churchill

The extent of the zone influenced by tunnelling majorly depends on the amount of over-excavation and stress changes induced in the soil, normally represented as a value of volume loss. This chapter combines the upper and lower estimates of volume loss for different soil conditions and cover-to-diameter ratios in order to identify the zones around the tunnel influenced by tunnelling. These zones are dealt with risk categories of damage of existing buildings in order to identify whether applying mitigating methods or taking additional control measures during tunnelling would be needed for a safe and damage-free tunnel construction. Effects of soil parameters on the influence zones are also investigated to identify their impact and quantity of the requirements for mitigating measures.

This chapter is based on a paper under review in Tunnelling and Underground Space Technology [Vu et al. \(2015b\)](#).

6.1. INTRODUCTION

One of the obstacles in the development of shallow tunnels in urban areas is the high risk of damage on existing nearby buildings. Although the areas where nearby structures are impacted were estimated in the studies of Kaalberg et al. (2005) and Selemetas et al. (2005), which are based on analyses of empirical data, theoretical understanding on the extent of influence zones induced by tunnelling is still limited. Chapter 2 investigates the stability of tunnelling when reducing the C/D ratio and shows the limitations on the range of the support pressure and the depth of the tunnel. Chapter 3 studies on the structural deformation and tunnel lining parameters and derives the optimal depth of the tunnel. In the analysis of ground movement in Chapter 4, the dependence of ground movement on the volume loss and the impact of shallow tunnelling on buildings are derived. The boundaries of volume loss in shallow tunnelling investigated in Chapter 5 depend on the support pressure, TBM machine parameters and the long-term consolidation. From these analyses, further study can be carried out by combining the boundaries of volume loss in Chapter 5 and the influence zones in Chapter 4 in order to derive the boundaries of influence zones.

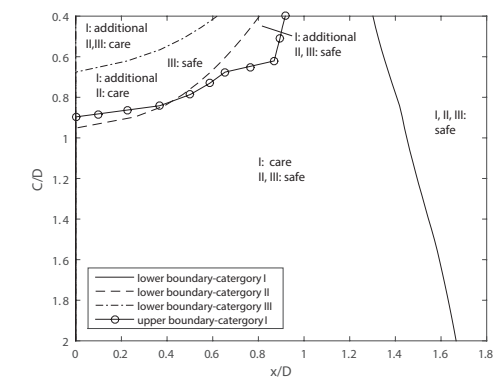
In this chapter, the impact of the range of volume loss in shallow tunnelling on ground movement and buildings is investigated in Section 6.2 with different categories of damage risk assessment and is also compared to some existing shallow tunnelling cases. When shallow tunnelling in urban areas, in order to reduce the influence of tunnelling on the buildings, ground improvement techniques are often applied. In Section 6.3, effects of soil parameters on the relative influence distance x/D induced by shallow tunnelling is also studied to identify possible ground improvement methods.

6.2. ON THE VARIATION OF INFLUENCE ZONES WITH DIFFERENT CATEGORIES OF DAMAGE RISK ASSESSMENT

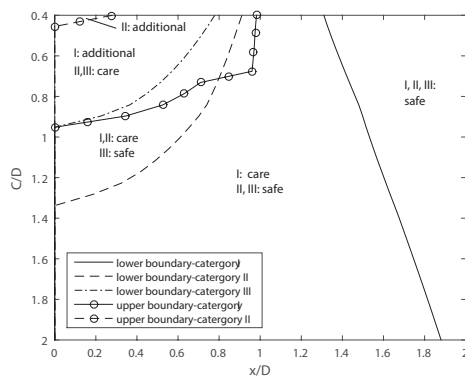
In order to estimate the impact of volume loss and the variation of the extent of the zones affected by tunnelling in relation to the different damage categories, allowable settlement values $u_{max} = 10, 50$ and 75 mm corresponding to the transitions between categories I, II, and III of damage risk assessment in Table 4.1 are applied. The analysis is carried out in the cases of tunnelling with diameters $D = 6, 8$, and 10 m .

Figure 6.1 shows the boundaries of relative influence distances from the tunnel axis to surface buildings x/D and the C/D ratio in these categories of damage risk assessment. In this figure, depending on the relative influence distances x/D , it is indicated whether additional ground improvement and/or careful monitoring control is required, or it should be possible to tunnel safely without additional measures. These relative influence distances are estimated for the three above risk categories.

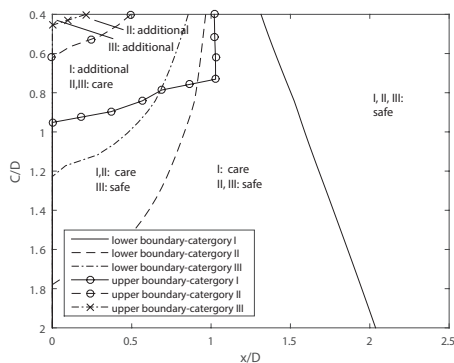
Figure 6.2 shows the effects of tunnel diameters on the relative influence distances due to tunnelling in clay for risk category I. In the case of $C/D = 0.4$ (the lowest C/D ratio value in this study), if buildings are at a relative influence distance x/D less than 0.8, ground treatment should be implemented. When the C/D ratio ranges from 0.8 to 2, careful monitoring is required during the tunnelling progress. In the case of C/D ratios larger than 1, surface buildings will normally deform less than $u_{max} = 10\text{ mm}$. As long as the TBM is properly operated, from this figure, it can also be seen that even if the buildings



(a) D=6m



(b) D=8m



(c) D=10m

Figure 6.1: Relative influence distances due to tunnelling in clay with Risk Categories I,II,III
additional: require additional ground improvement; care: require careful control; safe: safe area with allowable settlement

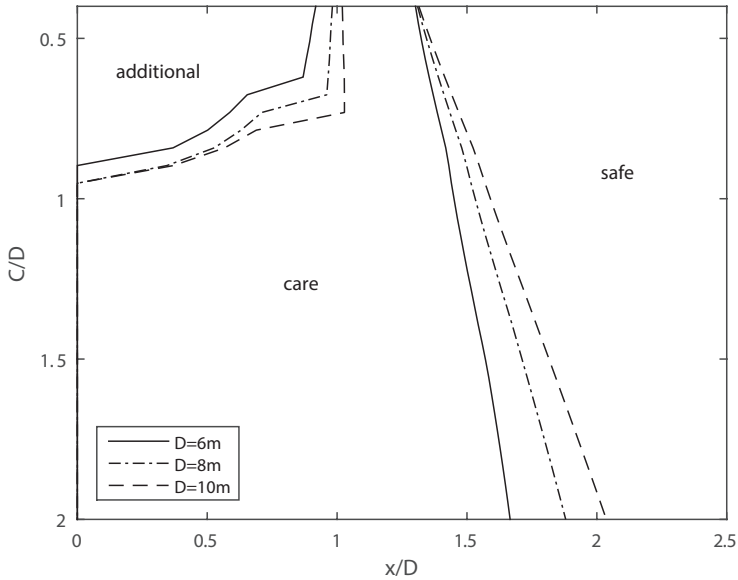


Figure 6.2: Relative influence distances due to tunnelling in clay for risk category I with various tunnel diameter D

are directly above the tunnel, ground improvement methods may not be necessary for tunnelling with an allowable settlement $u_{max} = 10\text{mm}$ with the C/D ratio larger than 1. However, when the relative influence distance x/D is less than 2, careful control is necessary.

In order to apply these results to shallow tunnelling, they should be compared to data observed from existing tunnelling cases. The validation of the impact of shallow tunnelling on ground movement in soft soils is shown in Figure 6.3 for relative influence distances from the tunnel axis to the existing surface buildings. The observed settlement data in shallow tunnelling cases described in Table 6.1 are taken from surface settlement trough data. Since there is only a small number of existing tunnels which have C/D values lower than 2 and detailed surface settlement monitoring data in order to validate, the discussion here will provide recommendations for future shallow tunnelling.

- In Figure 6.3, the cases with observed settlements of more than 10mm are derived from measuring points at or nearby the vertical axis of the tunnel where the surface settlements reach the maximum values as indicated in Chapter 4. Settlements further away from the tunnel axis in these projects, but still in the zone requiring attention are equal or less than 10mm .

- Settlements of approximate 10mm are almost always recorded in the zone indicating special care for projects where ground improvement methods were used and in the normally safe areas in the case of the Frankfurt and Heathrow tunnels, which were constructed without ground improvement.

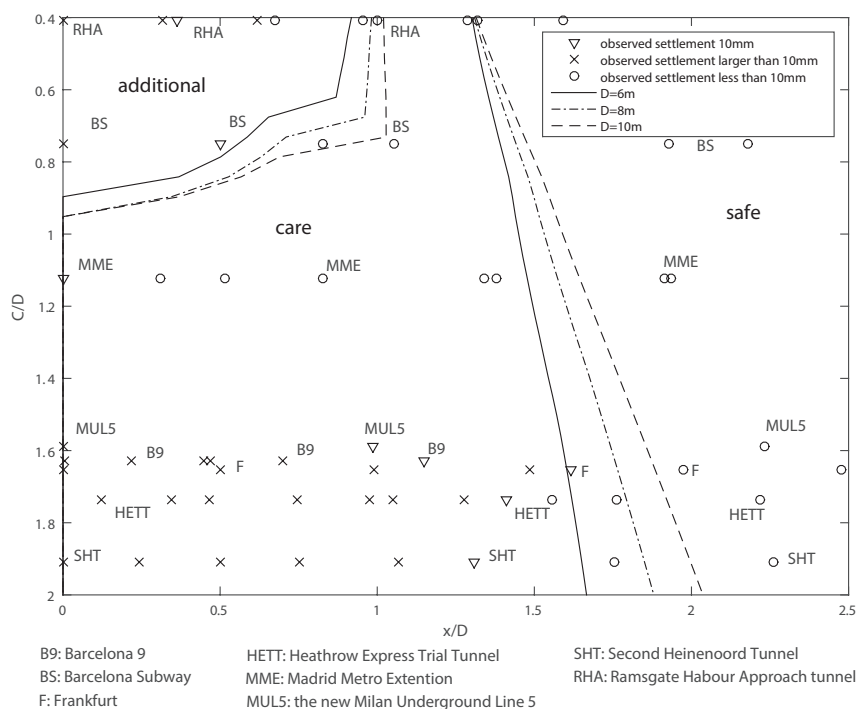


Figure 6.3: Comparison of relative influence distances to shallow tunnelling cases

- For settlements less than 10mm, there are two observed cases, namely the Barcelona Subway and the Madrid Metro Extension, where ground improvement methods were applied and followed with careful monitoring.

In the areas that additional measures are needed, Ramsgate Harbour Approach tunnel was constructed by Perforex pre-vaulting method combined with the fiberglass ground improvement methods (Bloodworth, 2002). This tunnel has a C/D ratio of 0.41, but is not strictly a bored tunnel.

Tunnel	$D(m)$	C/D	$u(mm)x(m)$		x/D	Construction method	Soil type	Ground improvement	Reference
Barcelona Line 9	9.4	1.63	10	10.8	1.149	EPB machine	Miocene material	jet grouting, compensation, structural jacking	Gens et al. (2011)
	9.4	1.63	11.1	10.7	0.7				
	9.4	1.63	17.9	7.2	0.47				
	9.4	1.63	14.9	6.85	0.45				
	9.4	1.63	20.58	3.34	0.22				
Barcelona Subway	9.4	1.63	22.37	0.06	0	-	Stiff clay with gravel	jet grouting	Ledesma and Romero (1997)
	8	0.75	0.24	17.4	2.2				
	8	0.75	0.34	15.41	1.93				
	8	0.75	1.3	6.5	0.83				
	8	0.75	1.5	8.5	1.06				
Frankfurt	8	0.75	10	4	0.5	Shield with bolted concrete segments	Frankfurt clay marl	-	Rowe and Kack (1983)
	8	0.75	23.4	0	0				
	6.5	1.65	3.0	19.27	2.965				
	6.5	1.65	4.85	16.11	2.479				
	6.5	1.65	7.8	12.82	1.972				
Heathrow Express Trial Tunnel	6.5	1.65	10	10.5	1.615	Open face	Stiff clay	-	Deane and Bassett (1995)
	6.5	1.65	12.8	9.652	1.48				
	6.5	1.65	20.9	6.433	0.99				
	6.5	1.65	28.6	3.257	0.5				
	6.5	1.65	32.1	0	0				
	8.5	1.735	0.91	27.64	3.25				
	8.5	1.735	2.83	18.87	2.22				
	8.5	1.735	5.82	14.98	1.76				
	8.5	1.735	8.19	13.22	1.56				
	8.5	1.735	10	12	1.41				
	8.5	1.735	12.54	10.85	1.28				
	8.5	1.735	16.54	8.93	1.05				
	8.5	1.735	18.71	8.29	0.9				
	8.5	1.735	26.65	6.33	0.74				
	8.5	1.735	34.34	3.97	0.47				
	8.5	1.735	36.66	2.92	0.34				
	8.5	1.735	38.84	1.04	0.12				

Table 6.1: Distance x to tunnel center axis corresponding to settlement $u_{max} = 10mm$ in shallow tunnelling cases (continue in next page)

Tunnel	D(m)	C/D	u(mm)	x(m)	x/D	Construction method	Soil type	Ground improvement	Reference
Madrid Metro Extension	8.88	1.12	0.57	17.2	1.94	EPB machine	Stiff Tertiary layers	-	Gonzalez and Sagaseta (2001)
	8.88	1.12	1.4	17	1.9				
	8.88	1.12	2.15	12.6	1.4				
	8.88	1.12	4.63	11.9	1.4				
	8.88	1.12	4.85	7.34	0.83				
	8.88	1.12	7.38	4.56	0.51				
	8.88	1.12	8.72	2.76	0.31				
Milan Underground Line 5	8.88	1.12	10	0	0	EPB machine	coarse-grained soil	Grout injection	Fagnoli et al. (2013)
	6.7	1.59	0.322	21	3.134				
	6.7	1.59	1.611	14.95	2.231				
	6.7	1.59	10	6.6	0.985				
Ramsgate Harbour Approach tunnel	6.7	1.59	21	0	0	Perforex pre-vaulting method	Weathered Chalk	fiberglass	Bloodworth (2002)
	11	0.41	0.72	14.51	1.32				
	11	0.41	1.66	17.5	1.6				
	11	0.41	1.87	11	1				
	11	0.41	2.65	14.1	1.29				
	11	0.41	4.8	7.4	0.67				
	11	0.41	8.9	10.5	1				
	11	0.41	10	4	0.364				
	11	0.41	11.9	0	0				
	11	0.41	12.5	6.8	0.62				
Second Heinenoord Tunnel	11	0.41	13.1	3.5	0.32	Slurry machine	Cohesive Holocene layers and sandy Pleistocene layers	-	Netzel (2009)
	8.3	1.91	1.41	29.2	3.52				
	8.3	1.91	3	18.77	2.26				
	8.3	1.91	5.26	14.56	1.76				
	8.3	1.91	10	10.87	1.31				
	8.3	1.91	15.1	8.87	1.07				
	8.3	1.91	21.8	6.26	0.75				
	8.3	1.91	26.4	4.154	0.5				
	8.3	1.91	29.3	2	0.241				
	8.3	1.91	30.1	0	0				

Table 6.1: Distance x to tunnel center axis corresponding to settlement $u_{max} = 10mm$ in shallow tunnelling cases

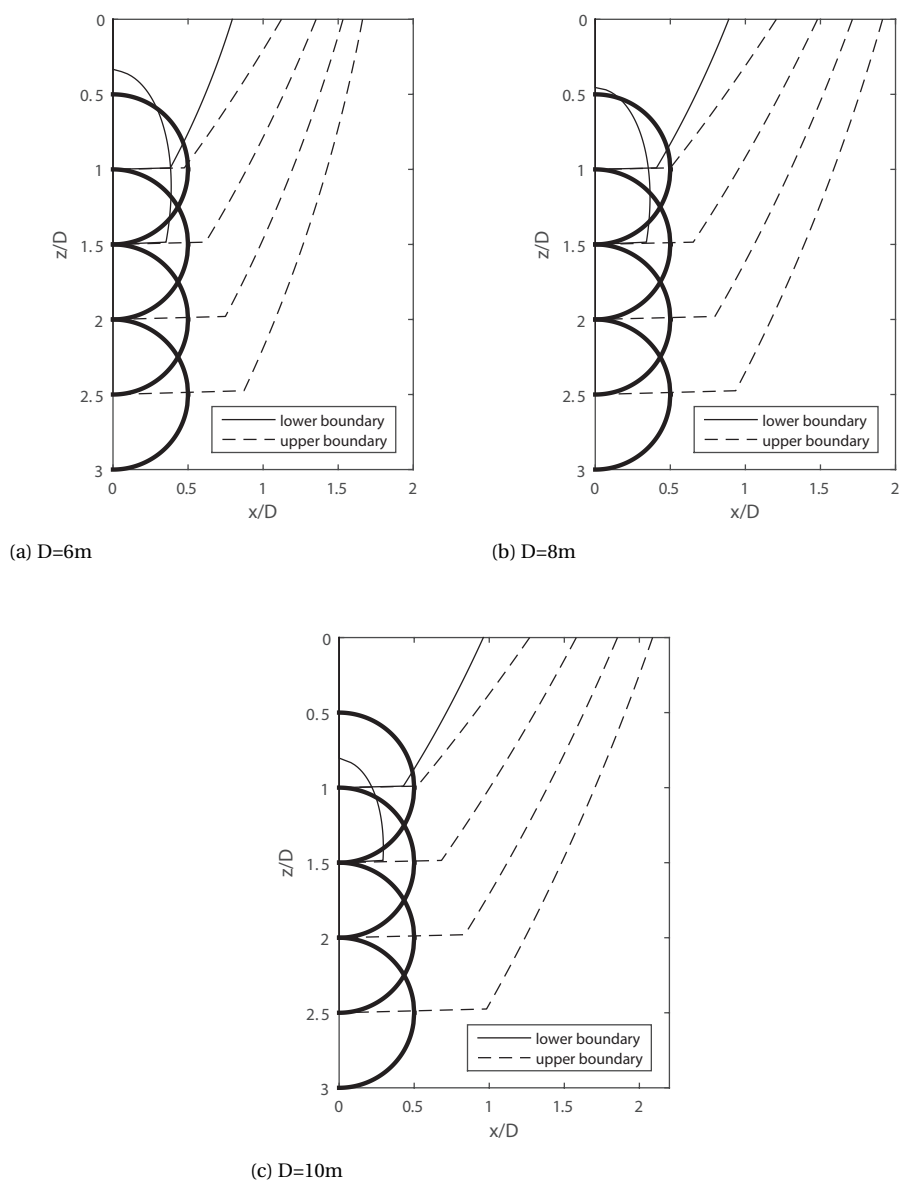


Figure 6.4: Influence zones when shallow tunnelling in clay

In the investigation of subsurface influence zones, Figure 6.4 shows the boundaries of the subsurface zones influenced by tunnelling in clay in the cases of $C/D = 0.5, 1, 1.5$ and 2 with diameters $D = 6, 8$, and 10m and an allowable settlement $u_{max} = 10\text{mm}$ in risk category I. In this zone, which is determined by lower and upper boundaries, careful

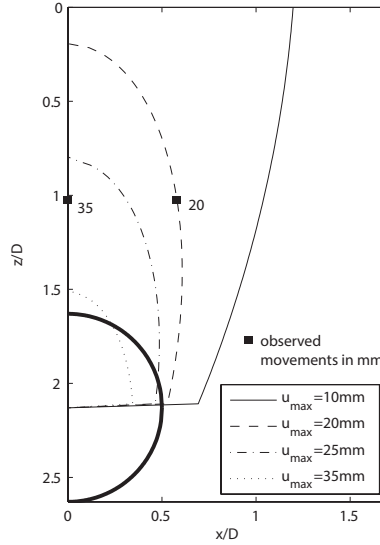


Figure 6.5: Comparison of shallow tunnelling influence zones for the Barcelona Line 9 case

control and monitoring is required when tunnelling. If subsurface structures appear in the zone from lower boundaries to tunnel axis, ground improvement methods are necessary. The area outside from the upper boundaries is safe for subsurface structures. It is shown that the larger the tunnel diameter is, the larger the influence zone is. Additionally, when the tunnel becomes shallower with a smaller C/D ratio, the influence zone reduces, the careful control area becomes smaller and the unsafe area becomes larger. From this analysis, designers can decide the C/D ratio for a particular tunnel with or without adding ground improvement methods to prevent unexpected deformations of existing buildings.

Figure 6.5 shows the validation for the subsurface influence zone in the Barcelona 9 case with $C/D \approx 1.6$ and $D = 9.4m$ at the level $-9.5m$ ($z/D \approx 1$). The observed settlement of $20mm$ at the distance $x/D \approx 0.6$ is on the analysis graph. The maximum settlement of subsurface curve is $35mm$ at the tunnel axis.

6.3. EFFECTS OF SOIL PARAMETERS ON INFLUENCE ZONES

In order to identify the method and quantity of ground improvement that should be applied when tunnelling, the impacts of soil parameters on relative influence distances x/D are investigated. In this study, the effects of the cohesion c , the friction angle ϕ and the modulus of elasticity E on boundaries of influence zones are studied.

Figure 6.6 shows the dependence of the relative influence distance x/D on the cohesion c in the case of tunnelling with $D = 6m$ in soil with friction angle $\phi = 35^\circ$ and elasticity

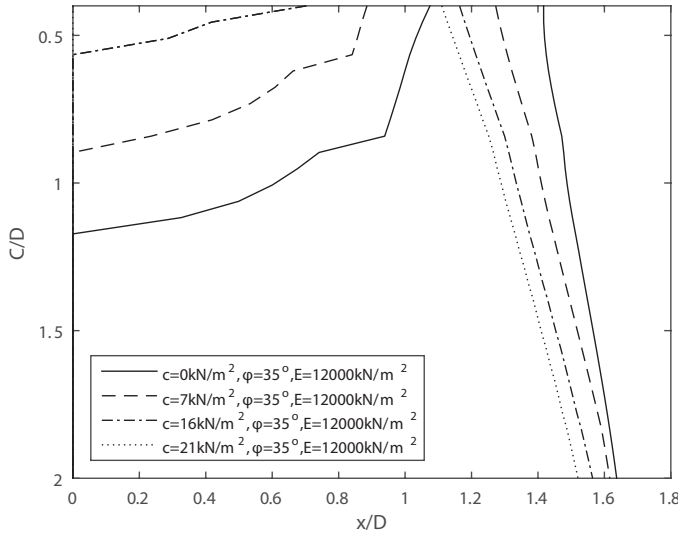


Figure 6.6: Effect of cohesion c on relative influence distance x/D in the case of tunnelling with $D = 6m$

modulus $E = 12000kN/m^2$. When the cohesion c increases, the unsafe relative distance x/D decreases. Moreover, it can also be seen that the gaps between lower boundaries are larger than the gaps between upper boundaries. Based on this analysis, in the case of tunnelling with a small C/D ratio, increasing the value of the cohesion c can be an effective method in order to reduce the relative influence distance x/D . When the value of the cohesion c is approximate $21kN/m^2$, the lower boundary becomes 0 with $C/D = 0.4$. It means that if ground treatment methods can improve the cohesion to $21kN/m^2$, the risk of settlements more than $10mm$ can be limited, but with careful control on grouting and support pressure still needed.

The effect of the friction angle ϕ on the relative influence distance x/D is shown in Figure 6.7. In this analysis, the friction angle ϕ is assessed in the range from 20° to 58° , which corresponds to the maximum friction angle of a grouted soil (Fujita et al., 1998) for a tunnel in soil with cohesion $c = 7kN/m^2$ and elasticity modulus $E = 12000kN/m^2$. It can be seen that when the friction angle ϕ increases, the relative influence distance x/D becomes smaller. However, due to the limitation of increasing of the friction angle ϕ further, a relative influence distance x/D will remain. Based on these results, increasing the friction angle ϕ can be a useful method to reduce the relative influence distance x/D .

Figure 6.8 shows an opposite impact of increasing the modulus of elasticity E on the relative influence distance x/D due to tunnelling for a tunnel in soil with cohesion $c = 7kN/m^2$ and friction angle $\phi = 33^\circ$. This figure shows that the higher the value of the elasticity modulus E is, the larger the relative influence distance x/D is. This is due to the increasing heave at the tail, which leads to more compensation of the settlement of

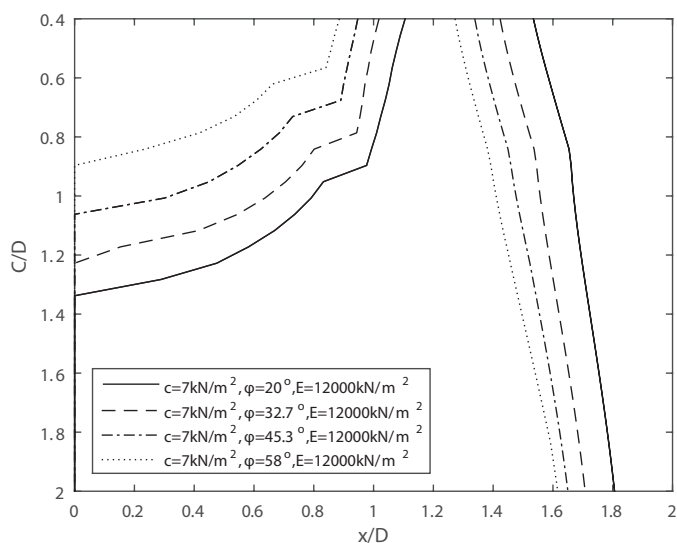


Figure 6.7: Effect of friction angle ϕ on relative influence distance x/D in the case of tunnelling with $D = 6m$

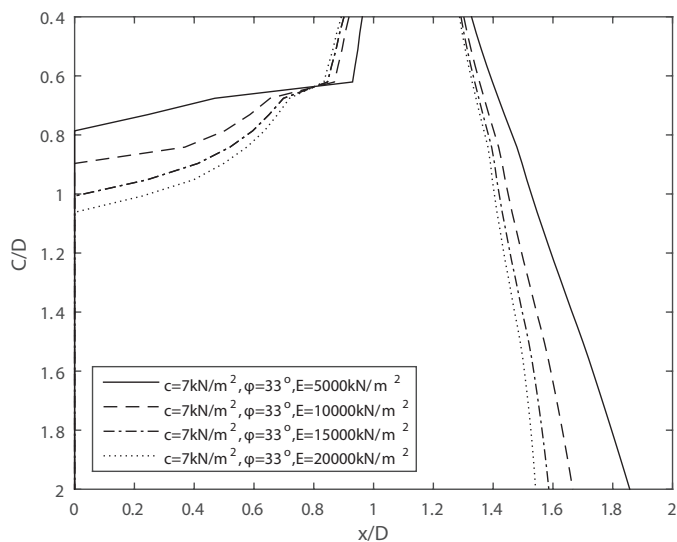


Figure 6.8: Effect of modulus of elasticity E on relative influence distance x/D in the case of tunnelling with $D = 6m$

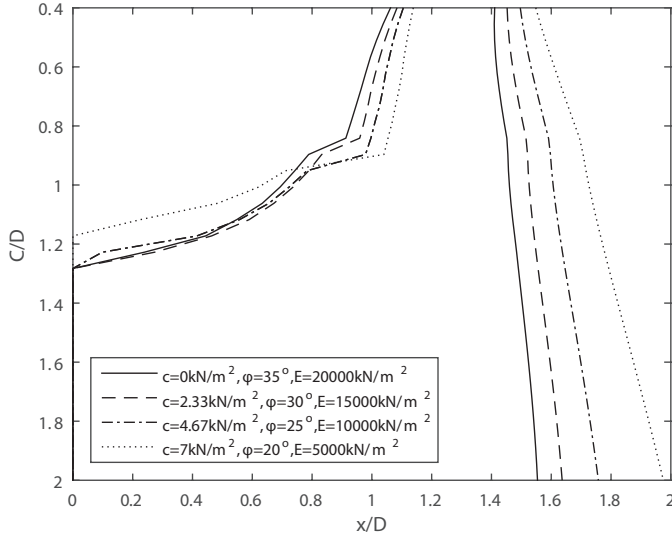


Figure 6.9: Combination influence of soil parameters on relative influence distance x/D in the case of tunnelling with $D = 6m$

tunnelling and a reduction of the total volume loss. However, in practice, when increasing the cohesion c value and friction angle φ value, the modulus of elasticity E of the soil also increases. In this case, it follows that the volume loss at the tunnelling face can be reduced but it is difficult to compensate any settlement at the tail.

Figure 6.9 shows the relationship between the C/D ratio and the relative influence distance x/D in the case of shallow tunnelling with diameter $D = 6m$ with the combination of changing all above soil parameters. With a given distance from the existing buildings to the tunnel axis, required soil parameters can be estimated in order to achieve settlements less than a given allowable settlement. It can be seen that although increasing stiffness and strength has opposite impacts on the width of the influence zone, the combination of these effects can lead to a reduction of the influence zone. On the basis of this analysis, designers can choose suitable ground improvement methods and identify quantities of ground treatment, for example, jet grouting, soil mixing and other mitigating measures.

6

6.4. CONCLUSION

By combining the upper and lower estimates of volume loss and ground movement analysis, the boundaries of influence zones induced by shallow tunnelling are derived both for surface and subsurface in this chapter. The combination of influence zones with different categories of risk damage assessment is investigated in order to identify the zones where mitigating measures should be applied or careful monitoring is needed. Al-

though there is a small number of existing case studies, it is a good agreement between the analysis results and observed data. In order to allow tunnelling in areas, which are deemed to lead to too large surface settlements without additional measures (unsafe zones), this chapter also shows that by improving soil properties, the boundaries of influence zones can be controlled. This analysis provides a theoretical basis to identify the mitigating methods and the required quantity of soil improvement with the aim of safe and damage-free tunnel construction.

7

CONCLUSIONS AND RECOMMENDATIONS

A good traveler has no fixed plans, and is not intent on arriving.

Lao Tzu

This dissertation investigates the effects of reducing the C/D ratio and estimates the limit and/or optimal C/D ratio for shallow tunnelling in soft soils. Moreover, a theoretical basis for protective methods is proposed in order to optimize the tunnelling process. This chapter synthesizes conclusions on the effects of shallow tunnelling and provides recommendations for further research.

7.1. CONCLUSIONS

Tunnels in urban areas are often designed well below the surface in order to reduce the effects on nearby structures. This leads to increased construction costs because of deep station boxes. Despite benefits such as lower construction costs and shorter travelling time between the surface and platforms, what limits understanding of shallow tunnelling effects is a barrier to the development of shallow tunnels in cities. This study firstly investigates the effects of reducing the C/D ratio and estimates the limits and/or optimal C/D ratio for shallow tunnelling in soft soils. Based on this study, recommendations and solutions for improving the shallow tunnelling process have been proposed. Reducing the C/D ratio of a shallow tunnel leads to many effects on the stability and ground movements in the tunnelling process, the deformations of the tunnel lining and the effects on existing nearby buildings.

Stability analysis

In the stability analysis for shallow tunnelling in this study, the range of the support pressures has been estimated for various types of soils and C/D ratios. It is found that it is possible to tunnel with a very low C/D ratio in sand, clayey sand, clay, or organic clay by changing the thickness of the tunnel lining or by adding ballast weight. In the case of tunnelling in peat, due to limitations in control of the margin between maximum and minimum support pressures, a tunnel lining with the d/D ratio larger than 1/12 would allow stable tunnel construction. The stability analysis for uplift has shown that it is possible to tunnel in sand, clayey sand, clay, organic clay but in the case of tunnelling in peat deep cover or ballast layer is required.

In this dissertation, new models for blow-out calculations, which are more accurate when applied to shallow tunnels, were proposed. The significant difference between the required support pressures at the top, the spring line of tunnel and the bottom of the tunnel in the case of shallow tunnels is taken into account. The new models in this study are divided into the uniform support pressures and the linear support pressures at the upper and the lower parts of the tunnel lining. The latter case includes the effect of the reducing pressure in grouting flows. A comparison to a case study and centrifuge results shows a good agreement between the maximum support pressures derived from the new models and field and experimental data. Comparing to the recent models for the maximum support pressure due to blow-out, it is concluded that while the calculated result in Balhaus's model is somewhat exaggerated due to activating a large soil body above the tunnel, Broere's model is probably too conservative. The new models can avoid the risk of blow-out at the top of the tunnel where only a thin soil layer above the tunnel is present while higher support pressures can be used at the spring line and the bottom in order to reduce the potential volume loss.

Structural analysis

The structural analysis in this study investigates the impact of cover on the tunnel lining when the C/D ratio reduces. From this analysis, the change of the maximum bending moments and deformations of the lining sections is estimated. An optimal C/D ratio for a particular cross-section d/D ratio in tunnelling without ballast can be derived in various soils by combining the structural analysis with the uplift analysis.

Commonly used models in the structural analysis for tunnels were proposed by [Duddeck and Erdmann \(1985\)](#). These models are only suitable for moderate and deep tun-

nels with $C/D \geq 2$ as they assume a symmetric load on the tunnel lining. In the case of shallow tunnels, the relative difference between the load at the top and the bottom of the tunnel is significant. A new model proposed for calculating the internal forces and deformations of the tunnel lining in this study is suitable in the case of shallow tunnels. This model takes into account the change of the load on the tunnel lining in each particular point of the tunnel section. The analysis results derived from the new model for a case study of Second Heinenoord Tunnel show an agreement with field data and other numerical analysis. When the tunnel is at a deeper location, the internal forces and deformations of the tunnel lining calculated by this new model come close to the results by Duddeck's model.

Comparing to Duddeck's model, while Duddeck's model uses a symmetric load at the top and the bottom and only radial springs for the soil-structure interaction and the same stiffness for the springs, the new model takes into account the radial and tangential interaction between structure and soil and can show the difference of the soil load at the top and the bottom of the tunnel. Moreover, the normalized internal forces and the deformations of the tunnel lining in the structural analysis by Duddeck's model become smaller when the tunnel is designed at shallow locations, while these values increase significantly in the case of with and without taking buoyancy in the new models. From the structural analysis with the new models, it is also found that there is a minimum value of the maximum deformations of the tunnel lining when changing the depth H of tunnels.

Ground movements

Tunnelling introduces ground movements which can lead to damage on existing nearby buildings. In order to assess the impact of tunnelling, the ground movements around the tunnel are investigated in this study. The ground movement analysis is carried out with the first risk category as proposed by Rankin (1988) and for the preliminary stage of risk assessment with the allowable settlement $u_{max} = 10\text{mm}$ and the allowable slope $w_{max} = 1/500$ according to Mair et al. (1996). On the basis of this theoretical analysis, the extent of the influence zones induced by shallow tunnelling were estimated.

This study proposes two models for assessing the impact of tunnelling on existing buildings for surface and subsurface settlements. From the extent of the influence zones, designers can easily identify if existing buildings are in the zones affected by tunnelling as a preliminary assessment. The influence zones for the subsurface settlement were also derived by assessing the ground movements of subsurface structures, such as the ground movements at the tip of piles.

The calculation models in this study can be applied to the preliminary assessment in the three stage methodology of building damage risk assessment proposed by Mair et al. (1996) and Burland et al. (2001). The allowable values of settlement and slope in this study are adaptable with Eurocode 7. Comparing to Kaalberg et al. (2005) which indicates that the safe distance between the piles and tunnels should be more than $0.5D$ for various volume losses, the results in this study show that the extent of the influence zones induced by tunnelling depends on the value of the u_{max}/V_L ratio. The unsafe zone A, as indicated by Kaalberg et al. (2005), mostly overlaps the zone where $u_{max}/V_L \geq 0.4m$ and the intermediate zone B overlaps the zone where $0.04m \leq u_{max}/V_L \leq 0.4m$. This indicates that the safe area derived from this study depends on the distance, volume loss and the designed allowable settlement of the buildings and the approach followed in this

dissertation can be used to estimate the safe zone also for different combinations of tunnel diameter, cover and soil conditions.

Volume loss

The analysis of ground movements in Chapter 4 shows that the extent of zones affected by shallow tunnelling depends on the volume loss in the tunnelling process. The volume loss in the tunnelling process includes the volume loss at the tunnelling face, along the shield, at the tail and behind the shield due to the long-term consolidation settlement. The upper and lower boundaries of volume loss are estimated for all these components in this study.

In design, the value of volume loss is often taken from experience. No detailed calculation of volume loss along and behind the shield has been published yet. There is only a method to calculate the volume loss at the tunnelling face by Macklin (1999) and Dimmock and Mair (2007) based on project data of tunnelling in London clay. This study used this method in calculating the volume loss at the tunnelling face.

The volume loss along the shield is estimated from the shape of the TBM in Loganathan (2011) or by numerical analysis in Nagel and Meschke (2011). For the volume loss behind the shield, only the consolidation and the cake formation in grout behind the shield have been investigated by Talmon and Bezuijen (2009). In this study, a model for calculating the volume loss along the shield is developed based on the study of Bezuijen and Talmon (2008) on the grout flow along the TBM. It is shown that the volume loss along the shield not only depends on the shape of the overcutting of the TBM but also on the support pressures at the tunnelling face and the tail. For the volume loss at the tail, a method to calculate the surface settlement due to the support pressures is proposed based on the cavity-expansion theory by Yu (2013). This also indicates that a high support pressure can create heave at the tail in order to compensate to the total settlement. In calculating the value of volume loss behind the tail, a method for estimating the long-term consolidation settlement is proposed. Based on this method, the effect of consolidation on the total volume loss is also derived.

From these models, volume loss estimated in this study is not only for the short-term in the tunnelling process (at the tunnelling face, along the TBM and at the tail), but also for the long-term consolidation settlement. The addition of consolidation settlement on the volume loss has been studied in more detail in this dissertation. From a comparison to field data, it shows that the approach proposed in this study can predict the volume loss when shallow tunnelling.

It is also shown that controlling the applied support pressure at the tunnelling face and tail can minimize the total volume loss. From the volume loss boundaries, a direct volume loss around 1% is the feasible volume loss for a very shallow tunnel with $C/D = 0.4$, for deeper tunnels, no volume loss can be achievable. The boundaries of total volume loss are also derived for both short-term tunnelling and long-term consolidation in this study.

Influence zones

Applying the boundaries of volume loss to the ground movement analysis, the boundaries of the zones affected by shallow tunnelling are derived. On the basis of this analysis results, designers can assess damages on existing nearby buildings induced by shallow tunnelling.

The boundaries of influence zones are derived with different categories of damage risk assessment. The effects of soil parameters on the extent of the zones affected by shallow tunnelling is also investigated in this study. With existing nearby buildings and a given tunnel design, the required soil parameters are estimated in order to reach allowable settlements and slopes. These results, therefore, can be a theoretical basis for estimating the amount of ground improvement needed in the case of tunnelling in soft clay or peat by for example, permeation grouting and soil mixing.

Some case studies of shallow tunnelling with $C/D \leq 2$ are used to corroborate the extent of influence zones induced by tunnelling and the application of ground improvement methods. However, the number of case studies is still small, especially the number of cases with $C/D \leq 1$ available. Therefore, these results are a first recommendation for the design of very shallow tunnels in the future only.

In tunnel construction, the quantity of ground improvement has a large contribution to the total cost. However, there are only recommendations for ground improvement or reinforcement in tunnelling based on experience and success in prior projects but little theoretical background for ground improvement in order to reduce the impact of tunnelling. Based on the impact analysis of soil parameters on the extent of zones affected by tunnelling, this study shows a first theoretical analysis for estimating the quantity of ground improvement that should be used in tunnelling in order to achieve the allowable settlements and slopes.

7.2. RECOMMENDATIONS FOR FUTURE RESEARCH

In order to improve our understanding on shallow tunnelling, the following areas should be further studied:

Stability analysis

The model in the uplift analysis in this study is a safe model which does not include soil friction when the soil volume above the tunnel moves. A more detailed analysis could include this effect.

Structural analysis

This dissertation investigates the impact of overburden on the tunnel lining. However, the grouting pressure at the tail is often larger than the soil stress, and as the result, the tunnel lining segments at the tail will experience larger loads due to the construction process. Also, the impact of grouting pressures on the lining at the stage of construction at the tail should be investigated.

Although underground structures are safer than surface structures in earthquakes, there is still a risk for shallow tunnels. Case studies have been shown that shallow tunnels seem to be vulnerable and unsafer comparing to deep tunnels. Moreover, in the case of very shallow tunnels, dynamic surface loading due to vehicles also has a large impact on the tunnel lining. Therefore, other loads such as seismic and dynamic surface loading in the case of very shallow tunnel should be studied. As mentioned in Chapter 3, the new model uses well established and commonly used design assumptions for the loads acting on the tunnel lining. However, these assumptions are deemed conservative and further study is recommended to improve these assumptions based on physical evidence and measurements.

Ground movements

As indicated in Chapter 5, this study focused on the preliminary stage of risk assessment of damage on buildings due to tunnelling. More detailed assessment of the next two steps in Mair et al. (1996) and Burland et al. (2001) should be studied such as the extent of the sagging and hogging influence zones when reducing the C/D ratio and the impact of the building stiffness.

Volume loss

The method of calculating the volume loss at the tunnelling face by Macklin (1999) in this dissertation is based on the data analysis of tunnelling projects in London clay. The volume loss at the tunnelling face in sand, soft clay, and peat should be investigated from other projects in order to have more accurate results.

Overcutting and the shape of the TBM also affect the volume loss along the shield. In the case of shallow tunnels which have a thin overburden, as the friction between soil and TBM is small, the TBM could reduce the difference of the diameter between the TBM and lining and the amount of overcutting. Therefore, an innovation of the TBM for shallow tunnelling could be investigated.

The occurrence of heave at the tail can compensate for the total settlement and reduce the total volume loss. However, while the support pressure is assumed as a uniform support pressure at the tail in volume loss calculation in this dissertation, it changes along the tunnel section in practice. A more detailed calculation for the influence of the change of support pressure at the tail should be investigated.

In the study on the impact of the long-term consolidation settlement on volume loss, only the final consolidation settlement is taken into account. The impact of the time independence of consolidation settlement should be studied.

Influence zones

This study investigated the effects of soil parameters on the boundaries of volume loss. However, there is hardly any literature on estimating the quantity of grout that needs to be injected into soils for improvement, which has a large contribution to construction cost. Therefore, a further study on the effect and estimate of grouting to improve the soil should be carried out.

Although many problems are listed for further study, this dissertation is the first investigation of the impact of reducing the C/D ratio for shallow tunnels in soft soil. The models and results in this study supply more understanding on the effects of shallow tunnelling in soft soils and will help designers optimize shallow tunnelling in the future.

BIBLIOGRAPHY

- ACI-506R-05 (2005). *ACI-506R.Guide to Shotcrete*. American Concrete Institute, Farmington Hills, USA.
- Ahmed, M. and Iskander, M. (2010). Analysis of tunneling-induced ground movements using transparent soil models. *Journal of Geotechnical and Geoenvironmental Engineering*, 137(5):525–535.
- Ahrens, H., Lindner, E., et al. (1982). Zur dimensionierung von tunnelausbauten nach "empfehlungen zur berechnung von tunneln im lockergestein, 1980". *Bautechnik*, 59(8&9).
- Anagnostou, G. and Kovári, K. (1994). The face stability of slurry-shield-driven tunnels. *Tunnelling and Underground Space Technology*, 9(2):165–174.
- Atkinson, J. and Potts, D. (1977). Stability of a shallow circular tunnel in cohesionless soil. *Geotechnique*, 27(2):203–215.
- Attewell, P. and Farmer, I. (1974). Ground disturbance caused by shield tunnelling in a stiff, overconsolidated clay. *Engineering Geology*, 8(4):361–381.
- Attewell, P. and Woodman, J. (1982). Predicting the dynamics of ground settlement and its derivatives caused by tunnelling in soil. *Ground Engineering*, 15(8).
- Attewell, P. B., Yeates, J., and Selby, A. R. (1986). *Soil movements induced by tunnelling and their effects on pipelines and structures*. Methuen, Inc., New York, NY.
- Bakker, K. (2003). Structural design of linings for bored tunnels in soft ground. *Heron*, 48(1):33–64.
- Bakker, K., Leendertse, W., Jovanovic, R., and van Oosterhout, G. (2000). Monitoring: Evaluation of stresses in the lining of the second heinenoord tunnel. *Geotechnical Aspects of Underground Construction in Soft Ground*. Balkema, Tokyo, Japan, pages 197–202.
- Bakker, K. J. (2000). *Soil retaining structures: development of models for structural analysis*. PhD thesis, Delft University of Technology.
- Balthaus, H. (1991). Tunnel face stability in slurry shield tunnelling. In *Proceeding 12th International Conference on Soil Mechanics and Foundation Engineering, Rio de Janeiro, 13–18 August 1989 V2, P775–778*, volume 28, page A391. Pergamon.
- Bezuijen, A. (2007). Bentonite and grout flow around a tbm. In *Underground Space–The 4th Dimension of Metropolises, Proceedings of the World Tunnel Congress 2007 and 33rd ITA/AITES Annual General Assembly, Prague, May 2007*, page 383. CRC Press.

- Bezuijen, A. and AM, T. (2005). Grout properties and their influence on back fill grouting. *Geotechnical aspects of underground construction in soft ground*. Amsterdam: Balkema, pages 187–93.
- Bezuijen, A. and Brassinga, H. E. (2006). Blow-out pressures measured in a centrifuge model and in the field. *Tunnelling: a decade of progress: GeoDelft 1995-2005*, page 143.
- Bezuijen, A. and Talmon, A. (2005a). Grout the foundation of a bored tunnel. *Tunnelling. A Decade of Progress. GeoDelft 1995-2005*, page 95.
- Bezuijen, A. and Talmon, A. (2005b). Monitoring and modelling during tunnel construction. *Tunnelling. A Decade of Progress. GeoDelft 1995-2005*, page 61.
- Bezuijen, A. and Talmon, A. (2008). Processes around a tbm. In *Proceedings of the 6th International Symposium on Geotechnical Aspects of Underground Construction in Soft Ground (IS-Shanghai 2008)*, pages 10–12.
- Bezuijen, A., Talmon, A., Joustra, J., and Grote, B. (2006). Pressure gradients and muck properties at the face of an epb. *Proceeding of Geotechnical aspects of underground construction in soft ground*, pages 195–201.
- Bezuijen, A. and van Seters, A. (2005). The stability of a tunnel face in soft clay. *Tunnelling. A Decade of Progress. GeoDelft 1995-2005*, page 149.
- Blom, C. B. M. (2002). *Design philosophy of concrete linings for tunnels in soft soils*. PhD thesis, Delft University of Technology.
- Bloodworth, A. G. (2002). *Three-dimensional analysis of tunnelling effects on structures to develop design methods*. PhD thesis, University of Oxford.
- Boscardin, M. D. and Cording, E. J. (1989). Building response to excavation-induced settlement. *Journal of Geotechnical Engineering*, 115(1):1–21.
- Bosch, J. W. and Broere, W. (2009). Small incidents, big consequences. leakage of a building pit causes major settlement of adjacent historical houses. amsterdam north-south metro line project. In *Safe Tunnelling for the City and Environment: ITA-AITES World Tunnel Congress, 23-28 May 2009, Budapest, Hungary*. Hungarian Tunneling Association.
- Bowers, K., Hiller, D., and New, B. (1996). Ground movement over three years at the heathrow express trial tunnel. In *Proceedings of the international symposium on geotechnical aspects of underground construction in soft ground, London*, pages 557–562.
- Brassinga, H. and Bezuijen, A. (2002). Modelling the grouting process around a tunnel lining in a geotechnical centrifuge. In *Proceedings of the International Conference on Soil Mechanics and Geotechnical Engineering*, volume 2, pages 1455–1458. AA BALKEMA PUBLISHERS.

- Broere, W. (2001). *Tunnel Face Stability & New CPT Applications*. PhD thesis, Delft University of Technology.
- Broere, W., Faassen, T., Arends, G., and van Tol, A. (2007). Modelling the boring of curves in (very) soft soils during microtunnelling. *Tunnelling and underground space technology*, 22(5):600–609.
- Broms, B. B. and Bennermark, H. (1967). Stability of clay at vertical openings. *Journal of Soil Mechanics & Foundations Div.*
- Burland, J. (1995). *Assessment of risk of damage to buildings due to tunnelling and excavation*. Imperial College of Science, Technology and Medicine.
- Burland, J. B., Standing, J. R., and Jardine, F. M. (2001). *Building response to tunnelling: case studies from construction of the Jubilee Line Extension, London*, volume 200. Thomas Telford.
- Celestino, T., Gomes, R., and Bortolucci, A. A. (2000). Errors in ground distortions due to settlement trough adjustment. *Tunnelling and Underground Space Technology*, 15(1):97–100.
- Chambon, P. and Corté, J.-F. (1994). Shallow tunnels in cohesionless soil: stability of tunnel face. *Journal of Geotechnical Engineering*.
- Cording, E. J. and Hansmire, W. (1975). Displacements around soft ground tunnels. In *5th Pan American Congress on Soil Mechanics and Foundation Engineering*, volume 4, pages 571–633, Buenos Aires.
- Davis, E., Gunn, M., Mair, R., and Seneviratne, H. (1980). The stability of shallow tunnels and underground openings in cohesive material. *Geotechnique*, 30(4).
- Deane, A. and Bassett, R. (1995). The heathrow express trial tunnel. *Proceedings of the ICE-Geotechnical Engineering*, 113(3):144–156.
- Dias, T. G. S. and Bezuijen, A. (2015). Data analysis of pile tunnel interaction. *Journal of Geotechnical and Geoenvironmental Engineering*, 141(12):04015051.
- Dimmock, P. S. and Mair, R. J. (2007). Estimating volume loss for open-face tunnels in london clay. *Proceedings of the ICE-Geotechnical Engineering*, 160(1):13–22.
- Do, N. A., Dias, D., Oreste, P., and Djeran-Maigre, I. (2014). A new numerical approach to the hyperstatic reaction method for segmental tunnel linings. *International Journal for Numerical and Analytical Methods in Geomechanics*.
- Duddeck, H. (1988). Guidelines for the design of tunnels. *Tunnelling and Underground Space Technology*, 3(3):237–249.
- Duddeck, H. and Erdmann, J. (1985). Structural design models for tunnels in soft soil. *Underground Space; (United States)*, 9.

- Einstein, H. H. and Schwartz, C. W. (1979). Simplified analysis for tunnel supports. *Journal of Geotechnical and Geoenvironmental Engineering*, 105(ASCE 14541).
- Fargnoli, V., Boldini, D., and Amorosi, A. (2013). Tbm tunnelling-induced settlements in coarse-grained soils: The case of the new milan underground line 5. *Tunnelling and Underground Space Technology*, 38:336–347.
- Farrell, R., Klar, A., Mair, R., et al. (2012). Tunnels in sands: the effect of size, depth and volume loss on greenfield displacements. *Géotechnique*, 62(5):385–399.
- Festa, D. (2015). *On the Interaction between a Tunnel Boring Machine and the Surrounding Soil*. TU Delft, Delft University of Technology.
- Festa, D., Broere, W., and Bosch, J. (2015). Kinematic behaviour of a tunnel boring machine in soft soil: Theory and observations. *Tunnelling and Underground Space Technology*, 49:208–217.
- Franzius, J. N. (2004). *Behaviour of buildings due to tunnel induced subsidence*. PhD thesis, University of London.
- Fujita, Y., Ishimaru, R., Hanai, S., and Suenaga, Y. (1998). Study on internal friction angle and tensile strength of plain concrete. *Proceedings of fracture mechanics of concrete structures FRAMCOS*, 3:325–334.
- Gemeente-Amsterdam (2009). Geotechnical base report alternative design deep stations and risk assessment bored tunnel. Technical report, Projectbureau Noord/Zuidlijn.
- Gens, A., Di Mariano, A., and Yubero, M. (2011). Epb tunneling in deltaic deposits: observations of ground movements. In *7th International Symposium Geotechnical Aspects of Underground Construction in Soft Ground*.
- Giardina, G. (2013). *Modelling of settlement induced building damage*. PhD thesis, Ph. D. thesis, Delft Univ. of Technology, Delft, Netherlands.
- Gonzalez, C. and Sagaseta, C. (2001). Patterns of soil deformations around tunnels. application to the extension of madrid metro. *Computers and Geotechnics*, 28(6):445–468.
- Grant, R. and Taylor, R. (2000). Tunnelling-induced ground movements in clay. *Proceedings of the ICE-Geotechnical Engineering*, 143(1):43–55.
- Groeneweg, T. (2007). *Shield driven tunnels in ultra high strength concrete: reduction of the tunnel lining thickness*. PhD thesis, MSc Thesis, Delft University of Technology, The Netherlands.
- Han, Y.-w., Zhu, W., Zhong, X.-c., and Jia, R. (2007). Experimental investigation on backfill grouting deformation characteristics of shield tunnel in sand. *Underground Space—The*, 4:303–306.

- Harris, D., Mair, R., Love, J., Taylor, R., and Henderson, T. (1994). Observations of ground and structure movements for compensation grouting during tunnel construction at Waterloo station. *Geotechnique*, 44(4):691–713.
- Hashimoto, T., Nagaya, J., Konda, T., and Tamura, T. (2002). Observation of lining pressure due to shield tunneling. *Geotechnical aspects of underground construction in soft ground, IS-Toulouse*, pages 119–124.
- Hoefsloot, F. (2001). Waterspanningen voor het boor- front: een eenvoudig geohydrologisch model. *Geotechniek oktober*, pages 26–33.
- ITA-Group2 (2000). Guidelines for the design of shield tunnel lining. *Tunnelling and Underground Space Technology*, 15(3):303–331.
- Jacobsz, S. W. (2003). *The effects of tunnelling on piled foundations*. PhD thesis, University of Cambridge.
- Jancsecz, S. and Steiner, W. (1994). Face support for a large mix-shield in heterogeneous ground conditions. In *Tunnelling'94. Papers presented at seventh International Symposium 'Tunnelling'94', held 5-7 July 1994, London*.
- JSSMFE (1993). *Underground Construction in Soft Ground in Japan*. Japanese Society of Soil Mechanics and Foundation Engineering.
- Kaalberg, F., Teunissen, E., Van Tol, A., and Bosch, J. (2005). Dutch research on the impact of shield tunnelling on pile foundations. In *Proceeding of the International Conference on Soil Mechanics and Geotechnical Engineering*, volume 16, page 1615. AA Balkema.
- Kanayasu, S., Kubota, I., and Shikibu, N. (1995). Stability of face during shield tunneling—a survey of Japanese shield tunneling. *Underground Construction in Soft Ground*, pages 337–343.
- Kimura, T. and Mair, R. (1981). Centrifugal testing of model tunnels in soft clay. In *Proceedings of the 10th international conference on soil mechanics and foundation engineering*, pages 319–322. ISSMFE: International Society for Soil Mechanics and Foundation Engineering.
- Leca, E. and Dormieux, L. (1990). Upper and lower bound solutions for the face stability of shallow circular tunnels in frictional material. *Géotechnique*, 40(4):581–606.
- Ledesma, A. and Romero, E. (1997). Systematic backanalysis in tunnel excavation problems as a monitoring technique. In *Proceedings of the International Conference on Soil Mechanics and Foundation Engineering- International Society for Soil Mechanics and Foundation Engineering*, volume 3, pages 1425–1428. AA Balkema.
- Loganathan, N. (2011). An innovative method for assessing tunnelling-induced risks to adjacent structures. *New York: Parsons Brinckerhoff Inc. One Penn Plaza New York*.
- Macklin, S. (1999). The prediction of volume loss due to tunnelling in overconsolidated clay based on heading geometry and stability number. *Ground engineering*, 32(4):30–33.

- Maidl, B. (2012). *Mechanised shield tunnelling*. Wilhelm Ernst & Sohn, Verlag für Architektur und technische Wissenschaften GmbH & Company KG.
- Mair, R. (1989). Discussion leader's report on session 9: Selection of design parameters for underground construction. In *Proceedings of the 12th International Conference on Soil Mechanics and Foundation Engineering, Rio de*, volume 5, pages 2891–2893.
- Mair, R., Gunn, M., and O'Reilly, M. (1982). Ground movement around shallow tunnels in soft clay. *Tunnels & Tunnelling International*, 14(5).
- Mair, R. and Taylor, R. (1999). Theme lecture: Bored tunnelling in the urban environment. *of XIV ICSMFE [131]*, pages 2353–2385.
- Mair, R., Taylor, R., and Bracegirdle, A. (1993). Subsurface settlement profiles above tunnels in clays. *Geotechnique*, 43(2).
- Mair, R., Taylor, R., and Burland, J. (1996). Prediction of ground movements and assessment of risk of building damage due to bored tunnelling. In *Fourth International Symposium of International Conference of Geotechnical Aspects of on Underground Construction in Soft Ground*, pages 713–718. AA Balkema.
- Mashimo, H. and Ishimura, T. (2005). Numerical modelling of the behavior of shield tunnel lining during assembly of a tunnel ring. *Earth*, 60(80.0):100–0.
- Matter, J. and Portner, J. (2004). Successful grouting for the zimmerberg base tunnel. *Tunnelling and Underground Space Technology*, 19:504–505.
- Melis, M., Medina, L., and Rodríguez, J. M. (2002). Prediction and analysis of subsidence induced by shield tunnelling in the madrid metro extension. *Canadian Geotechnical Journal*, 39(6):1273–1287.
- Miki, K., Yokomizo, F., Ueda, H., Hino, Y., and Yamamoto, H. (2009). Development of construction method for a road underpass at intersection. In *Proceedings of 2009 World Tunnel Congress. Budapest*.
- Moh, Z., Ju, D. H., and Hwang, R. (1996). Ground movements around tunnels in soft ground. In *Proc. Int. Symposium on Geotechnical Aspects of Underground Constructions in Soft Ground. London: Balkema*, pages 725–730.
- Molins, C. and Arnau, O. (2011). Experimental and analytical study of the structural response of segmental tunnel linings based on an in situ loading test.: Part 1: Test configuration and execution. *Tunnelling and Underground Space Technology*, 26(6):764–777.
- Möller, S. C. (2006). *Tunnel induced settlements and structural forces in linings*. Univ. Stuttgart, Inst. f. Geotechnik.
- Mollon, G., Dias, D., and Soubra, A.-H. (2009a). Face stability analysis of circular tunnels driven by a pressurized shield. *Journal of geotechnical and geoenvironmental engineering*, 136(1):215–229.

- Mollon, G., Dias, D., and Soubra, A.-H. (2009b). Probabilistic analysis and design of circular tunnels against face stability. *International Journal of Geomechanics*, 9(6):237–249.
- Mollon, G., Phoon, K. K., Dias, D., and Soubra, A.-H. (2010). Validation of a new 2d failure mechanism for the stability analysis of a pressurized tunnel face in a spatially varying sand. *Journal of Engineering Mechanics*, 137(1):8–21.
- Morgan, H. (1961). A contribution to the analysis of stress in a circular tunnel. *Geotechnique*, 11(1):37–46.
- Mori, A., Tamura, M., Kurihara, K., and Shibata, H. (1991). A suitable slurry pressure in slurry-type shield tunneling. *Proc Tunnelling '91, London*, pages 361–369.
- Muir Wood, A. (1975). The circular tunnel in elastic ground. *Geotechnique*, 25(1):115–127.
- Muir Wood, A. (1976). Discussion: The circular tunnel in elastic ground. *Geotechnique*, 26(1):231–237.
- Nagel, F. and Meschke, G. (2011). Grout and bentonite flow around a tbm: Computational modeling and simulation-based assessment of influence on surface settlements. *Tunnelling and Underground Space Technology*, 26(3):445–452.
- NEN-3650 (2012). *NEN 3650-2012 nl Eisen voor buisleidingsystemen*.
- NEN-EN 1992-1-1, C. E. (1992). Design of concrete structures - part 1-1 : General rules and rules for buildings. *European Prestandard ENV*, 1.
- NEN-EN 1997-1, C. E. (1997). Eurocode 7 geotechnical design - part 1: General rules. *European Prestandard ENV*, 1.
- Netzel, H. D. (2009). *Building response due to ground movements*. TU Delft, Delft University of Technology.
- Ng, C. and Springman, S. (1994). Uplift resistance of buried pipelines in granular materials. In *Centrifuge*, volume 94, pages 753–758.
- O'Reilly, M. (1988). Evaluating and predicting ground settlements caused by tunnelling in london clay. In *Tunnelling*, volume 88, pages 231–241.
- O'Reilly, M. and New, B. (1982). Settlements above tunnels in the united kingdom-their magnitude and prediction. Technical report, Institution of Mining and Metallurgy.
- Oreste, P. (2007). A numerical approach to the hyperstatic reaction method for the dimensioning of tunnel supports. *Tunnelling and underground space technology*, 22(2):185–205.
- Peck, R. B. (1969). Deep excavations and tunnelling in soft ground. In *Proc. 7th Int. Conf. on SMFE*, pages 225–290.

- Plizzari, G. and Tiberti, G. (2006). Steel fibers as reinforcement for precast tunnel segments. *Tunnelling and Underground Space Technology*, 21(3):438–439.
- Rankin, W. (1988). Ground movements resulting from urban tunnelling: predictions and effects. *Geological Society, London, Engineering Geology Special Publications*, 5(1):79–92.
- Rowe, R. and Kack, G. (1983). A theoretical examination of the settlements induced by tunnelling: four case histories. *Canadian Geotechnical Journal*, 20(2):299–314.
- Sagaseta, C. (1988). Analysis of undrained soil deformation due to ground loss. *Geotechnique*, 38(4).
- Schmid, H. (1926). *Statische Probleme des Tunnel-und Druckstollenbaues und ihre gegenseitigen Beziehungen*. Springer.
- Schulze, H. and Duddeck, H. (1964). Spannungen in schildvorgetriebenen tunneln. *Beton-und Stahlbetonbau*, 59(8):169–175.
- Selemetas, D., Standing, J., and Mair, R. (2005). The response of full-scale piles to tunnelling. In *Proceedings of the 5th International Symposium on Geotechnical Aspects of Underground Construction in Soft Ground*, pages 763–769. Taylor and Francis.
- Stein, D. (2005). *Trenchless technology for installation of cables and pipelines*. Stein & Partner Bochum, Germany.
- Strack, O. E. (2002). *Analytic solutions of elastic tunneling problems*. PhD thesis, Delft University of Technology.
- Talmon, A. and Bezuijen, A. (2005). Grouting the tail void of bored tunnels: the role of hardening and consolidation of grouts. In *Geotechnical Aspects of Underground Construction in Soft Ground: Proceedings of the 5th International Symposium TC28. Amsterdam, the Netherlands, 15-17 June 2005*, page 319. Taylor & Francis US.
- Talmon, A. and Bezuijen, A. (2009). Simulating the consolidation of tbm grout at noord-plaspolder. *Tunnelling and Underground Space Technology*, 24(5):493–499.
- Taylor, R. (1993). Prediction of clay behaviour around tunnels using plasticity solutions. In *Predictive Soil Mechanics: Proceedings of the Wroth Memorial Symposium Held at St. Catherine's College, Oxford, 27-29 July 1992*, page 449. Thomas Telford.
- Trautmann, C. H., O'Rourke, T. D., and Kulhawy, F. H. (1985). Uplift force-displacement response of buried pipe. *Journal of Geotechnical Engineering*, 111(9):1061–1076.
- Verruijt, A. (1997). A complex variable solution for a deforming circular tunnel in an elastic half-plane. *International Journal for Numerical and Analytical Methods in Geomechanics*, 21(2):77–89.
- Vorster, T. E. B. (2006). *The effects of tunnelling on buried pipes*. PhD thesis, University of Cambridge.

- Vu, M. N., Broere, W., and Bosch, J. W. (2015a). Effects of cover depth on ground movements induced by shallow tunnelling. *Tunnelling and Underground Space Technology*, 50:499–506.
- Vu, M. N., Broere, W., and Bosch, J. W. (2015b). Estimating the influence zones induced by shallow tunnelling. *In under review in Tunnelling and Underground Space Technology*.
- Vu, M. N., Broere, W., and Bosch, J. W. (2015c). The impact of shallow cover on stability when tunnelling in soft soils. *Tunnelling and Underground Space Technology*, 50:507–515.
- Vu, M. N., Broere, W., and Bosch, J. W. (2015d). The impact of shallow cover on tunnelling in soft soil. In Kolic, D., editor, *ITA WTC 2015 Congress and 41st General Assembly*.
- Vu, M. N., Broere, W., and Bosch, J. W. (2015e). Structural analysis for shallow tunnels in soft soil. *In under review in International Journal of Geomechanics*.
- Vu, M. N., Broere, W., and Bosch, J. W. (2016a). Effects of cover depth on ground movements induced by shallow tunnelling. In *ITA WTC 2016 Congress and 42nd General Assembly*.
- Vu, M. N., Broere, W., and Bosch, J. W. (2016b). Volume loss in shallow tunnelling. *Tunnelling and Underground Space Technology*, 59:77–90.
- White, D., Barefoot, A., and Bolton, M. (2001). Centrifuge modelling of upheaval buckling in sand. *International Journal of Physical Modelling in Geotechnics*, 1(2):19–28.
- Windels, R. (1966). Spannungstheorie zweiter ordnung für den teilweise gebetteten kreisring. *Die Bautechnik*, 43:265–274.
- Windels, R. (1967). Kreisring im elastischen kontinuum. *Der Bauingenieur Bd*, 42:429.
- Winkler, E. (1867). Theory of elasticity and strength. *Dominicus Prague*.
- Yu, H.-S. (2013). *Cavity expansion methods in geomechanics*. Springer Science & Business Media.

A

BLOW-OUT MODEL

A.1. UNIFORM SUPPORT PRESSURE

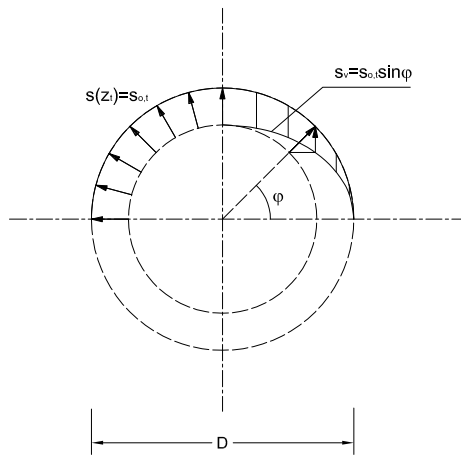


Figure A.1: Uniform support pressure at the upper part of the tunnel

The weight of soil layers above the tunnel is given by:

$$G_1 = DH\gamma - \frac{\pi}{8}D^2\gamma \quad (\text{A.1})$$

where $H = C + \frac{D}{2}$.

In Figure 2.23 and 2.25, the weight of the tunnel lining is estimated as:

$$G_2 \approx \pi\gamma_T Dd \quad (\text{A.2})$$

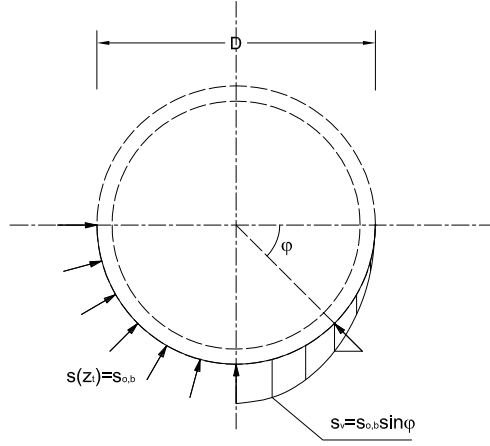


Figure A.2: Uniform support pressure at the lower part of the tunnel

The shear forces between soil column and the surrounding soil are:

$$2\tau_y = 2 \left(C + \frac{D}{2} \right) \left[c + \frac{1}{2} \left(C + \frac{D}{2} \right) K_y \gamma' \tan \varphi \right] \quad (\text{A.3})$$

The total vertical support force is given by:

$$S_v = \int_0^\pi d\varphi \int_0^R s \sin \varphi dr = Ds \quad (\text{A.4})$$

From the equilibrium condition at the upper part of the tunnel, the total vertical support force equals the sum of the soil body weight and the shear forces between the soil column above the tunnel and surrounding ground. We have:

$$S_v = G_1 + 2\tau \quad (\text{A.5})$$

Or:

$$Ds = \gamma \left[\left(C + \frac{D}{2} \right) D - \frac{\pi}{8} D^2 \right] + 2 \left(C + \frac{D}{2} \right) \left[c + \frac{1}{2} \left(C + \frac{D}{2} \right) K_y \gamma' \tan \varphi \right] \quad (\text{A.6})$$

From this, the uniform support pressure at the upper part can be estimated as:

$$s_{t,max} = s_{0,t} = \gamma' \left(H - \frac{\pi}{8} D \right) + 2 \frac{H}{D} \left(c + \frac{1}{2} H K_y \gamma' \tan \varphi \right) \quad (\text{A.7})$$

At the lower part of the tunnel in Figure A.2, the soil body weight, the shear forces between the soil column and the surrounding ground, and the weight of the tunnel are taken into account. Therefore, the equilibrium condition can be shown as:

$$S_v = G_1 + G_T + 2\tau \quad (\text{A.8})$$

Or:

$$Ds = \gamma \left[\left(C + \frac{D}{2} \right) D - \frac{\pi}{8} D^2 \right] + 2 \left(C + \frac{D}{2} \right) \left[c + \frac{1}{2} \left(C + \frac{D}{2} \right) K_y \gamma' \tan \varphi \right] + \gamma_T \pi D d \quad (\text{A.9})$$

From this, the maximum uniform supporting pressure at the lower part of the tunnel can be estimated as:

$$s_{b,max} = s_{0,b} = \gamma \left(H - \frac{\pi}{8} D \right) + 2 \frac{H}{D} \left(c + \frac{1}{2} H K_y \gamma' \tan \varphi \right) + \gamma_T \pi d \quad (\text{A.10})$$

A.2. LINEAR SUPPORT PRESSURE WITH GRADIENT δ_p

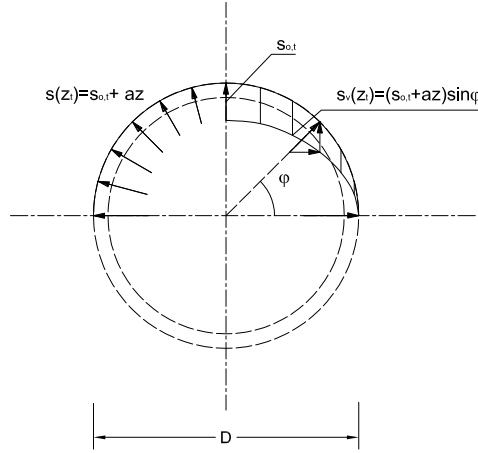


Figure A.3: Linear support pressure at the upper part of the tunnel

At upper part of the tunnel section in Figure A.3 ($0 \leq \varphi \leq \pi$), support pressure on the upper part of the tunnel section is given by:

$$s = s_{0,t} + \delta_p R \cos \varphi \quad (\text{A.11})$$

where δ_p is the vertical pressure gradient and $s_{0,t}$ is the support pressure at the top of the tunnel face.

The total vertical support force can be estimated by:

$$S_v = \int_0^\pi d\varphi \int_0^R (s_{0,t} + \delta_p R \cos \varphi) \sin \varphi dr = D s_{0,t} + \delta_p \frac{D^2}{4} \quad (\text{A.12})$$

From the vertical equilibrium condition at the upper part of the tunnel, the total vertical support force equals the sum of the weight of soil column above the tunnel and the shear forces between the soil column and the surrounding ground. We have:

$$D s_{0,t} + \delta_p \frac{D^2}{4} = \gamma \left[\left(C + \frac{D}{2} \right) D - \frac{\pi}{8} D^2 \right] + 2 \left(C + \frac{D}{2} \right) \left[c + \frac{1}{2} \left(C + \frac{D}{2} \right) K_y \gamma' \tan \varphi \right] + \delta_p \frac{D^2}{4} \quad (\text{A.13})$$

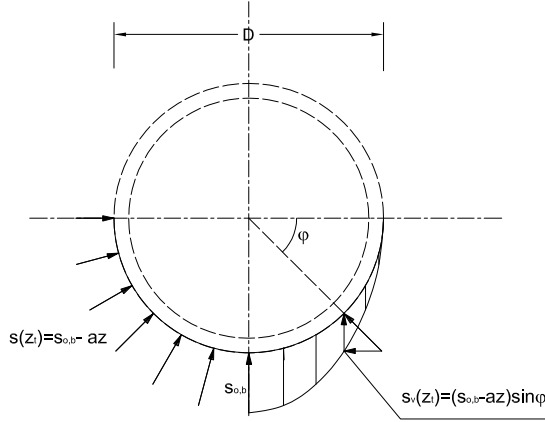


Figure A.4: Linear support pressure at the lower part of the tunnel

From this, the maximum support pressure at the top of the tunnel face can be estimated as:

$$s_{0,t,max} = \gamma \left(H - \frac{\pi}{8} D \right) + 2 \frac{H}{D} \left(c + \frac{1}{2} HK_y \gamma' \tan \varphi \right) - \frac{\delta_p D}{4} \quad (A.14)$$

Support pressure at the lower part of the tunnel in Figure A.4 with $-\pi \leq \varphi \leq 0$ is given by:

$$s = s_{0,b} + \delta_p R \cos \varphi \quad (A.15)$$

where $s_{0,b}$ is the support pressure at the bottom of the tunnelling face.

The total vertical support force at the lower part of the tunnel is estimated as:

$$S_v = \int_0^\pi d\varphi \int_0^R (s_{0,b} + \delta_p R \cos \varphi) \sin \varphi dr = D s_{0,b} - \delta_p \frac{D^2}{4} \quad (A.16)$$

At the lower part of the tunnel, besides the soil body weight and the shear forces between the soil column and the surrounding ground, the weight of the tunnel is also taken into account. Therefore, the vertical equilibrium condition is shown as:

$$D s_{0,b} - \delta_p \frac{D^2}{4} = \gamma \left[\left(C + \frac{D}{2} \right) D - \frac{\pi}{8} D^2 \right] + 2 \left(C + \frac{D}{2} \right) \left[c + \frac{1}{2} \left(C + \frac{D}{2} \right) K_y \gamma' \tan \varphi \right] + \gamma_T \pi D d - \delta_p \frac{D^2}{4} \quad (A.17)$$

From this, the maximum support pressure at the bottom of the tunnelling face is estimated as:

$$s_{0,b,max} = \gamma \left(H - \frac{\pi}{8} D \right) + 2 \frac{H}{D} \left(c + \frac{1}{2} HK_y \gamma' \tan \varphi \right) + \frac{\delta_p D}{4} \quad (A.18)$$

B

GROUND MOVEMENT

In Equation 4.17, the distance x from the building to tunnel axis with a given settlement u_{max} is:

$$x = \sqrt{-2i^2 \ln\left(\frac{u_{max}}{S_{v,max}}\right)} = \sqrt{-2i^2 \ln\left(\frac{u_{max} i 4\sqrt{2}}{V_L D^2 \sqrt{\pi}}\right)}$$

With $A = \frac{u_{max} i 4\sqrt{2}}{V_L D^2 \sqrt{\pi}}$, Equation 4.17 becomes:

$$x = \sqrt{-2i^2 \ln(Ai)} \quad (\text{B.1})$$

In Figure 4.14, the distance x value is equal to x_0 when the first derivative of x equals 0:

$$x' = \frac{1}{2} \frac{-4i \ln(Ai) - 2i}{\sqrt{-2i^2 \ln(Ai)}} = 0 \quad (\text{B.2})$$

Solving Equation B.2 yields:

$$i = \frac{1}{A\sqrt{e}} \quad (\text{B.3})$$

and from Equation B.3 and B.1, the distance x_0 follows as:

$$x_0 = \sqrt{-2 \left(\frac{1}{A\sqrt{e}}\right)^2 \ln\left(A \frac{1}{A\sqrt{e}}\right)} = \frac{1}{A\sqrt{e}} = \frac{V_L D^2 \sqrt{\pi}}{u_{max} 4\sqrt{2}e} \approx 0.19 \frac{V_L D^2}{u_{max}} \quad (\text{B.4})$$

LIST OF SYMBOLS

General

c	cohesion
c_u	undrained shear strength of the ground
C	cover depth
C_s	compression constant
C_{swel}	swelling constant
d	thickness of the tunnel lining
D	diameter of the tunnel
E_s	stiffness modulus of the ground
g	acceleration of gravity
H, z_0	depth of the tunnel
K	coefficient of lateral earth pressure
R	radius of the tunnel
γ'	soil volumetric weight
γ'_g	effective volumetric weight of soil
γ_w	volumetric weight of water
γ_T	weight unit of the tunnel lining (concrete)
ν	Poisson's ratio
φ, ϕ	friction angle

Stability analysis

a	relaxation length
d_{gr}	width of the tail void gap
G_1	weight of the soil layers above the tunnel
G_2	weight of the tunnel
G_A	uplift force
K_{A3}	three dimensional earth pressure coefficient
K_0	coefficient of neutral horizontal effective stress
N	stability ratio
N_{TC}	critical stability ratio
N_s, N_γ	Leca & Dormieux weighting coefficients
N_c	Mollon's coefficient

p	pore pressure
q_s	surface load
q_0	arbitrary surface surcharge in Broere's model
s	support pressure
s_{min}	minimum support pressure
s_{max}	maximum support pressure
$s_{t,max}$	maximum allowable uniform support pressure at the top of the tunnel
$s_{b,max}$	maximum allowable uniform support pressure at the bottom of the tunnel
$s_{0,t,max}$	maximum allowable linear support pressure at the top of the tunnel
$s_{0,b,max}$	maximum allowable linear support pressure at the bottom of the tunnel
δ_p	vertical pressure gradient
$\eta_{blow-out}$	safety index for blow-out
η_{uplift}	safety index for uplift
$\eta_{porepressure}$	safety index for pore pressure
$\eta_{\sigma'_h}$	safety index for effective horizontal pressures
ρ_{gr}	the density of the grout
τ_y	shear strength of the grout

Structural analysis

E	Young's modulus of the ground
E_s	stiffness modulus of the ground
E_c	elasticity modulus of the ground
$E_l I_l$	normal stiffness of the tunnel lining
k	ground reaction modulus (spring stiffness)
k_s	stiffness of tangential spring
k_r	stiffness of radial spring
$k_{n,i}$	stiffness of radial spring in each element
$k_{s,i}$	stiffness of tangential spring in each element
p	ground bedding pressure
p_{lim}	maximum reaction pressure
S	radial displacement of tunnel lining
ϕ	angle between the element axis and the vertical axis of a tunnel section
α_D	relative stiffness
β	dimensionless factor for the ground reaction modulus in the Oreste's model
η^*	apparent stiffness of the ground
$\eta_{n,0}$	radial ground reaction modulus
η_s, η_n	stiffness of tangential and radial (normal) springs

Ground movement analysis

D_0	diameter where for D less than D_0 the surface settlement is always less than the allowable settlement u_{max}
i	width of the settlement trough
K	trough width parameter
L_p	pile length
s_h	horizontal displacement
s_v	transverse settlement of the ground surface
$s_{v,max}$	maximum transverse settlement of the ground surface
$s_v(y)_{(x=0)}$	vertical settlement in the longitudinal direction
$s_h(y)_{(x=0)}$	horizontal settlement in the longitudinal direction
u_{max}	maximum allowable settlement
V_L	volume loss
V_s	volume of settlement trough
x	distance from tunnel axis to existing building
x_0	distance from tunnel axis to existing building where settlement is always less than u_{max}
ω	slope or ground distortion
ω_{max}	maximum allowable slope

Volume loss analysis

a	reduction of shield diameter
G	shear modulus of soil
$h_{overcut}$	overcutting width
k	constant corresponding to cylindrical or spherical models
LF	load factor
p_0	pre-tunnelling pressure
R_p	plastic zone radius
r	distance from the assessment point to the tunnel centre
s_f	maximum fracturing pressures
s_{tail}	grout pressure in the tail
u_c	consolidation settlement at the surface
u_s	soil displacement in the elastic/plastic zone
u_t	surface settlement at the tail
V_{cons}	volume of consolidation settlement at the surface
$V_{L,f}$	volume loss at tunnelling face
$V_{L,s}$	volume loss along the shield
$V_{L,t}$	volume loss at the tail
$V_{L,c}$	volume loss due to consolidation

w_j	joint width between the tunnel and the soil
Δp	change of the pressure due to flow
Δx	length increment
σ_r	radial stress in cavity expansion theory
σ_θ	tangential stress in cavity expansion theory
σ_{soil}	stress in the soil
σ_0	initial stress in the soil
τ_y, τ_y^{grout}	shear strength of the grout around the TBM
$\tau_y^{bentonite}$	shear strength of bentonite

SUMMARY

In urban areas, tunnels are often constructed well below the surface to minimize damage to existing nearby buildings. This comes with deep station boxes and increases the construction costs. Although shallow tunnels have many benefits because of the lower short-term construction costs and the long-term operational costs, the limitations in the understanding of shallow tunnelling in soft soils form obstacles to development in urban areas.

This study investigates the impact of reducing the C/D ratio of shallow tunnels in soft soils in relation to the following issues: stability, structure, ground movement and effects on existing buildings and volume loss. From this, the limit and/or optimal C/D ratio for shallow tunnelling is derived and recommendations and/or solutions for improving the shallow tunnelling process have been proposed.

Firstly, the stability analysis for shallow tunnelling was carried out on the basis of the uplift, face stability and blow-out mechanisms. The relationships between the C/D ratio and the required d/D ratio and required support pressures were investigated with various soils. Related models in the literature were applied and new models were proposed and compared. The ranges of support pressures were estimated for TBM machines, especially for EPB. It was found that in the case of shallow tunnelling in peat, a tunnel lining with a d/D ratio larger than $1/12$ would allow stable tunnel construction.

Secondly, structural analysis investigated the effect on deformations and the internal forces of the tunnel lining when the C/D ratio was decreased. Since recent models in tunnel design are only applied for moderate and deep tunnels with $C/D \geq 2$, a new structural analysis model for shallow tunnels, which includes the different loads at the top and at the bottom of the tunnel, was proposed and validated with a case study. The variation in internal forces and deformations of the tunnel lining was analyzed when reducing the C/D ratio. The results showed that a significant difference between the new models and the existing models lies in the increasing of the maximum deformations of the tunnel lining in the cases of very shallow tunnels. It also derived optimal C/D ratios with various d/D ratios for shallow tunnels in soft soils. These values were combined with the results of stability analysis in order to derive optimal C/D and d/D values.

Tunnelling leads to ground movement not only on the surface but also in the subsurface. Such movements might lead to the damage of existing nearby buildings. This research investigated the affected areas of the shallow tunnelling and the relationship between these areas and the C/D values. Two analysis models were proposed to estimate the affected areas for the preliminary assessment of the risk of building damage. The affected areas were derived with different tunnel diameters in various soil types and were compared with recent studies.

The next part of this study studied volume loss due to shallow tunnelling. The total volume loss was estimated at the tunnelling face, along the TBM, at the tail and with long-term consolidation settlement. At the tunnelling face, the method of [Macklin \(1999\)](#),

which was derived from case study analysis, was applied. A new calculation method was proposed based on the research of [Bezuijen and Talmon \(2008\)](#) on grouting flows along the TBM. At the tail, an analysis model based on cavity-expansion theory was presented. A calculation for estimating the volume loss attributed to long-term consolidation settlement was also carried out. From these analyses, boundaries for volume loss induced by shallow tunnelling were derived both for short-term construction and for long-term consolidation and compared to case studies. This showed that in the case of very shallow tunnelling, no volume loss is feasible with a very careful control of support pressure.

In the fifth part of this study, the boundaries of the affected areas were derived by combining the ground movement analysis and volume loss for surface and subsurface displacements and was then discussed with the case studies. The effect of soil parameters was also investigated in order to estimate the required soil strength for stable tunnelling. The investigation when reducing the C/D ratio in this study provides more understanding on the effects of shallow tunnelling in soft soils and will help designers to optimize shallow tunnelling in the future.

SAMENVATTING

Tunnels in stedelijk gebied worden veelal ver beneden maaiveld aangelegd, om schade aan bestaande bebouwing te beperken. Dit resulteert in diepe stations en hoge bouwkosten. Hoewel ondiepe tunnels vele voordelen bieden gezien de lagere bouwkosten en de lagere operationele kosten, leidt de beperkte kennis over het boren van ondiepe tunnels in slappe grond tot obstakels bij de inzet in stedelijk gebied.

Dit onderzoek richt zich op de invloed van het verminderen van de C/D verhouding van ondiepe tunnels in slappe grond met aandacht voor de volgende aspecten: stabiliteit, constructie, zettingen en de invloed op bestaande bebouwing en volumeverliezen. Op basis hiervan zijn de limitaties en de optimale C/D verhouding voor ondiepe tunnels afgeleid en oplossingen voor het verbeteren van het ondiepe boorproces voorgesteld.

Ten eerste is het evenwicht van ondiepe tunnels beschouwd met betrekking tot opdrijven, frontstabiliteit en blow-out. De relatie tussen de C/D verhouding en de benodigde d/D verhouding en de benodigde steundrukken is onderzocht voor verschillende grondsoorten. Hierbij zijn zowel bestaande modellen toegepast als nieuwe modellen ontwikkeld. De bandbreedte van toelaatbare steundrukken is afgeschat voor tunnelboormachines, met name voor gronddrukbalansschilden. Het is aangetoond dat voor een ondiepe tunnel in veen een tunnelmantel met een d/D verhouding groter dan $1/12$ tot een stabiele tunnelconstructie zal leiden.

Ten tweede is op basis van constructieel het effect van deformaties en de interne krachten op de tunnelmantel bepaald voor afnemende C/D verhoudingen. Aangezien recente ontwikkelde modellen voor het ontwerp van tunnelmantels ontwikkeld zijn voor middeldiepe tot diepe tunnels met $C/D \geq 2$, is een nieuw model voorgesteld dat rekening houdt met verschillende belastingen aan boven- en onderzijde van de tunnel. De verandering van de interne krachten en deformaties van de tunnelmantel is beschouwd bij afnemende C/D verhouding. De resultaten laten zien dat een significant verschil tussen de nieuwe en bestaande modellen de toenemende maximum deformaties van de tunnelmantel bij zeer ondiepe tunnels is. Tevens zijn de optimale C/D verhoudingen voor verschillende d/D verhoudingen voor tunnels in slappe grond bepaald. Deze waarden zijn gecombineerd met de resultaten van de evenwichtsbeschouwingen om tot optimale C/D en d/D waarden te komen.

Het boren van tunnels leidt niet alleen tot grondverplaatsingen aan maaiveld maar ook in de ondergrond. Deze verplaatsingen kunnen tot schade aan nabijgelegen bestaande bebouwing leiden. Dit onderzoek heeft de invloedzone van ondiepe tunnels onderzocht en het verband tussen deze zones en de C/D verhouding. Twee modellen zijn opgesteld om de invloedzone af te schatten en een eerste inschatting te maken van de kans op gebouwschade. De invloedzones zijn afgeleid voor verschillende tunneldiameters in verschillende grondslag en vergeleken met recente projecten.

Het volgende deel van dit onderzoek heeft zich gericht om het volumeverlies door ondiepe boren van tunnels. Het totale volumeverlies is geschat aan het graaffront, langs

het tunnelschild, nabij de staartspleet en ten gevolge van lage duur consolidate. Bij het graaffront is de methode van [Macklin \(1999\)](#), welke op basis van projectervaringen was afgeleid, toegepast. Een nieuwe berekeningsmethode is voorgesteld op basis van onderzoek van [Bezuijen and Talmon \(2008\)](#) naar stroming van grout langs de tunnelbormachine. Voor de volumeverliezen bij de staartspleet is een nieuw model op basis van cavity expansion opgesteld en tevens is voor de volumeverliezen ten gevolge van consolidatie een nieuw model voorgesteld. Op basis van deze analyse zijn onder- en bovengrenzen aan de verwachte volumeverliezen bij ondiepe tunnels bepaald, zowel tijdens de bouw als ten gevolge van lange termijn consolidatie. Deze analyse laat zien dat bij het zeer ondiep boren van tunnels een nul volumeverlies haalbaar is met zeer nauwkeurige controle van de steundrukken.

In het vijfde deel van dit onderzoek zijn de grenzen van de invloedzones afgeleid door de resultaten van de zettingsberekeningen en de volumeverlies-berekeningen te combineren, zowel aan maaiveld als in de ondergrond. De resultaten zijn vergeleken met praktijkmetingen. Daarnaast is de invloed van grondeigenschappen onderzocht om een schatting van de benodigde sterkte van de grond voor een stabiel boorproces te geven. Dit onderzoek naar het reduceren van de C/D verhouding heeft meer inzicht in de effecten van ondiep tunnelboren in slappe grond opgeleverd en zal ontwerpers helpen bij het optimaliseren van toekomstige ondiepe tunnels.

CURRICULUM VITÆ

Minh Ngan Vu was born on the 4th of November 1982 in Hanoi, Vietnam. He started his Civil Engineering study at National University of Civil Engineering in Vietnam in September 2000. He graduated in March 2005. He began his M.Sc. course on civil engineering in 2005 and obtained the M.Sc. degree in 2008 on bridge and tunnel construction. In that period, he also worked in a construction company on several road and bridge projects in Vietnam.

In October 2009, he started as a lecturer in Hanoi University of Mining and Geology. Since February 2012, he has worked at Faculty of Civil Engineering and Geoscience in Delft University of Technology on the topic of shallow tunnelling in soft soils.